NUTRIENTS AND ENERGY RECOVERY FROM ECOLOGICAL SANITATION SYSTEM

AUSTINE OWUOR OTIENO

DOCTOR OF PHILOSOPHY

(Environmental Engineering and Management)

JOMO KENYATTA UNIVERSITY

OF

AGRICULTURE AND AGRICULTURE

2023

Nutrients and Energy Recovery from Ecological Sanitation System

Austine Owuor Otieno

A Thesis Submitted in Partial Fulfilment of the Requirements for the Degree of Doctor of Philosophy in Environmental Engineering and Management of the Jomo Kenyatta University of Agriculture and Technology

2023

DECLARATION

This thesis is my original work and has not been presented for a degree in any other university.

Signature……..Date…….

Austine Owuor Otieno

This thesis has been submitted for examination with our approval as University supervisors.

Signature……..Date…….

Prof. Patrick G. Home, PhD

JKUAT, Kenya

Signature……..Date…….

Prof. (Eng). James M. Raude, PhD

JKUAT, Kenya

Signature……..Date…….

Dr. Sylvia I. Murunga, PhD

JKUAT, Kenya

DEDICATION

I dedicate this work to my father Mr. Elias Otieno Ongowo, and mother Mrs. Grace Akinyi Otieno for motivating me to achieve the best in my academic pursuit. I also dedicate this work to my family for their encouragement and enduring my absence during my studies.

ACKNOWLEDGEMENT

I express my sincere gratitude to my supervisors Prof. Patrick G. Home, Prof. (Eng). James M. Raude, and Dr. Sylvia I. Murunga from Jomo Kenyatta University of Agriculture and Technology for their guidance and support throughout my studies. I would also like to thank Prof. Tuula Tuhkanen, from the University of Jyvaskyla, Finland, to whom I owe gratitude for the Erasmus+ exchange programme between JKUAT and University of Jyvaskyla, which not only accorded me an opportunity to conduct experiments in world class facilities but also enabled me to network with professionals in my area of research. I appreciate the technicians at the Department of Biological and Environmental Science at the University of Jyvaskyla, Finland, for their guidance in conducting adsorption experiments. I am grateful to Dr. Dickson O. Ojwang from Uppsala University, Sweden who contributed immensely towards materials characterization at Angstrom Laboratory, Department of Chemistry. I appreciate Prof. Anthony Gachanja from the Department of Chemistry at Jomo Kenyatta University of Agriculture and Technology for his invaluable ideas in carrying out experiments and providing equipment for conducting emission analysis. The Kenya Forestry Research Institute, Karura is acknowledged for providing the facilities used for characterization of the briquettes and charcoal. I also acknowledge my employer the Technical University of Kenya for granting me study leave during the exchange programme. Finally, I am sincerely proud of my family that not only offered me overwhelming support and encouragement, but also endured my absence during my studies.

TABLE OF CONTENTS

LIST OF TABLES

LIST OF FIGURES

LIST OF APPENDICES

ABBREVIATIONS AND ACRONYMS

ANOVA	Analysis of Variance
APS	Adequate Precision Statistics
ASTM	American Standard for Testing and Materials
CCC	Central Composite Circumscribed Design
CCD	Central Composite Design
CCF	Central Composite Face-Centered Design
CCI	Central Composite Inscribed Design
C_e,	Concentration of adsorbate remaining in solution (mg/L)
CO	Carbon monoxide
CO_2	Carbon dioxide
DI	Deionized water
DTF	Decentralized Treatment Facilities
DTG	Derivative Thermogravimetry
D-R	Dubinin-Radushkevich
E_α	Activation Energy (kJ/mol)
EDS	Energy Dispersive Spectroscopy
ERes	Externally Studentised Residual

FC	Fixed Carbon
FTIR	Fourier Transform Infrared Spectroscopy
FWO	Flynn-Wall-Ozawa
GCV	Gross Calorific Value
HHV	Higher Heating Value
ICTAC	International Confederation for Thermal Analysis and Calorimetry
ISRes	Internally Studentised Residual
KAS	Kissinger-Akahira-Sunose
LHV	Lower Heating Value
LS	Lateritic Soil
LSD	Least Significance Difference
NH_4^+-N	Ammonium Nitrogen
OSHA	Occupational Safety and Health Administration
P	Phosphorous
PPB	ineapple Peel Biochar
PRESS	Predicted Residual Sum of Squares
q_e	Amount adsorbed per unit mass of adsorbent (mg/g),

q_m	Maximum monolayer adsorption capacity (mg/g)
RSM	Response Surface Methodology
SEM	Scanning Electron Microscopy
SD	Standard Deviation
SDG	Sustainable Development Goals
SPSS	Statistical Package for Social Sciences
TGA	Thermogravimetric Analysis
UBSUP	Up-scaling of Basic Sanitation for the Urban Poor Programme
UDDT	Urine Diversion and Dehydration Toilet
UNICEF	United Nations Children's Fund
VM	Volatile Matter
WHO	World Health Organization
XRD	X-ray powder Diffraction

ABSTRACT

Human excreta are abundant waste streams whose safe disposal to the environment is a challenge in many developing countries due to inadequate sewerage system and poor faecal sludge management. The growing practice of resource recovery from human excreta could minimize the challenge of unsafe disposal thereby contributing to protection of the environment and human health. The overall aim of the study was therefore to recover nutrients from human urine and energy from human faeces. On nutrient recovery, the study focused on adsorption of ammonium nitrogen (NH_4^+-N) and phosphorous (P) in human urine using pineapple peel biochar (PPB) and lateritic soil (LS). Physicochemical properties of PPB, and LS were characterized by Scanning Electron Microscopy-Energy Dispersive Spectroscopy (SEM-EDS), X-ray powder Diffraction (XRD), Fourier Transform Infrared Spectroscopy (FTIR) and Thermogravimetric Analysis (TGA) to investigate the relationship of their properties with adsorption of NH_4^+-N and P. Langmuir, Freundlich, and Dubinin-Radushkevich (D-R) isotherm models were fitted to correlate the experimental equilibrium adsorption data with the coefficient of correlation (R^2) used to determine the model that offered the best fit. The effect of contact time and initial concentration of NH_4^+-N and P on adsorption was evaluated. Factors influencing adsorption process such as the contact time, agitation speed, and adsorbent loading were optimised using Response Surface Methodology (RSM) in order to predict the optimum conditions for achieving the highest adsorption of NH_4^+-N and P. For adsorption of NH_4^+-N, the D-R isotherm model best described the behaviour of its adsorption on both PPB and LS based on the coefficient of correlation values. This model showed that the adsorption of NH_4^+-N on both samples was a physical process with PPB and LS having mean surface adsorption energies of 1.826×10^{-2}, and 1.622×10^{-2} kJ/mol, respectively. The PPB exhibited a slightly higher adsorption capacity for NH_4^+-N (13.40 mg/g) than LS (10.73 mg/g) with the difference attributed to its higher contact surface area and porosity. The adsorbed NH_4^+-N on PPB at optimal conditions described by RSM of 60 contact time, 80 rpm agitation speed, and adsorbent loading of 0.1g, yielded experimental adsorption capacity of 36.42 mg/g, which agreed well with the predicted adsorption capacity of 36.80 mg/g. These values are good indicators for assessing the effectiveness of the materials for adsorption of NH_4^+-N from human urine. For adsorption of P, PPB exhibited a tendency to adsorb and gradually release P into the human urine thereby not attaining equilibrium. LS on the other hand adsorbed P upto equilibrium. The P adsorption data on LS fitted the Langmuir model best ($R^2 = 0.984$) compared to the Freundlich model ($R^2 = 0.966$). The mean surface adsorption energy of 1.313×10^{-2} kJ/mol obtained from the D-R model ($R^2 = 0.858$) indicated that the adsorption of P on LS occurred through weak forces of interaction. The amount of adsorbed P on LS at equilibrium (q_e) increased with the initial concentration of urine as well as with the contact time. The Langmuir maximum adsorption of P on LS was found to be 45.25 mg/g. The RSM demonstrated that contact time 30 min, agitation speed 80 rpm, and adsorbent loading 0.1 g in 25 mL of urine were optimum for highest adsorption of P (112.80 mg/g). The results show that LS is a promising inexpensive adsorbent for effective removal and recovery of P from

human urine. On energy recovery, the study examined the kinetic analysis of the thermal decomposition of faecal char, sawdust char and their blend using thermogravimetric analysis (TGA) under air to assess their reaction rates and thermal stability as potential sources of fuel. The kinetic parameters during the degradation were tested by combining the Kissinger-Akahira-Sunose (KAS), and Flynn-Wall-Ozawa (FWO) iso-conversional methods. The TGA and deconvoluted DTG curves indicated moisture release followed by devolatilization of hemicellulose, cellulose, and lignin between ~300 and 450 °C, before ash formation. Both KAS and FWO methods described the kinetic processes realistically and yielded similar activation energy values. The lowest activation energy required to initiate degradation as calculated by KAS were found to be 80.4, 80.0, and 86.4 kJ/mol for faecal char, sawdust char, and blend, respectively. On the other hand, the activation energy for the whole conversion range was 103.7, 108.7, and 104.8 kJ/mol for faecal char, sawdust char, and blend, respectively. These results suggest that the compositional differences between the samples translated to variability in the weight loss rates, shapes of decomposition peaks, and parallel, competitive, and complex reaction schemes resulting to irregular trend in the activation energy. Furthermore, the study on energy recovery compared the heating properties and toxic flue gases namely; carbon monoxide (CO), nitric oxide (NO), and hydrogen sulphide (H_2S), emitted during combustion of charcoal and co-combustion (50:50 wt. %) of charcoal with briquettes densified from human faecal char, sawdust char, and molasses. The physicochemical properties (fixed carbon, volatile matter, moisture content, ash content, and gross calorific value) of the briquettes and charcoal was determined and characterization of the flue gases (concentration, oxygen level, combustion temperature) conducted using E8500P industrial integrated emissions system combustion gas analyser. It was observed that combustion of charcoal did not emit NO, however the concentration of the CO was above the critical short-term limits of 35 ppm. The level of emission of the CO and H_2S was above the short-term exposure limits of 35 and 0.005 ppm, respectively during co-combustion whereas NO concentration was below dangerous exposure levels of 100 ppm throughout the combustion period. Co-combustion resulted into release of higher heat energy as evidenced by the flue gas temperatures reaching upto 475 °C compared to 222 °C during charcoal combustion. The gross calorific value for briquettes was 19.8 MJ/kg which was comparable to those reported for fuel wood although lower than 25.7 MJ/kg reported for charcoal. These results suggest that co-combustion of charcoal with briquettes densified from faecal and sawdust char is a promising alternative approach to generate safe and sufficient heat energy for indoor use, reduce deforestation, and mitigate unsafe faecal waste disposal issues. In conclusion, this research demonstrates that nutrients can be captured from human urine to produce enriched biomass that can be used as slow-release fertilizers. The study findings also demonstrated that human faeces are a potential biomass for production of safe solid fuels. Hence, nutrients and energy recovery from human excreta could mitigate the environmental and health impacts associated with their unsafe disposal into the environment.

.

CHAPTER ONE

INTRODUCTION

1.1 Background Information

Proper management of human excreta is essential in maintaining a healthy and safe environment for biodiversity. Target 6.2 of the Sustainable Development Goals (SDG) which aims at increasing access to adequate and equitable sanitation and hygiene for all and end open defecation has seen many governments continuously invest in this vital sector. Despite attempts to improve sanitation situation globally, 46% of the global population (3.6 billion people) still lack access to safely managed sanitation services implying that significant amount of human excreta generated daily is unsafely disposed of in the environment (WHO & UNICEF, 2021) thereby posing threat to human health and biodiversity (Nguyen-Viet et al., 2009; Cheng et al., 2012).

With on-site sanitation facilities being the most common systems used globally (Strande et al., 2014; WHO & UNICEF, 2017), the entire faecal sludge management chain from containment of human excreta, emptying, transport, treatment, safe disposal or reuse is of paramount importance in order to protect the population from water borne diseases. However, inadequate financial resources have hampered the emptying and or safe disposal of the accumulated sludge in these facilities, often resulting to their abandonment or disposal of the untreated sludge into the environment thereby contaminating water resources (Bassan et al., 2015). The practice of recovery of valuable resources from human excreta contained in the on-site sanitation facilities with the aim of revenue generation is considered as a promising way of sustainably managing the waste (Diener et al., 2014; Gold et al., 2014). This approach to management of human excreta could potentially improve overall access to properly managed sanitation facilities by promoting frequent desludging. Noteworthy is the development of the ecological sanitation concept also commonly referred to as Ecosan. Ecological sanitation is a sanitation approach that aims at collecting the different waste streams separately at

source and treating them individually with the objective of recovering valuable nutrients, energy, and clarified water (Langergraber & Muellegger, 2005). Urine diversion and dehydration toilet (UDDT) is a form of ecological sanitation system which operate on the principle of separation of human faeces and urine at the point of generation thus enabling utilization of these waste streams separately (Langergraber & Muellegger, 2005).

The potential of both human urine and faeces for agricultural production have been widely reported (Harder et al., 2019; Gwara et al., 2021). There have also been few studies at laboratory scale aimed at recovering energy from human urine (Kuntke et al., 2014; Salar-García et al., 2017), while for human faeces, a variety of options have recently been explored at both lab and field scale such as for production of solid fuel, protein for animal feed, biogas and as a component in building materials (Diener et al., 2014). For human urine, the World Health Organization (WHO) recommends storage for 6 months to achieve complete sanitization (WHO, 2006), a practice likely not to be ideal especially in urban and peri-urban areas due to odour problems and large space requirements. This has prompted a focus on nutrients extraction or capture by many researchers. Human urine is rich in macro-nutrients such as Nitrogen (N), and Phosphorous (P) (Udert et al., 2003; Maurer et al., 2006; Etter et al., 2011) which are readily up taken by plants and thus can contribute to enhanced crop production if captured and incorporated in the soil. However, ammonium (NH_4^+-N), and P are the major cause of eutrophication in water bodies as a result of wastewater inflows, with human urine being the major contributor of these nutrients in municipal wastewater flows (Nguyen et al., 2019; Preisner et al., 2021).

Among the technologies already reported aimed at recovering NH_4^+-N from human urine are microbial electrolysis cell (Kuntke et al., 2014), microbial fuel cells (Ledezma et al., 2015), ammonia stripping (Behrendt et al., 2002), and adsorption using adsorbents such as ion exchange resins (BelerBaykal et al., 2004), geological materials (Kithome et al., 1998), biochar (Wang et al., 2015), and activated carbon (Pillai et al., 2014). Similarly, researchers have explored various technologies for recovery of P from

wastewater or human urine, with struvite ($MgNH_4PO_4.6H_2O$) precipitation upon addition of magnesium being the most widely investigated method (Ban and Dave, 2004; Ganrot et al., 2007; Wang et al., 2018; Li et al., 2019). Other techniques reported are solar thermal evaporation (Antonini et al., 2012), freeze thaw (Ganrot et al., 2007), electrochemical (Perera & Englehardt, 2020) and adsorption (Mansing R & Rout, 2013; Pitawala et al., 2013; Ling Zhang et al., 2014). Of the reported NH_4^+-N and P recovery techniques, adsorption is considered the most ideal method for nutrients recovery especially in developing nations due to its flexibility of design, ease of operation and low cost (Martin et al., 2020). The use of biochar and geological materials for adsorption of nutrients from aqueous solutions has been demonstrated to be effective. Thus, investigating the adsorption of NH_4^+-N, and P in human urine on biochars derived from organic wastes, and geological materials that have not been reported on is attractive. Utilization of biochar derived from pineapple peels, and lateritic soil for nutrients recovery from human urine is rather scarce and hence investigation of their physicochemical properties, mechanisms of nutrient removal and their adsorption capacities would be key in optimising their use to produce slow-release fertilizers or an enriched medium for crop growth. Biochar is a carbon material formed as a result of combustion of biomass material under minimal or no oxygen conditions whereas Lateritic soil (LS) is formed as a result of rapid weathering of rocks and high rate of leaching in the tropical climate and is normally nutrient deficient, thus majorly used for construction purposes (Ehujuo et al., 2017; Stoops & Marcelino, 2018; Ng et al., 2019).

Production of solid fuels (briquettes) from human faeces for domestic heating is an approach that is currently practiced in Kenya (Karahalios et al., 2018). It is however recommended to pyrolyze human faeces at temperatures > 300 ^oC to eliminate all pathogens to make it safe for briquetting (Atwijukye et al., 2018). During pyrolysis, biomass materials are heated under inert conditions to yield a charcoal-like material called biochar (Mishra & Mohanty, 2018). Pyrolysis however reduces the calorific values of human faeces due to degradation of aliphatic hydrocarbons (Ward et al., 2014). On the other hand, the calorific values of wood biomass such as sawdust are

known to increase with pyrolysis temperature due to an increase in their fixed carbon content (Bulmau et al., 2010). Thus, it is recommended that pyrolyzed human faeces and other carbonized woody waste streams could be blended to improve the resultant calorific values (Atwijukye et al., 2018). Normally charred materials lack plasticity and therefore it is common practice to moisten them with binders such as starch and molasses before densification so as to produce durable briquettes. Blending pyrolyzed human faeces (hereon referred to as faecal char) with sawdust char and using molasses as a binder in order to produce briquettes has been the most widely reported approach (Kabok et al., 2018; Karahalios et al., 2018). Sawdust is a widely abundant waste from saw milling activities in Kenya while molasses is widely abundant as a by-product of sugar processing and hence they are sustainable source of raw materials in the production of briquettes.

Despite the ongoing practice of briquettes production from faecal char and sawdust char, studies involving thermal degradation characteristics, and reaction kinetics of the pyrolyzed pathogen free human faeces, sawdust char and their blend using thermogravimetric analysis (TGA) under ambient conditions are lacking. Studying the thermal degradation characteristics and reaction kinetics is vital in giving insights on the practical thermal behaviour of briquettes densified from the charred faeces and sawdust char. Furthermore, studies on the safety of the briquettes containing faecal char for indoor heating in terms of their level of emission of toxic gases such as CO, H_2S and NO are scarce.

1.2 Statement of the Problem

The WHO/UNICEF Joint Monitoring Programme (JMP) report for Water Supply, Sanitation and Hygiene published in 2021, revealed that 46% of the global population (3.6 billion people) lack safely managed sanitation service in which excreta is safely disposed of in situ or treated off-site (WHO & UNICEF, 2021). This implies that nearly half of the global human population generates excreta whose safe disposal cannot be accounted for, a situation that pose significant health risks to humans as a result of

environmental pollution. Other studies have reported that inadequate management of human excreta is among the major contributors of diseases causing death of children under the age of five (Cheng et al., 2012; Bassan et al., 2015). Coupled with increase in waterborne diseases due to inadequate management of human excreta, is the rising level of eutrophication of aquatic systems due to domestic wastewater inflows, a situation which has resulted into hypoxic conditions that affect aquatic life (Nguyen et al., 2019). Human urine is the major contributor of macronutrients in wastewater conveyed to centralized treatment plants with approximately N (80–90%), P (50–65%), and K (50–80%) (Lienert et al., 2007; Jana et al., 2012). Recovery of valuable resources from human excreta contained in on-site facilities is currently considered as a sustainable way of managing both faecal matter and urine in unsewered areas. Production of briquettes from human faeces has been established to be the most profitable venture compared to its tradition use as soil amender in sub-Saharan Africa (Muspratt et al., 2014). On the other hand, application of human urine as fertilizer has been reported to yield higher produce compared to chemical fertilizers (Viskari et al., 2018), with WHO recommending its storage for 6 months to achieve complete sanitation for use in agriculture (WHO, 2006). Nevertheless, studies that have reported on briquettes production from human faecal char for domestic heating and cooking have majorly focused on the influence of organic binder types (molasses and starch), binder ratios, densification pressures, and carbonization temperatures on the combustion behaviour and heating values of the solid fuels (Ward et al., 2014; Kabok et al., 2018). However, investigations on the thermal decomposition behaviours and reaction kinetics of human faeces, using thermogravimetric analysis (TGA) under air conditions to depict their practical behaviours have not been reported. Furthermore, despite the increasing attention on briquettes production from human faeces, studies on emission of toxic gases liberated during combustion of these briquettes are lacking. For human urine, there has been increasing attention on nutrients adsorption from source separated human urine on biochars and geological materials to produce an enriched biomass for use as slow-release fertilizers. Nutrients adsorption from human urine is not only considered low cost but also environmentally friendly since it eliminates the need for prolonged urine

storage for 6 months that often generates offensive odours (Alhashimi & Aktas, 2017). However, studies aimed at investigating the physicochemical properties, adsorption mechanisms and nutrients adsorption capacities of pineapple peel biochars and lateritic soil in human urine are lacking despite their wide availability. Moreover, adsorption process being influenced by a number of factors, the one at a time factor approach used in obtaining optimum conditions cannot capture the interactive effects of the various factors. Hence employing interactive tool such as Response Surface Methodology (RSM) that captures all interactions (Myers et al., 2004) could be useful in predicting optimum conditions to attain the highest level of adsorption.

1.3 Objectives

1.3.1 Main Objective

The main objective of this study was to evaluate and optimize nutrients and energy recovery from ecological sanitation system.

1.3.2 Specific Objectives

The specific objectives of this study were to:

i. Determine the behaviour and capacity of pineapple peel biochar and lateritic soil in adsorbing ammonium nitrogen and phosphorous from human urine.
ii. Optimise the adsorption of ammonium nitrogen and phosphorous from human urine on pineapple peel biochar and lateritic soil.
iii. Determine the thermal degradation and kinetic behaviours of pyrolyzed human faeces, sawdust char and their blend.
iv. Evaluate emission properties of briquettes densified from pyrolyzed human faeces, sawdust char and molasses.

1.4 Research Questions

i. What are the behaviours and capacities of pineapple peel biochar and lateritic soil in adsorbing ammonium nitrogen and phosphorous from human urine?
ii. What are the optimum conditions for adsorption of ammonium nitrogen and phosphorous from human urine on pineapple peel biochar and lateritic soil?
iii. Are the thermal degradation and kinetic behaviours of pyrolyzed human faeces, sawdust char and their blend different?
iv. What are the emission properties of briquettes densified from pyrolyzed human faeces, sawdust char and molasses?

1.5 Justification of the Study

With bioresource recovery from human excreta gaining attention as a sustainable approach towards managing both human faeces and urine, a focus on production of safe and good quality products from the waste streams could enhance investments in the sector which consequently will improve access to safely managed sanitation services and overall human health. The advent in the adoption of Urine Diversion and Dehydration Toilets (UDDTs) also referred to as ecological sanitation systems, has further enabled separate utilization of human excreta for diverse applications. With the increasing energy and fertilizer demand globally, seeking alternative safe and sustainable sources is immediate. Human faeces are considered a potential biomass for production of solid fuels which has a high market potential compared to its tradition use as soil amender (Muspratt et al., 2014). Human urine has also been demonstrated at field scale to promote high agricultural productivity compared to chemical fertilizers, with no potential threats to human health (Viskari et al., 2018). Nutrient capture from human urine through adsorption to produce enriched biomass for use as slow release fertilizer is however considered suitable compared to prolonged storage for 6 months before use as recommended by WHO due to space constraints and odour problems (Alhashimi & Aktas, 2017).

This study therefore investigated the thermal stability and reaction rates of faecal char in comparison to sawdust char and their blends under air atmospheres, as well as the heating and emission properties of briquettes densified from faecal char, sawdust char, and molasses. On nutrients recovery, pineapple peel biochar and lateritic soils were used to adsorb ammonium nitrogen (NH_4^+-N) and phosphorous (P) from the human urine to produce slow-release fertilizer.

The findings of this study will be useful to;

i. Public and private sanitation companies engaged in large scale production of briquettes from human excreta since the findings can be used to improve the quality of their product to compete other existing fuels.
ii. Researchers actively involved in seeking low-cost and sustainable materials for effective capture of nutrients from human urine in order to produce an enriched slow-release fertilizer to supplement the non-renewable sources of chemical fertilizers
iii. Advocates for circular economy that considers human excreta as a resource rather than a waste

1.6 Scope and Limitations of the Study

The overall aim of the study was to recover nutrients and energy from ecological sanitation systems. Pineapple peel biochar (PPB) and lateritic soil (LS) were used as bio-sorbents for recovery of ammonium nitrogen (NH_4^+-N) and phosphorous (P) from the human urine. Langmuir, Freundlich, and Dubinin-Radushkevich (D-R) isotherm models were employed to correlate the experimental equilibrium adsorption data, while Response Surface Methodology (RSM) was used to optimise the adsorption process. It was assumed that both PPB and LS could effectively adsorb the cationic NH_4^+-N, and anionic PO_4^{3-} species upto equilibrium to enable adsorption isotherm modelling to be conducted so as to calculate the NH_4^+-N and P adsorption capacities of both adsorbents from human urine. Although LS could adsorb NH_4^+-N and P upto equilibrium, PPB

adsorbed and gradually released P into the human urine solution thereby not attaining equilibrium conditions. The PPB surface could have been modified with metal cations so as to attract and retain the anionic PO_4^{3-} species on its surface. On energy recovery, kinetic analysis of the thermal decomposition of pyrolyzed human faeces, sawdust char and their blend using thermogravimetric analysis under air was conducted to assess their thermal stability and reaction rates as potential as sources of fuel. Furthermore, briquettes densified from faecal char, sawdust char and molasses were produced and co-combusted with charcoal to characterize their emission properties to determine their safety for indoor household heating and cooking. It was assumed that briquettes densified from faecal char, sawdust char, with molasses (10 wt.%) used as a binder could easily ignite without the need for co-combustion with other fuels. It was however observed that upon heating, molasses melts causing disintegration of the densified briquettes thereby making ignition difficult. Although co-combustion of the briquettes with charcoal enabled the briquettes to ignite easily, lower amounts of charcoal (< 50 wt.%) could have been used to monitor their effect on the heating and emission properties during co-combustion.

CHAPTER TWO

LITERATURE REVIEW

2.1 Human Urine

Human urine is a complex water solution excreted from the body through the urethra. The biological, physical, and chemical properties of human urine have been extensively studied (Kirchmann & Pettersson, 1994 Etter et al., 2011; Bischel et al., 2015). The use of urine for agricultural production has attracted attention of researchers due to its high concentration of major macronutrients (NPK) required for plant growth (Simha et al., 2017; Viskari et al., 2018; Pradhan et al., 2019). Moreover, according to WHO, complete pathogen elimination in human urine can be attained by storing it for a period of six months making it suitable for direct application in the field for agricultural production after dilution (WHO, 2006).

2.1.1 Liquid Generation

Approximately 91–96% of human urine is water (Höglund et al., 2000) with inorganic salts, urea, organic compounds, and organic ammonium salts constituting the remaining fraction (Putnam, 1971). Therefore, the amount of urine generated is dependent on the water intake of individuals. Normally, one person produces 0.6 to 2.6 L of urine daily with an average value estimated at 1.4 L daily (Rose et al., 2015). Other factors influencing urine generation are body size and age with adults producing twice as much urine as children (Karak & Bhattacharyya, 2011). The high generation rates of urine by adults is attributed to greater physical activity, obesity and higher medication intake than children (Clark et al., 2011). It can be recommended that urine from children is safer for use in agriculture since they contain less pharmaceuticals.

2.1.2 Composition

Since urine is an excretion from the human body, its composition is influenced largely by the diet. The most predominant constituent in urine (>50%) is urea [$CO(NH_2)_2$] which is the major source of total nitrogen in fresh urine (Udert et al., 2003; Etter et al., 2011). Urea is produced through metabolism of protein. The other major solutes (macronutrients) excreted in urine are Na (2.5-3.4 g/L), P (0.8–2.0 g/L), K (1.8-2.7 g/L) and Cl (3.7-4.9 g/L) which are largely derived from dietary intake (Maurer et al., 2006). Ammonium (NH_4^+) is produced through hydrolysis of urea by urease enzyme with the process also yielding carbamate that spontaneously decomposes to carbonic acid and another molecule of ammonia through a process called ureolysis as shown in Equation 2.1 (Udert et al., 2003).

$$NH_2(CO)NH_2 + 2.H_2O \rightarrow NH_3 + NH_4^+ + HCO_3^- \quad (2.1)$$

According to Hotta & Funamizu (2008), without urease, urea is a very stable compound with a half-life time of 3.6 years at 38 ºC. Although fresh urine is normally acidic with pH ranging 5.6 – 7.2 (Udert et al., 2003; Etter et al., 2011), the release of ammonia during ureolysis increases pH (Udert et al., 2003). Variations in urine pH amongst individuals has also been reported to be influenced by diet and alcohol intake (Kanbara et al., 2012). Noteworthy is that urine also contains enzymes, uric acid, vitamins, chlorides, oxalates, amino acids (Lind et al., 2000; Winker et al., 2009), heavy metals (Kirchmann & Pettersson, 1994), pharmaceuticals and hormones (Lienert et al., 2007), viruses and bacteria (Björn Vinnerås et al., 2008). Therefore, pre-treatment of fresh urine before use for agricultural production is recommended.

2.2 Source Separation of Urine

The concept of source separation involves the separate collection of urine from faeces in the toilet consequently allowing each of these waste streams, which have significantly different properties from one another, to be treated in a specific and appropriate manner.

This concept of source separation of human excreta also referred to as ecological sanitation (Eco-San), was originally developed to achieve the Millennium Development Goals in the sanitation sector with the target of preventing pollution, and sanitizing excreta for use in agriculture (Esrey et al., 1998; Langergraber & Muellegger, 2005). The Eco-San concept includes a number of toilet designs and systems that are appropriate for various contexts. The most common and widely researched Eco-San technology is the Urine Diversion and Dehydration Toilets (UDDTs), in which urine is diverted so that it does not come into contact with faeces (Langergraber & Muellegger, 2005). The whole structure of UDDTs is built above the ground and typically consists of a bowl divided into two parts. That is, the front bowl collects the urine and the rear bowls the faeces (Larsen et al., 2009). After separation, both faeces and urine are collected in containers located beneath the superstructure above ground and treated on-site or transported further to a centralized treatment unit (Larsen et al., 2009). In many cases, it is advisable that each user sprinkles a desiccant in form of ash, soil, or dry leaves to the excrement to minimize foul smells and keep away flies. In Kenya, there has been a growing trend of sanitation entrepreneurs installing UDDTs to meet sanitation needs in the slum areas and in market centre's of major towns with the aim of recovering resources from the waste streams (www.sanergy.com).

2.2.1 Urine Diversion and Dehydration Toilets and Associated Problems with Urine Fertilizer Recovery

Diversion of urine for storage and reuse that UDDTs promotes exhibit inherent challenges. Loss of nitrogen through ammonia volatilization during storage as a result hydrolyses of urea and subsequent elevation of pH reduces potential reusability of nitrogen in post storage application (Udert et al., 2003). A further concern of UDDT is cross faecal contamination of the relatively sterile source separated urine (WHO, 2006). Inactivation studies with urine point towards significant pathogenic risks over its use due to persistence of faecal sterols, *Escherichia Ecoli*, *Salmonella Typhimurium*, *Ascaris Suum eggs* and rhesus rotavirus (Nyberg et al., 2014; Winker et al., 2009). WHO therefore recommends that urine should be stored for a period of 6 months at a

temperature of 20 ºC to achieve complete sterilization (WHO, 2006). However this promotes ureolysis (Udert et al., 2003). Studies on optimization of pathogen die-off in recovered fertilizers from urine however indicates that the pathogens can be eliminated within a shorter duration by increasing drying temperature to less than 55 ^{0}C and pH of urine to a level ≥ 10.5 (Randall et al., 2016a; Winker et al., 2009). Alkalinization therefore is an effective approach to stabilize and preserve nutrients in urine.

2.3 Technologies for Nitrogen and Phosphorous Recovery from Human Urine

In order to produce enough food for the growing world population, farmers will need to rely increasingly on fertilizer to replenish soil. Nitrogen and phosphorous are the key components in most fertilizers in use. Currently, the Haber-Bosch process is used to produce nitrogen for fertilizer but consumes more than 1% of world's total energy production (Kitano et al., 2012). Phosphorus is a non-renewable resource that is quickly being mined to depletion (Neset & Cordell, 2012). Fortunately, a large portion of the nitrogen and phosphorus used in fertilizers eventually become present in human urine (Bonvin et al., 2015; Kirchmann & Pettersson, 1994). Recycling these components from urine to fertilizer would make agriculture more sustainable in the future. Recent research effort has been devoted towards the development of technologies that can safely harness nutrients from human excreta to yield usable end products.

Although N exist in different forms in human urine, N in the form of free ammonia (NH_3-N) and ammonium (NH_4^+-N) constitute the largest proportion (Udert et al., 2003; Etter et al., 2011). However, NH_3-N in urine is easily lost through volatilization, while NH_4^+-N increases gradually with time due to ureolysis caused by the urease enzyme (Udert et al., 2003). Technologies aimed at recovery of NH_4^+-N from human urine without the necessity of prolonged storage have drawn the attention of many researchers. Among them are microbial electrolysis cell (Kuntke et al., 2014), microbial fuel cells (Ledezma et al., 2015), ammonia stripping (Behrendt et al., 2002), and adsorption using adsorbents such as ion exchange resins (BelerBaykal et al., 2004), geological materials (Kithome et al., 1998), biochar (Wang et al., 2015), and activated carbon (Pillai et al.,

2014). Despite the possibility of recovering NH_4^+-N from the aforementioned technologies, operational costs and the sensitivity of a given approach to slight changes in operational parameters could determine the choice of one approach over the other. For instance, NH_4^+-N recovery using biological processes (microbial electrolysis cell, microbial fuel cell) are likely to be sensitive to changes such as pH and temperature since they are microorganism dependent. Ammonia stripping on the other hand requires energy input, and may be expensive to run for large scale production. According to Kavvada et al. (2017), large scale recovery of NH_4^+-N through ion exchange process is quite expensive but not detrimental to the environment. Currently, adsorption is considered the most ideal method of NH_4^+-N recovery since it is less costly, flexible, efficient and environmentally friendly, and thus can be ideal for the developing countries (Alhashimi & Aktas, 2017).

Phosphorous is mainly present in human urine in the form of phosphates (PO_4^{3-}) (Maurer et al., 2006). Researchers have explored various technologies for P recovery from wastewater or human urine, with struvite ($MgNH_4PO_4.6H_2O$) precipitation upon addition of magnesium being the most widely investigated method (Ban and Dave, 2004; Ganrot et al., 2007; Wang et al., 2018; Li et al., 2019). Other techniques reported are solar thermal evaporation (Antonini et al., 2012), freeze thaw (Ganrot et al., 2007), electrochemical (Perera & Englehardt, 2020), and adsorption (Mansing & Rout, 2013; Pitawala et al., 2013; Zhang et al., 2014). Of the reported P recovery techniques, adsorption is considered the most ideal especially in developing nations due to its flexibility of design, ease of operation and low cost (Martin et al., 2020). However, energy requirements of these processes are a major determent.

2.3.1 Adsorption Process

Adsorption is a mass transfer process which involves the accumulation of substances at the interface of two phases, such as, liquid–liquid, gas–liquid, gas–solid or liquid–solid interface (De Gisi et al., 2016). The substance being adsorbed is the adsorbate and the adsorbing material is termed the adsorbent. In a solid–liquid system, adsorption results

in the removal of solutes from solution and their accumulation at solid surface. The adsorption of solutes continues until equilibrium is attained. This process is however influenced by a number of factors. Öztürk & Bektaş (2004) demonstrated that increase in contact time, pH and adsorbent dosage increases nutrient removal from aqueous solutions. Mouni et al. (2018) also showed that adsorption is spontaneous and enhanced at higher temperatures because as temperature rises, solution viscosity drops, which is favorable to the subsequent adsorption stages. Increase in the surface area of the adsorbent which is achieved by decreasing the particle sizes of the adsorbent has also been found to increase adsorption level (Khamparia & Jaspal, 2016; Matsui et al., 2015). Agitation speed has also been reported to increase collision resulting to higher adsorption (Shen and Duvnjak, 2005).

Activated carbons which are processed carbonaceous materials with high porosity and internal surface area available for adsorption of liquids and gases or chemical reactions (Saleem et al., 2019), are the most popular and widely used adsorbents in recovery of nutrients from human urine throughout the world (Ganrot et al., 2007). In spite of large use, the cost of their production may be a hindrance to their sustainability for field scale application and hence seeking alternative but efficient adsorbents is ideal. It is worth noting that although both activated carbon and biochars are produced via heating biomass under minimal oxygen or anaerobic conditions the significant difference lies in their production temperature with biochar being produced at lower temperature less than 700 ℃ while activated carbon is produced at higher temperatures more than 700 ℃ (e.g. 800-1000 ℃) resulting to higher porosity (Saleem et al., 2019).

Low-cost sorbents sources can be classified as; agricultural and household by-products, industrial by-products, sludge, sea materials, soil and ore materials and novel low-cost adsorbents (Ali et al., 2012). The use of wastes from agricultural and household sources as well as geological materials (soil, ore, etc.) as adsorbents is an attractive option due to their ease of availability and low processing cost and hence sustainability. Researchers have thus reported the use of geological materials such as zeolite (Kithome et al., 1998; Wu et al., 2006; Huang et al., 2010), and biochar derived from pyrolysis of biomass

derived from different materials (Hale et al., 2013; Zhang et al., 2014) for extracting nutrients from human urine.

2.4 Adsorption Isotherms

Adsorption isotherms is a representation of the amount of adsorbate on the adsorbent as a function of its pressure (if gas) or concentration (if liquid) at constant temperature (Sulaymon et al., 2013). Isotherm analysis through mathematical modeling provides insights into sorbent capacity and its surface properties (Hameed & El-Khaiary, 2008). The quantity adsorbed is nearly always normalized by the mass of the adsorbent to allow comparison of different materials (Sulaymon et al., 2013). Adsorption isotherm is normally determined by plotting the amount of adsorbate per unit weight of adsorbent (*qe)* against the equilibrium concentration of the adsorbate remaining in solution (*Ce).*

2.4.1 Langmuir model

Langmuir model assumes a monolayer adsorption on homogeneous adsorption sites (Ayawei et al., 2017). The linearized form is given as in Equation 2.2 (Vijayaraghavan et al., 2006).

$$\frac{1}{q_e} = \frac{1}{q_m} + \frac{1}{K_L q_m C_e} \tag{2.2}$$

Where:

q_e = the amount of adsorbate adsorbed at equilibrium (mg/g)

C_e = the equilibrium concentration of the adsorbate (mg/L)

q_m = the saturated monolayer adsorption capacity (mg/g)

K_L = the binding energy between the adsorbate and the adsorbent (L/mg)

The plot of $1/q_e$ against $1/C_e$ gives a linear plot from which the parameters q_m (mg/g), and K_L (L/mg) are obtained.

The Langmuir model constant (K_L), can further be used to compute the dimensionless separation factor (R_L) according to Equation 2.3 given as:

$$R_L = \frac{1}{1 + K_L C_o} \tag{2.3}$$

Where:

C_o = the initial concentration of adsorbate in the solution (mg/L)

K_L = the Langmuir constant (L/mg)

R_L = a dimensionless separation factor

If R_L is in the range between 0 and 1, then the adsorption process is considered favorable (Hameed and ElKhaiary, 2008).

2.4.2 Freundlich model

This model is based on the assumption that adsorption occurs in multilayer on heterogeneous adsorption sites (Ayawei et al., 2017). Its linearized form is expressed as in Equation 2.4 (Kumar et al., 2008).

$$\log q_e = \log K_f + \frac{1}{n} \log C_e \tag{2.4}$$

Where:

q_e = the quantity of adsorbate adsorbed at equilibrium (mg/g)

C_e = the equilibrium concentration of the adsorbate (mg/L)

K_f = the constant incorporating the factors affecting the adsorption capacity

1/n = the constant incorporating the factors affecting the adsorption intensity

The plot of log q_e versus log C_e gives a linear plot, from which the empirical parameters K_f and *1/n* are obtained from the intercept and the gradient, respectively.

2.4.3 Dubinin-Radushkevich (D-R) Model

The D-R model is often employed to determine whether an adsorption process is chemical or physical based on the mean surface adsorption energy (Foo & Hameed, 2010). The linearized form is expressed as presented in Equation 2.5 (Mahmoud, 2015).

$$\ln q_e = \ln Q_o - K_{DR}[RT\ln(1+1/C_e)]^2 \quad (2.5)$$

Where:

q_e = the amount of adsorbate adsorbed at equilibrium(mg/g)

R = the universal gas constant (8.314 J/mol·K)

T = the temperature (Kelvin)

C_e = the equilibrium concentration of the adsorbate (mg/L)

The plot of lnq_e versus $[RTln(1+1/C_e)]^2$ gives a linear plot from which the parameters K_{DR} (mol^2/kJ^2), and Q_o (mg/g) are calculated from the gradient and the intercept, respectively.

The mean surface adsorption energy (E) (kJ/ mol) is calculated using Equation 2.6 (Hu & Zhang, 2019) given as:

$$E = \frac{1}{\sqrt{2K_{DR}}} \quad (2.6)$$

Adsorption process is considered physical if E < 8 kJ/mol, whereas chemisorption occurs if E > 18 kJ/mol (Mahmoud, 2015).

2.5 Response Surface Methodology Approach for Optimization Process

Response Surface Methodology (RSM) is a collection of statistical and mathematical techniques that are useful for the modeling and analysis of problems in which a response of interest is influenced by several variables and the objective is to optimize the response (Myers et al., 2004). Most optimization is done using conventional one factor at a time strategy, which changes a single factor while maintaining other factors constant whereas RSM demonstrate the combined effect of all factors.

In order to apply RSM as an optimization tool, some stages need to be followed (Dutta et al., 2018). They include:

i. Designing of a series of experiments for adequate and reliable measurement of the response of interest.
ii. Developing a mathematical model of the second order response with the best fittings.
iii. Finding the optimal set of experimental parameters that produce a maximum or minimum value of response.
iv. Representing the direct and interactive effects of process parameters through two and three -dimensional plots.

Response Surface Methodology design allows estimation of interaction and even quadratic effect and therefore, gives an idea of the shape of the response surface under investigation. Central composite design (CCD) is an effective design for a fitting second-order model to response surface because it uses a relatively small number of observations to estimate the parameters (Bezerra et al., 2008).

2.5.1 Experimental Scheme and Design

2.5.1.1 Central Composite Designs

Central Composite Design (CCD) is of three types namely; central composite circumscribed design (CCC), central composite inscribed design (CCI), and central composite face-centered design (CCF). Zhang & Baixiaofeng (2009) demonstrated the similarities and differences of CCC, CCI and CCF is shown in Table 2.1.

Table 2.1: Similarities and Differences of CCC, CCI, and CCF

Properties	CCC	CCI	CCF
Design domain shape	Sphere	Sphere	Cubic
Design level	5	5	3
Complexity	High	High	Low
Factorial points position	±1	±0.7	±1
Axial points position	$\alpha = \sqrt{k}$	$\alpha = 1.0$	$\alpha = 1.0$
Recommend the center number	3-5	3-5	1-2
Rotatability	Rotatable	Rotatable	Not Rotatable
Uniformity of prediction error	Good	Good	Bad
Model based parameter estimation	Most effective	Worst	Second

2.5.1.2 RSM-Mathematical Model

Besides analyzing the independent variables effects, this experimental methodology also generates a mathematical model. The graphical viewpoint of the mathematical model has led to the term RSM. The relationship between the responses and the inputs are represented by Equation 2.7.

$$Y = f(x_1, x_2, x_3 \ldots\ldots\ldots\ldots x_k) + \varepsilon \qquad (2.7)$$

Where:

Y = the response

f = the response function

$x_1, x_2, x_3 \ldots x_k$ = the input variables which affects the response

k = the number of the independent variables

ε = the statistical error that represents other sources of variability not accounted for by f

After selection of the design, the model equation and coefficients are defined and predicted. As a result of sequential model sum of squares, a quadratic model is selected by Design Expert software. Usually a second-order model is utilized in response surface methodology as shown in Equation 2.8.

$$y = \beta_o + \sum_{i=1}^{k} \beta_i x_i + \sum_{i=1}^{k} \beta_{ii} x_i^2 + \sum_{i=1}^{k} \beta_{ij} x_i x_j + \varepsilon \quad (2.8)$$

Where:

β_o = the value of the fixed response at the center point of the design

$\beta_i, \beta_{ii}, and\ \beta_{ij}$ = the linear, quadratic and interaction effect regression terms, respectively

x_i = Denotes the level of the independent variable

k = is the number of independent variables

ε = the random error

The model correlates the dependent variables to the independent variables considered through second- order polynomial response equation according to Equation 2.9 given as:

$$Y = \beta_o + \beta_1 x_1 + \beta_2 x_2 + \beta_3 x_3 + \beta_{12} x_1 x_2 + \beta_{13} x_1 x_3 + \beta_{23} x_2 x_3 + \beta_{11} x_1^2 + \beta_{22} x_2^2 + \beta_{33} x_3^2 + \varepsilon \quad (2.9)$$

The selected independent variables are coded according to Equation 2.10 given as:

$$x_i = \frac{X_{i-} X_o}{\Delta X} \tag{2.10}$$

Where:

X_i = the un-coded value of the ith independent variable

X_o = the value of X_i at the centre point of the investigation area

ΔX = the step change

2.5.1.3 Statistical Analysis by RSM

Design expert software is used for statistical and diagnostic studies in response surface modeling. RSM offers adequacy measures such as the Analysis of Variance (ANOVA), sequential F-test and lack-of-fit test. The sum of square for the deviations in all the trials is known as the total sum of square (SS*T*). It is computed by adding the sum of square caused by the residual (SS_E) and the sum of square caused by the regression (SS_R) as shown in Equation 2.11.

$$SS_T = SS_E + SS_R \tag{2.11}$$

During repetition of experiments for accuracy and confidence in the results, errors and deviations result. Hence, the SS_R is found by adding the sum of square due to the lack of- fit (SS_L) and the sum of square due to the pure error (SS_P) as shown in Equation 2.12.

$$SS_R = SS_L + SS_P \tag{2.12}$$

The Fischer test (F-test) of a model evaluates the significance of the model by calculating the ratio of the mean square of regression (MS_R) to the mean square of residuals (MS_E). A small F-value for the model is not desired since it indicates that the variance is caused by random unexplained disturbances referred to as noise. The p-value

(p > F) provides an indication of the significance of a model in relation with the F-value. It can be defined as the probability that a variable did not affect the response for a given F-value. If the p > F for the model is less than 0.05, a model is said to be significant, meaning that there is 5% chance that the F-value is due to noise. If the p > F is above 0.1, the model is insignificant (Trinh & Kang, 2011).

The lack-of-fit test (LOF) determines the inability of a model to fit experimental data that are not represented in the experimental domain. This is commonly done by calculating its F-value. A small F-value for the LOF is desired, since the experimenter wants the model to fit. If the p > F is greater than 0.05 the LOF for the model is insignificant and the model is able to fit any data that are not specified in the experimental domain (Trinh & Kang, 2011). A good LOF does not guarantee the adequacy of a model, the coefficient of determination (R^2) as shown in Equation 2.13 must be considered, given the fact that it measures the overall performance of a model and its value should be close to 1 (Trinh & Kang, 2011).

$$R^2 = 1 - \left(\frac{SS_R}{SS_T} \right) \tag{2.13}$$

The adjusted R^2 (Equation 2.14) is computed by arranging the number of terms in a regression relative to the number of design points and it is usually equal to or lower than R^2. It has the particularity of being less subjected to variation than the R^2 when a new term is added to the regression (Myers et al., 2004).

$$Adjusted\ R^2 = \left(\frac{SS_E / df_E}{SS_T / df_T} \right) \tag{2.14}$$

The PRESS (Predicted residual sum of squares) is used to measure the predicted R^2, which indicates the level of change in the data using the model (Myers et al., 2004). During the selection of a model, the aim is to maximize the adjusted and predicted R^2

values. For a best fit, the difference between the adjusted and predicted R^2 must be less than 0.2. PRESS is calculated using Equation 2.15 given as:

$$PRESS = \sum_{I=1}^{n} \left(\frac{e_i}{1 - h_{ii}} \right)^2 \tag{2.15}$$

Where:

e_i = the residual

h_{ii} = the leverage which is the difference between the adjusted and predicted R^2

Other parameters in the analysis of a model include the standard deviation (SD) expressed in Equation 2.16 and Adequate Precision Statistics (AP) as in Equation 2.18 given as:

$$SD = \sqrt{MS_E} \tag{2.16}$$

The coefficient of variation (CV) measures the unexplained changes in the data and it is expressed as shown in Equation 2.17 given as:

$$CV = \left[\frac{SD}{\bar{Y}} \right] . * 100 \tag{2.17}$$

Where:

Y = the mean of the response variable

The adequate precision statistics (AP) determines the performance of the model in predicting the responses. A value of AP greater than four means that the model will give good predictions (Myers et al., 2004).

$$AP = \tilde{Y}_{\max} - \tilde{Y}_{\min} \tag{2.18}$$

Where:

Y_{max} = the maximum predicted response

Y_{min} = the minimum predicted response

2.5.1.4 Model Diagnostics

Diagnostic plots such as predicted versus actual plot, normal plot of residual, residuals versus predicted and residual versus the run predicts the reliability of the developed model and thus confirms that the ANOVA assumptions are correctly met. The residual is calculated as shown in Equation 2.19;

$$\text{Re}sidual = e_i = Y - \tilde{Y}_i \tag{2.19}$$

Where:

Y = the actual response

$\tilde{Y}_i$ = the response predicted by the model.

The residuals are classified as externally studentized (ESRes) or internally studentized (ISRes). A residual is said to be studentized when it is divided by the estimate of its standard deviation (SD). The ISRes (r) as shown in Eq. 2.20 compares the value of a residual to the residual variance in order to measure the number of standard deviation that separates the actual from predicted values.

$$IS\,\text{Re}s = r = \frac{e_i}{S\sqrt{(1 - h_{ii})}} \tag{2.20}$$

Where:

S = the standard deviation.

ESRes (t) as shown in Eq. 2.21 makes a comparison between the residual and the residual variance, excluding the first case of SD (s_{-1}). It represents the number of SD between the predicted value and the actual response (Myers et al., 2004).

$$ES\,\mathrm{Re}\,s = t = \frac{e_i}{S_{-1}\sqrt{(1-h_{ii})}} \tag{2.21}$$

2.5.1.5 The process of optimization

The optimization can be done graphically or numerically using Design Expert Software after the goals or criteria of the conditions desired for a given process is set by the experimenter. The RSM optimizes its factors through an objective function called the desirability function (D) (Equation 2.22) and transforms an estimated response to a scale free vale (*di*) called desirability. The desirability is a dimensionless entity that represents the closeness of a response to its ideal value and usually ranges from 0 to 1 with d = 0 being unacceptable, and d = 1 indicating that the model response is equal to that of the target value (Myers et al., 2004; Li et al., 2007).

$$D = (d_1 \times d_2 \times d_3 \times .....\times d_n)^{1/n} = \left[\prod_{i=1}^{n} di\right]^{1/n} \tag{2.22}$$

Where:

n = the number of responses in the measure

di = desirability

2.6 Pineapple Peel Wastes and Application of Pineapple Peel Biochar as an Adsorbent

In Africa, Nigeria, Kenya, Democratic Republic of Congo, Ivory Coast, Guinea and South Africa are the major pineapple producing countries (Hossain, 2016). According to Hossain (2016), in Kenya, large scale producers of pineapples namely; Delmonte (K) Limited based in Thika, Kakuzi limited based in Murang'a and Ndemo farm based in Kilgoris contribute close to 90% of all pineapples grown in Kenya. Other medium and small-scale producers account for about 10% of the total pineapple production. The increasing demand for pineapples with the ever growing human population consequently results into an increase in the amount of waste generated. Approximately 80% of pineapple parts (crown, peels, leaves, core and stems) are discarded during pineapple processing, transportations and storage and ends as waste (Hikal et al., 2021). The conventional techniques commonly applied in managing peel residues has been disposal to landfill, composting, and incineration. However, these traditional approaches are increasingly raising environmental concerns such as emission of methane gas from landfilling and discharge of toxic compounds like dioxin from incineration (Sial et al., 2019). Composting has also been reported to result in release of foul odour thereby affecting air quality (Bu et al., 2014). Conversion of pineapple peels into biochar for use as adsorbents is an approach that is currently being explored(Lam et al., 2018; Sial et al., 2019). Among the adsorption studies commonly reported for biochar is on organic contaminants (Fu et al., 2016; Zhou et al., 2015), heavy metals (Wang et al., 2016), and dyes (Foo & Hameed, 2012). Despite this, the application of pineapple peel biochar (PPB) for nutrient recovery from aqueous solutions is rather scarce with the very recent report (Hu et al., 2020) on its use for NH_4^+-N recovery from wastewater exhibiting an adsorption capacity of 5 mg/g. This value is significantly lower than those reported for other biochars. This variation could be attributed to factors such as the initial concentrations of adsorbate, and physicochemical characteristics of the adsorbents. Consequently, human urine whose pH is unaltered with addition of alkaline solutions

such as NaOH becomes an interesting solution to determine the adsorption capacity of the PPB.

2.7 Lateritic soil and its Application as an Adsorbent

Lateritic soil (LS) are commonly found in the tropical climatic regions and are formed as a result of chemical weathering of pre-existing soils such as granite, sandstone, shale and quartzite (Ehujuo et al., 2017). Due to humid conditions in the tropics, these soils are excessively leached making them nutrient deficient and unsuitable for crop production and thus majorly used in construction industry (Ehujuo et al., 2017; Ng et al., 2019; Stoops & Marcelino, 2018). These soils are highly rich in metal oxides of Fe and Al with the Fe2O3 content responsible for the characteristic reddish brown coloration (Stoops & Marcelino, 2018). Most of the studies on the use of LS for adsorption have mainly focused on the removal of fluorides (Osei et al., 2016; Sarkar et al., 2006), and heavy metals (Glocheux et al., 2013; Mitra et al., 2016) from water or wastewaters. Exploring its capacity for adsorption of nutrients could provide an insight into its suitability for producing slow release fertilizer and its surface properties. An investigation on its application for the removal of PO_4^{3-} from wastewater is very recent (Bhattacharjee et al., 2021). The concentrations of PO_4^{3-} in human urine are orders of magnitude greater than in the domestic wastewater (Maurer et al., 2006a), and so determining the LS adsorption capacity in natural human urine would be important to optimize its use for the removal of phosphorous. Its application for NH_4^+-N adsorption have however not been reported.

2.8 Human Faeces

Human faeces is composed of undigested materials that pass through the intestines, usually mixed with extracts from the blood stream, mucus and bile from the glands and the intestines impacting the characteristic brown colour (Rose et al., 2015).

2.8.1 Generation Rate

The amount of faeces produced by a person depends on the composition of the food consumed with higher fiber intake resulting to significant increase in faecal weight (Chen et al., 1998). The faecal production in the developed countries is approximately 80-140 g/p/d (wet weight) of faeces (Vinnerås et al., 2006). Faecal excretion rate in the developing countries is on average 350 g/p/d in rural areas and 250 g/p/d in urban areas, giving a range of 250-350g/p/day (Feachem et al., 1984).

2.8.2 Composition

The biological and physicochemical characteristics of human faeces vary depending on individual's health and diet. Generally, faecal solids are composed of proteins, fats, fibre, bacterial biomass, inorganic materials and carbohydrates. In terms of nutrient composition, it contains 10 – 20% nitrogen (N), 20 – 50% phosphorus (P) and 10 – 20% potassium (K) (Vinnerås et al., 2006). It has also been reported that human faeces may contain heavy metals (Yabe et al., 2018) and pathogens (WHO, 2006) that may pose health risk if faeces is discharged untreated into the environment. Faeces pH ranges between 5.3 and 7.5, with biological oxygen demand (BOD) ranging between 14 and 33.5 g/cap/day and chemical oxygen demand (COD) between 46 and 96 g/cap/day (Rose et al., 2015).

2.8.3 Human Faeces as a Source of Solid Fuel

Resource recovery from human excreta is currently considered as a sustainable way of managing the waste. Treated human faeces have traditionally been used in agriculture selectively. However it has been reported that its use as a source of energy in developing countries is more marketable (Diener et al., 2014), a venture that could offset the cost of maintaining the sanitation facilities as well as reduce the cost met by households for desludging the filled up faecal containment facilities. Several studies have been conducted to assess the suitability of dried human faeces as a source of fuel with results

depicting that they have calorific values ranging from 19 – 25 MJ/kg (Onabanjo et al., 2016; Afolabi et al., 2017; Somorin et al., 2020) which is comparable to that of wood fuel (Ruiz-Aquino et al., 2019).

In order to render human faeces safe for handling, pyrolyzing the waste at temperatures > 300 ^{o}C can lead to complete elimination of pathogens (Atwijukye et al., 2018). Pyrolysis, which is the decomposition of a feedstock through heating in the absence of oxygen, is highly affected by a variety of parameters such as heating rate, temperature, gas flow rate, biomass composition, residence time, moisture content, and particle size (Mishra & Mohanty, 2018). During pyrolysis, dried human faeces are heated under inert conditions to yield a charcoal-like material called biochar. For solid fuel production, the char is then densified by moistening with binders such as starch, and molasses. Other advantages of pyrolysis is that it minimizes oxygen containing functional groups, while also increasing the aromatic carbon content, which in turn lessens the emission of CO_2 and smoke (C. He et al., 2013). However, this process also lowers the calorific values of human faeces due to the degradation of energy rich aliphatic hydrocarbons with increasing pyrolysis temperature (Ward et al., 2014). Despite this feature, the gross calorific values of human faeces pyrolyzed between 300 ^{o}C and 450 ^{o}C are within 18 – 26 MJ/kg (Ward et al., 2014), a range comparable to 19 – 25 MJ/kg of wood fuel (Ruiz-Aquino et al., 2019). The calorific values of wood biomass are known to increase with pyrolysis temperature due to an increase in their fixed carbon content (Bonelli et al., 2003; Bulmau et al., 2010). Thus, pyrolyzed human faeces and other waste streams such as sawdust char could be blended to improve the calorific values (Atwijukye et al., 2018). In Kenya, sanitation entrepreneurs like Sanivation company limited (www.sanivation.com) have ventured into the large scale production of solid fuels (briquettes) from human faeces collected in dry toilets for domestic use.

2.9 Application of Sawdust Biochar for Solid Fuel Production

Biomass conversion to different forms of bioenergy has recently attracted the attention of scientific community, policy makers, and industry advocates as a way of meeting the escalating energy demands with minimal carbon footprint (Reid et al., 2020). The sustainability of bioenergy production from biomass is definitely dependent on the availability of the raw materials. Thus, seeking sustainable biomass sources for energy generation which simultaneously provide an additional benefit of environmental protection against degradation could be an attractive approach. Sawdust, a woody biomass residue generated from sawmilling activities by wood-based industries, is widely abundant in developing countries and have potential to replace energy sources such as firewood in meeting domestic energy needs (Elehinafe et al., 2017). However, only a small proportion of the residues are used as fuel because of their high moisture and low energy density (Njenga et al., 2013). It has been demonstrated that the calorific values of wood biomass such as sawdust increases with pyrolysis temperature due to an increase in their fixed carbon content (He et al., 2018). Carbonization could therefore overcome the drawbacks of using uncarbonized sawdust as a fuel source. Additionally, carbonized sawdust hereon referred to as sawdust char, could be a suitable material to blend with faecal char to improve their calorific values.

2.10 Solid Fuel Production Process

Biomass briquettes can be defined as compressed blocks of organic wastes aimed at producing heat for domestic and industrial applications. The general process followed in the production of fuel briquettes are; drying the raw materials, grinding, mixing, densification, drying, packaging, storage and use. The briquettes can be made solely from one particular organic waste such as faecal sludge (Muspratt et al., 2014) or a mixture of different wastes to improve calorific value and compressive strength (Supatata et al., 2013). The dry material can either be carbonized by pyrolysis to produce carbonized briquettes or it can be used to produce uncarbonized briquettes. In the case of carbonized briquettes, the char are ground into smaller and uniform sizes and the

processed raw material is then mixed with binder before briquetting (Ward et al., 2014). However, if densification pressure is adequate, no extra binder is added (Ngusale et al., 2014). Uncarbonized material on the other hand is compressed at low pressure when mixed with binder whereas high compaction pressure and high temperature are required in the absence of binder for adequate bonding (Asamoah et al., 2016).

2.11 Factors Affecting Briquette Quality

For briquettes to compete effectively with other sources of fuel, then its calorific value, emission levels and ease of transportation and handling are of vital consideration. Reviewed literature indicates that among the critical factors that affect the quality of briquettes during production are geometry, compaction pressure, binders, particle size and moisture.

2.11.1 Effect of Geometry of Briquettes

The shape of the briquettes depends on the discretion of the producers. However it has been demonstrated that shape has an effect on the combustion (ignition and burning time) properties of briquettes. Kabok et al. (2018) demonstrated that ignition time which is the average time required to ignite the composite briquettes was significantly influenced by the surface area of the briquettes exposed to the airflow. The study observed that the spherical briquettes with higher surface area had the shortest ignition time than cylindrical and triangular briquettes. However, the burning time which is the duration taken to bring a certain amount of water to boiling was insignificantly influenced by the shape of briquettes. This could be attributed to the fact that the calorific value of the fuel was the same since the briquettes were of the same materials.

2.11.2 Effect of Compaction Pressure/Density

The compaction pressure is usually exerted using a briquetting machine which can either be a screw or a piston press (mechanical or hydraulic). Compression not only helps in preventing the briquettes from crumbling (Ugwu, 2013) but also increases briquette

density which consequently decreases porosity making it burn longer (Ufot, 2013). Studies on the effect of compression pressure on heating values of briquettes shows that higher compression pressures (50 – 150 Mpa) does not significantly influence the calorific values (Tanui et al., 2018). Mambo (2016) using lower compression pressures (2 – 8 MPa) to produce briquettes from carbonized maize cobs, observed that the briquettes produced could withstand crumbling during handling and transportation, however the author recommended 8 Mpa as the best compression pressure. The findings suggest that focus should be on producing quality briquettes at low pressures to minimize energy consumption during production process.

2.11.3 Effect of Binders

Binders are sticking or agglomerating materials that are mixed with biomass material that lacks plasticity and densified to form strong briquettes. The quality and quantity of binders used is of key consideration in the production process since they affect the strength, thermal stability, combustion performance and cost of briquette (Altun et al., 2001). Generally, the desirable properties of briquette binder is that they should form a strong bond, be pollution free, have no effect on the heat released and combustibility of the biomass materials, environmentally acceptable and economically available (Githeko., 2013; Habib et al., 2014; Ngusale et al., 2014; Zhang et al., 2018). According to Zhang et al. (2018), briquette binders can be divided into three types based on the difference of their material composition, namely; (a) organic binder, (b) inorganic binder, and (c) compound binder.

2.11.3.1 Inorganic Binder

Clay, lime, plaster, cement, and sodium silicate are common types of inorganic briquette binders (Altun et al., 2001; Njenga et al., 2013). These binders have many excellent advantages, such as good thermal stability, strong adhesion, low pollution level, low-cost, good sulphur retention, and good hydrophilicity while the disadvantages

exhibited are high ash content, low gross calorific value and poor water repellency/ proofing (Zhang et al., 2018).

2.11.3.2 Organic Binder

Briquettes bonded with organic binders have high crushing strength thus durable, lower ignition temperature, high heating values and emit less smoke (Ngusale et al., 2014; Kabok et al., 2018; Aransiola et al., 2019). However, organic binders are reported to decompose easily at high temperatures, some are costly, in addition to possessing poor water repellency and poor thermal stability (Altun et al., 2001; Zhang et al., 2018). Among the commonly used organic binders for briquetting in developing countries are starch sources (cassava flour, wheat flour, potato starch, rice flour, corn starch, and maize flour), gum arabica, waste papers, and molasses (Njenga et al., 2013; Ngusale et al., 2014). However, the challenge of using starch sources is that they could create competition with food for human consumption and therefore making the entire process unsustainable.

2.11.3.2.1 Molasses Binder

Molasses is a heavy, viscous dark brown liquid produced as a by-product of sugar extraction and are widely used for ethanol production and animal nutrition (Palmonari et al., 2020; Dirbeba et al., 2021). There has been a growing trend of using molasses as a binder in briquette production due to its properties that enhances the combustion properties of fuels such as increasing volatile matter content, calorific values and ability to agglomerate particle of low plasticity (Altun et al., 2001; Ward et al., 2014; Tanui et al., 2018). Most studies have often reported on the chemical composition of molasses with results indicating that they are mainly composed of sucrose, water, reducing sugars (glucose and fructose) ashes and other organic compounds (Palmonari et al., 2020). However, there has been a recent study by Dirbeba et al. (2021) that has reported on the proximate parameters and heating values of cane molasses with results indicating that they have ash content of 19 wt. %, volatile matter of 28 wt. %, fixed carbon of 53 wt.

% , and higher heating value of 15 MJ/kg. Despite the potential of molasses in improving the physical and combustion properties of briquettes, it has been reported that the fructose content in molasses is highly hygroscopic (Davis, 1995). The hygroscopic property of molasses could result in high moisture content in briquettes densified with molasses consequently making their ignition difficult. Hence further research on alternative organic binders is necessary. Studies using molasses as a binder have reported that 10% of molasses by weight can produce durable briquettes of higher heating values than fuel wood (Githeko., 2013; Habib et al., 2014; Kabok et al., 2018; Tanui et al., 2018).

2.11.3.3 Compound Binder

There are advantages and disadvantages associated with both organic and inorganic binders. For instance, briquettes produced with inorganic binders are more thermally stable than those produced with organic binders. However, the briquettes produced with compound binders have low heating values, low combustion efficiency and high ash content compared to briquettes produced with organic binders. The concept of compound binder involves mixing two or more binders to combine all advantages of different kind of binders (Zhang et al., 2018). Examples of these binders include, cements (85% – 90%), hydrated lime (5% – 10%), polyvinyl alcohol (5% – 10%), coal tar pitch phenolic resins, and corn straw (70%), sodium hydroxide (7%), and MgCl/MgO (23%) (Zhang et al., 2018).

2.11.4 Effect of Particle Size

The particle sizes of the raw materials densified to form briquettes affect their physical and thermal properties. Studies have reported that increase in particle size of constituent materials increases calorific value, reduces ash content and increases thermal efficiency (Davies, 2013; Tokan et al., 2014; Mambo, 2016). Thus, medium sized particles should be used in briquetting.

2.11.5 Effect of Moisture

During densification of briquettes, moisture enhances bonding however minimal amounts should be maintained since increases in moisture content reduces combustion efficiency (Grover & Mishra, 1996). Hence, the raw material/ feedstock should be dried to moisture content within a range of 10% to 15% for ease of combustion (Grover & Mishra, 1996).

2.12 Higher Heating Value , Proximate and Ultimate Analysis of Briquettes

2.12.1 Higher Heating Value

Heating value of fuel can be defined as the amount of heat produced by complete combustion of fuel and it is measured as a unit of energy per unit mass or volume of substance (Xu & Yuan, 2015). It is normally expressed by the higher (gross calorific value) and lower heating values. The higher heating value (gross calorific value) is measured experimentally using a bomb calorimeter. Uzun et al. (2017) defines higher heating value of fuel as equal to the amount of heat released when a unit mass of the fuel is burnt completely, accounting for the enthalpy of condensation of liquid water as a combustion product under standard conditions. That is, the heat of condensation of the water is included in the total measured heat.

2.12.2 Proximate Analysis

The proximate analysis serves as a simple means for determining the behaviour of a solid biomass fuel when it is heated. It determines the contents of moisture, volatile matter, ash and fixed carbon of the fuel (ASTM, 1984). The proximate parameters provide the potential efficiency and durability of the briquettes that will be produced as discussed in the following sub sections.

2.12.2.1 Fixed Carbon

Fixed carbon is the solid combustible carbon that remains in the pyrolyzed material after volatile matter is released. Briquettes made of materials with higher fixed carbon content therefore combust and release heat energy for a longer time and have higher heating values (Falemara et al., 2018).

2.12.2.2 Volatile Matter

Volatile matter refers to the non-water gases formed from the thermal degradation of a material. Materials with higher volatile content ignite faster at lower temperatures and release higher amount of heat due to higher oxygen consumption rates (Sha et al., 2021).

2.12.2.3 Ash Content

Ash is a powdery residue consisting of incombustible materials that remains after complete burning of a material. Materials with high ash content have lower heating value since the portion of heat liberated is also absorbed by the incombustible fraction (Tokan et al., 2014; Ward et al., 2014; Hafford et al., 2018). In addition, higher ash content will result in ash slagging which inhibits the combustion process by supporting overheating of the burning device and subsequently its corrosion (Asamoah et al., 2016). Therefore, optimum ash content in feedstock is needed to control the burning process and to maintain the machine parts.

2.12.2.4 Moisture Content

Higher moisture content in feedstock may increase the production cost in terms of energy, due to the fact that more energy is required to reduce the water content during drying and densification. Biochar however have lower moisture content and only little moisture is required to assist the bonding process of the feedstock. Higher moisture content in briquettes reduces their heating value (Yank et al., 2016).

2.12.3 Ultimate Analysis

The main purpose of ultimate analysis is to determine the elemental composition (Carbon, Hydrogen, Nitrogen, Sulphur and Oxygen) of a solid biomass fuel (Ceylan & Sungur, 2020). Its determination is relatively time consuming and expensive compared to proximate analysis. Carbon and Hydrogen content has been shown to increase the heating value of fuel while oxygen content reduces heating value (Avelar et al., 2016). Higher Nitrogen and Sulphur on the other hand significantly contributes to NO_x and SO_x pollutants respectively (Parikh et al., 2007). The percentage of Carbon, Hydrogen, Nitrogen, and Sulphur on dry basis can be determined using an elemental analyser while the Oxygen content is determined by the difference (Equation 2.23).

Oxygen (%) = 100 - Carbon (% Dry Basis) - Hydrogen (% Dry Basis) - Nitrogen (% Dry Basis) -Sulphur (% Dry Basis) (2.23)

2.13 Toxic Air Emissions from Combustion of Biomass

A flue gas emission from biomass combustion refers to the gas product resulting from burning of biomass solid fuel (Pilusa et al., 2013). Combustion of biomass normally releases gases which can pose health hazard to humans depending on their inherent toxicity and duration of exposure. A good fuel should therefore emit gases below the threshold limit value as recommended by the occupational safety and health administration (OSHA). OSHA (2010) defines threshold limit value as the upper permissible concentration limit of the gases believed to be safe for humans even with an exposure of 8 hours per day, 5 days per week over a period of many years. OSHA limits are based on industrial settings, however, short term exposure limits for various toxic gases which is applicable for domestic settings are also defined by organizations such as WHO, Environmental Protection Agencies (EPA), and National Institute for Occupational Safety and Health (NIOSH) (Schieb, 1976; WHO, 1981; EPA, 2002). Among the critical emissions of concern to human health are the carbon monoxide (CO), hydrogen sulphide (H_2S), and nitric oxide (NO).

CO_2 is produced as a result of complete combustion of biomass and therefore regarded harmless to human health , while CO emission results from incomplete combustion (Obernberger et al., 2006). Inhalation of CO even for shorter exposure period (< 1 hr) can cause disastrous health effects such as limited oxygen supply in the blood, fatigue, headache and sudden death (Townsend & Maynard, 2002). Fuels emitting CO concentrations above the critical limit of 35 ppm allowed for human exposure for one hour are normally considered unsafe for indoor heating (EPA, 2002). Proper ventilation is thus necessary to enhance oxidation of carbon during biomass combustion.

Hydrogen sulphide (H_2S) gas is among the common hazardous substances whose concentrations at elevated levels (1000 – 2000 ppm) can lead to immediate death (Frame & Schandl, 2015). It has a characteristic offensive odour (rotten eggs) which makes it to be easily detected at very low concentrations by sense of smell. Many countries have short term exposure limits for ambient H_2S with the WHO recommending its concentrations not to exceed 0.005 ppm within 30 minute exposure time in order to avoid substantial complaints about odour annoyance (WHO, 1981). Very short lived peak concentrations have also been reported to cause discomfort (Collins & Lewis, 2000). Also, Bhambhani and Singh (1991) reported that exposure of human population to 2.5 – 5 ppm of H_2S after 15 minutes resulted to coughs, throat irritation and impaired oxygen uptake in the blood. It is worth noting that the corrosive nature of H_2S (Malone Rubright et al., 2017) may also pose challenge by corroding metal wares.

The most important oxides of nitrogen that are considered air pollutants are nitric oxide (NO) and nitrogen dioxide (NO_2) (EPA, 1971). NO is a colourless and odourless gas which is readily oxidised in the atmosphere to form NO_2 which is a reddish-brown gas with a characteristic pungent smell and is more toxic (EPA, 1971; Ku, 1991). NO is classified as a respiratory irritant with inhalation being the main route of exposure, however eye and skin irritation also occurs if one is exposed to NO (Ku, 1991). Although little scientific data is available regarding exposure to NO compared to NO_2, its concentration above 100 ppm is considered dangerous to life or health according to

National Institute for Occupational Safety and Health (NIOSH) (Schieb, 1976). Monitoring emission of these gases from combustion of the briquettes will give useful information regarding their safety for indoor household use.

2.14 Thermogravimetric and Kinetic Analysis

Thermogravimetric analysis (TGA) has often been employed in kinetic modelling of the thermal degradation of biomass-type wastes. This technique determines the thermal stability of materials by monitoring the change of weight that occurs as a sample is heated. For example, the thermal behavior of various biomass sources have been studied including, rice husks, corn residues, and sawdust (Sittisun et al., 2015; Lim et al., 2016; Mishra & Mohanty, 2018). The information gained from thermal degradation can also be used in conducting kinetic analysis to determine the activation energy of the material (Sittisun et al., 2015; Lim et al., 2016; Mishra & Mohanty, 2018). That is, the experimental data from TGA is routinely fitted to different reaction models and the one that offers the best fit chosen to be the best that describes the kinetics of the process. Two approaches that can be used to adequately describe the kinetics of a given reaction process under both isothermal and non-isothermal conditions are; model-fitting kinetics and model-free (iso-conversional) kinetics (Vyazovkin & Wight, 1998). The model-fitting method is based on a single heating rate and therefore not able to account for multiple reaction steps. This is a disadvantage because the activation energy varies with the heating rate, due to mass and heat transfer effects. The model-free or iso-conversional method on the other hand uses multiple heating rates allowing for a change in mechanism during reactions hence accounting for multiple reaction steps. The iso-conversional method is used to estimate the activation energy independent of the reaction mechanism, with no prior assumptions about the analytical form of $f(\alpha)$. Model-free methods are thus recommended by the ICTAC Kinetics Committee due to the mentioned advantages (Vyazovkin et al., 2011). Kinetic data are of major interest in the technological development of processes related to energy production (pyrolysis, gasification, and combustion). Most studies on TGA of biomass materials have been performed under different heating rates, and under different reaction atmospheres (e.g.,

nitrogen, oxygen, and air) (Farrow et al., 2013; Lim et al., 2016; Yacob et al., 2018) leading to different thermal behaviors. For example, Ma et al. (2018) has demonstrated that palm kernel shell loses more weight under air (~95.22%) than under nitrogen flow (~72.39%). Zhang et al. (2019) reported that cattle manure exhibited lower activation energy when combusted under oxy-fuel atmosphere (CO_2/O_2) than under air conditions (N_2/O_2). Similar studies on human faeces (Somorin et al., 2020; Yacob et al., 2018) are available in the literature albeit with variations, especially on how blending affects their thermal decomposition properties and kinetic behaviour. For instance, when human faeces is blended with wood biomass in different ratios, the thermal behaviour of the blend markedly vary with the wood biomass content as explained by Fidalgo et al. (2019). Conversely, Somorin et al. (2020), acknowledged that regardless of the wood biomass content, blended samples exhibited similar thermal decomposition profile to that of human faeces. Additionally, Somorin et al. (2020), and Yacob et al. (2018) found activation energy values for human faeces to be between 122 – 382 kJ/mol, and 141 – 409 kJ/mol, respectively, for the same degree of conversion (10 – 90 %). The combustion properties of these biowastes vary depending on factors such as the composition, nature, particle size, moisture, and the volatile content. Although the reported studies have focused on the thermal behaviour and kinetics of dried human faeces under nitrogen atmospheres, investigating the behaviours of these materials after pyrolysis is important since the practice of solid fuel production from faeces is based on densification of charred faeces which is considered pathogen free. Moreover, studying their combustion characteristics under air conditions depicts the practical properties of these materials.

2.15 Summary of Related Literature Reviewed

The summary of related literature reviewed presented in Table 2.2 highlights the potential of biochars such as pineapple peel biochars and geological materials such as lateritic soil in adsorbing nutrients from human urine and the capability of response surface methodology in accurately predicting the optimum conditions for achieving maximum adsorption of nutrients from aqueous solutions. The summary also delved into

the factors affecting thermal stability of biomass materials and the suitability of model-free kinetic analysis methods over model-fitting kinetic analysis methods in determining activation energies of materials. The short-term limits of exposure to carbon monoxide (CO), nitric oxide (NO) and hydrogen sulphide (H_2S) applicable for domestic settings are also highlighted.

Table 2.2: Summary of Related Literature Reviewed

S/No	Objectives	Cited Literature	Remarks
1	Determining the ammonium nitrogen and phosphorous adsorption behaviours and capacities of pineapple peel biochar and lateritic soil from human urine	(Maurer et al., 2006; Ali et al., 2012; De Gisi et al., 2016 Alhashimi & Aktas, 2017; Ayawei et al., 2017)	• Human urine is an abundant rich source of nitrogen and phosphorous • Adsorption technology is less costly, flexible, efficient and environmentally friendly • Adsorption isotherms can describe the adsorption behaviours and enable calculation of the adsorption capacities of the adsorbents • Biochars and geological materials are effective and low-cost adsorbents
2	Optimising the ammonium nitrogen and phosphorous adsorption on pineapple peel biochar and lateritic soil from human urine.	(Myers et al., 2004; Bezerra et al., 2008 Trinh & Kang, 2011; Dutta et al., 2018)	• Response Surface Metho-dology (RSM) is a reliable technique for determining optimal conditions of factors that influence adsorption process so as to achieve maximum adsorption or removal of ions or molecules from aqueous phase • Central Composite Circum-scribed Design (CCCD) in RSM is most preferred because it uses a relatively small number of observations to effectively estimate the model parameters
3	Determining the thermal degradation and kinetic behaviours of pyrolyzed human faeces, sawdust char and their blend.	(Vyazovkin et al., 2011; Farrow et al., 2013; Lim et al., 2016; Mishra & Mohanty, 2018; Yacob et al., 2018)	• The thermal degradation behaviours of biomass materials varies with the heating rates, reaction atmospheres (nitrogen, oxygen, and air) and material properties • Blending of pyrolyzed human faeces with biochar from woody biomass materials such as sawdust is recommended since pyrolysis lowers calorific value of human faeces • Biomass materials with lower activation energies undergo ignition at lower temperatures • Model-free kinetic analysis methods are preferred over model-fitting methods since they use multiple heating rates hence accounting for multiple reaction steps
4	Evaluating the emission properties of briquettes densified from pyrolyzed human faeces, sawdust char and molasses	(Schieb,1976; WHO, 1981; EPA, 2002; Ward et al., 2014)	• Combustion of biomass fuels releases gases which can pose health hazard to humans depending on their inherent composition and duration of exposure • Short-term exposure limits applicable in domestic settings for CO is 35 ppm, NO is 100 ppm, and H_2S is 0.005ppm

2.16 Research Gap

Despite the progress made in adsorption technology for recovery of nutrients from wastewater using low cost adsorbents, the potential of pineapple peel biochars and lateritic soils for nutrients recovery from human urine haven't been reported despite the wide availability. Intricate studies on how the physicochemical properties of the pineapple peel biochars and lateritic soils influence adsorption process and how their surfaces interact with the NH_4^+-N and P in human urine gave an insight on their potential applicability for large scale recovery of these nutrients from human urine. Moreover, estimating their NH_4^+-N and P adsorption capacities from human urine will enable their optimal use for producing enriched slow-release fertilizers or medium for crop growth. Also, although the concept of briquettes production from human faecal chars blended with sawdust char has been reported (Kabok et al., 2018), investigations on the thermal decomposition characteristics and reaction rates of faecal char and their blend with sawdust char under air atmospheres haven't been reported. Hence this study reveals the practical thermal stability and reaction rates of faecal char and their blend with sawdust char when used as energy source for household cooking. Moreover, studies on emission of toxic gases during combustion of briquettes containing faecal char have not been reported by previous studies and this study therefore adds vital information that depicts the safety of the briquettes for indoor household cooking and heating.

2.17 Conceptual Framework

Conceptual framework is a model that employs the use of drawing or diagram to explain the interrelationships between the independent and dependent variables. The conceptual framework for this study can be represented as shown in Figure 2.1

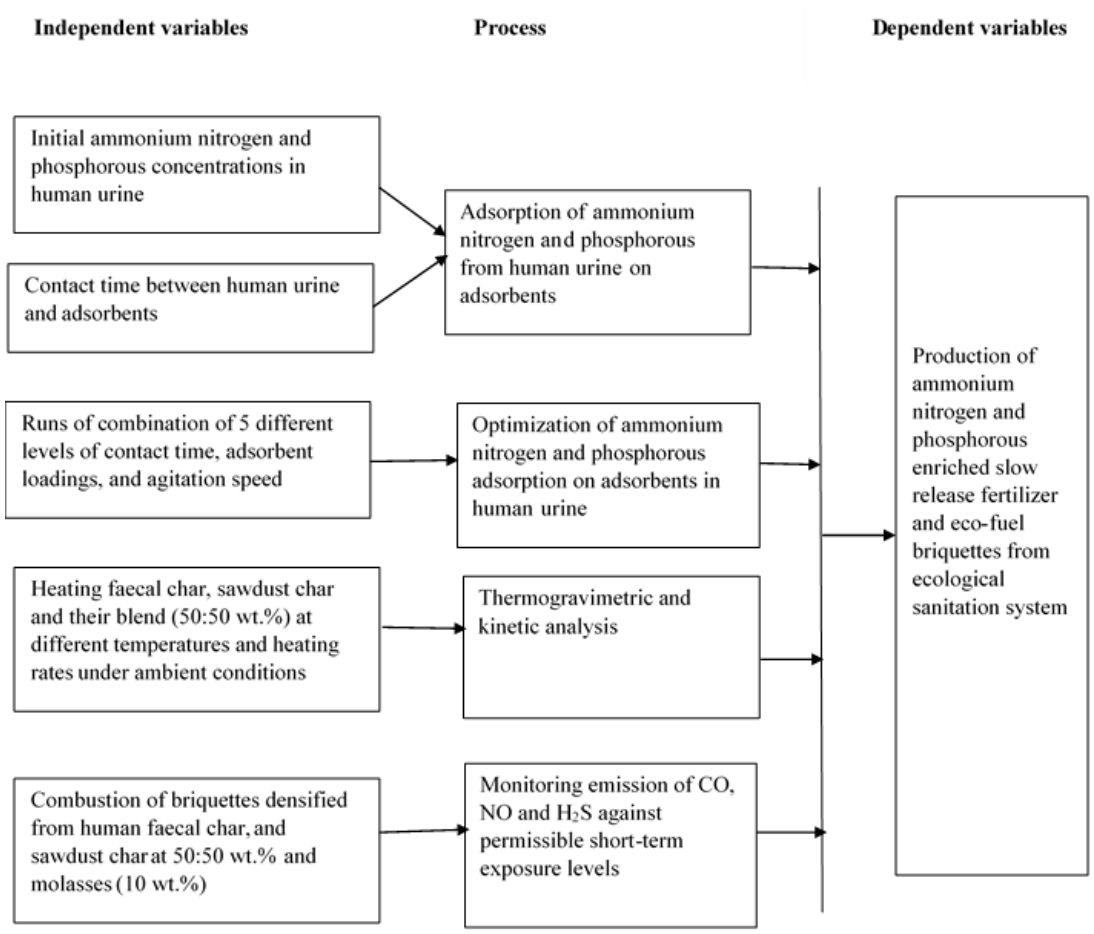

Figure 2.1: Conceptual Framework of the Study Variables

CHAPTER THREE

MATERIALS AND METHODS

3.1 Determining the Behaviour and Capacity of Pineapple Peel Biochar and Lateritic Soil in Adsorbing Ammonium Nitrogen and Phosphorous from Human Urine

3.1.1 Materials Preparation

Fresh undiluted urine was collected from volunteers and used directly without further purification. Fresh pineapple peels were collected from vendors, dried in a greenhouse for 48 hours and then carbonized at 400 °C under vacuum for 4 hours. The resulting char was crushed and particles with ≤ 300 μm sieved with 300 micron stainless steel sieve. The powder was then kept in an air tight plastic container for further analysis. Lateritic soil was excavated 20 cm from the ground surface, and impurities such as leaves and roots removed. The soil was then dried in an oven at 104 ±1 °C for 24 h under vacuum. The dried soil was then crushed, sieved to ≤ 300 μm and kept in an airtight plastic container for further studies.

3.1.2 Materials Characterization

Thermogravimetric Analysis (TGA) of pineapple peel biochar and lateritic soil was performed on a TGAQ500 thermogravimetric analyzer (TA instruments, USA) from 30 to 800°C at a heating rate of 5°C/min under flowing N_2. FTIR spectra were obtained using a Spectrum One attenuated total reflection (ATR)-FTIR spectrometer. Spectra for each run were averaged over 40 scans at a 4 cm^{-1} resolution in the range 4000 – 650 cm^{-1}. X-ray powder diffraction (XRD) patterns were recorded at room temperature on a Bruker AXS D8 Advance X-ray diffractometer using CuK_α radiation (λ = 1.54056 Å) operating at 45 kV, and 40 mA in the 2θ scan range of 5 – 90° with a step size of 0.009° and a total measuring time of 3 hours. The pH of lateritic soil (LS) and pineapple peel biochar (PPB) were determined by shaking 500 mg of sample powders with 20 mL

deionized (DI) water for 30 min. The samples were let to settle for 1 hour before recording the pH using a pH electrode Seven Compact pH meter S220 (Mettler Toledo, Switzerland). The Brunauer-Emmett–Teller (BET) surface area, pore volume, and pore size distribution of the samples were analyzed using a Micromeritics ASAP 2020 analyzer. Prior to the measurements, samples (200 – 400 mg) were degassed under vacuum at 150°C overnight to eliminate moisture before N_2 adsorption. The surface areas of the samples were calculated by the BET method in relative pressure (p/p^0) range of 0.05 – 0.30 at 77 K. The morphological and elemental mapping studies were performed by a LEO-1530 scanning electron microscope (SEM) equipped with an Oxford AZtec energy dispersive spectrometer (EDS).

3.1.3 Batch Adsorption and Ammonium Nitrogen and Phosphorous Determination

3.1.3.1 Batch Adsorption Studies

Nutrient removal ability of lateritic soil (LS) and pineapple peel biochar (PPB) was evaluated using parallel experiments. Dilution of urine to obtain six varying concentrations of the solute (NH_4^+-N and P) was done using DI water. 0.2 g of LS and PPB were separately added to 25 mL of urine in a beaker at 21 °C, and the solution shaken in a thermostatic mechanical shaker (Heidolph unimax orbital shaker 2010, Germany) at a rate of 100 rpm. Samples were filtered using Whatman filter paper no. 42 to separate the adsorbents from the urine at time intervals of 30, 60, 90, 120 min. The control samples consisted of human urine with no adsorbent added. The NH_4^+-N and P levels in the filtrates were measured for all the treated samples and control samples. Equation 3.1 was used in calculating the amount of nutrients adsorbed at various time intervals, q_t, until the equilibrium concentration, C_e, was reached.

$$q_t = \frac{(C_o - C_t)V}{W} \tag{3.1}$$

Where:

C_o = the concentrations of solute at the initial time (mg/L)

C_t = the concentrations of solute at a certain time t (mg/L)

V = the volume of urine (mL)

W = the mass of adsorbent (g)

3.1.3.2 Analytical Methods for Ammonium Nitrogen Determination

The NH_4^+-N concentration in urine samples was determined using Kjeldahl method ISO standard. Briefly, 2.5 mL of sample was put in a distillation glass tube, and the pH adjusted to 9.5 by 0.1M NaOH and 5 mL of borate buffer. 25 mL of 2% boric acid was then added to a separate beaker for collecting the distillate. As the distillation process continued, the volume of the distillate was monitored until it reached 125 mL upon which the distillation unit (Kjeltec 1002 System Distilling Unit, Sweden) was switched off. The pH of the collected sample was measured and 0.01M H_2SO_4 added until a pH of 5.1 was reached. The final volume titrated was used in calculating the NH_4^+-N concentration in the sample using Equation 3.2. Normally a blank sample (DI water) was also subjected to the same procedure to verify the accuracy of the method since DI water is theoretically expected to have no ions. This procedure was followed each day prior to analyzing urine samples. In case of any level of NH_4^+-N detected in the blank samples, it was subtracted from the values read in the urine samples according to Equation 3.2 given as:

$$c = (a-b) \times M \times 2 \times 14.007 \times 1000 / V \tag{3.2}$$

Where:

c = the NH_4^+-N concentration (mg/L),

a = the consumption of H_2SO_4 when titrating sample (mL),

b = the consumption of H_2SO_4 when titrating the blank (DI water) sample (mL),

M = the concentration of H_2SO_4 (mol/L),

14.007 = the molecular mass of nitrogen (g/mol),

V = the sample volume (mL).

3.1.3.3 Analytical Methods for Phosphorous Determination

Phosphorous in the samples was determined according to Finnish standards (SFS 3026) for determination of total phosphorous in water (SFS, 1986).

3.1.3.3.1 Preparation of Phosphorous Stock Solution and Working Standards

Phosphorous stock solution (50 mg/L P) was prepared by dissolving 0.2197 g of dry potassium di-hydrogen phosphate (KH_2PO_4) in deionized (DI) water. 10 mL of 4 M H_2SO_4 was then added and the solution diluted to a total volume of 1 L. Phosphorous working solution (1/50 dilution of the stock solution) was prepared by diluting 10 mL of the stock solution with DI water to a total volume of 500 mL.

3.1.3.3.2 Determining the Calibration Curve and Concentration Levels of Phosphate in Human Urine

The first step in the SFS 3026 method for determining phosphate concentrations was to develop the standard calibration curve using five working standards. In this method, calibration standards are prepared by pipetting different amounts (1, 2, 10, 25 and 75 mL) of phosphate working solution into 100 mL volumetric flasks. They are then acidified with 1.0 mL of 4.0 M H_2SO_4 and diluted with DI water to the 100 mL mark. The calibration solutions therefore contained 10, 20, 100, 250 and 750 µg/L of P. Blank or zero samples were also prepared by pipetting 10 mL of 4.0 M H_2SO_4 in 1000 mL

volumetric flask and then adding DI water to the 1000 mL mark. Each sample investigated was prepared in three replicates. 5 mL of potassium persulfate (5g $K_2S_2O_8$ per 100 mL DI water) solution was added into each bottle to transform phosphorous into phosphates. The bottles were autoclaved at 120 °C for 40 min to expedite the transformation process and then cooled to room temperature, 21±1 °C. 1 mL of each ascorbic acid ($C_6H_8O_6$) and ammonium molybdate $(NH_4)_6Mo_7O_{24}$) reagents were then added for color development. UV-Spectrophotometer (880 nm wavelength) was used to obtain the total P readings. The absorbance and concentration values of blank (zero) samples were read first followed by absorbance of the standards whose concentration had been predetermined in the experiment. The plot of absorbance against concentration of the blanks and the standards gave a calibration curve from which the P concentration of the samples of unknown concentration was calculated based on the absorbance readings obtained by the spectrophotometer.

For the human urine whose concentrations of P were unknown, 0.5 mL of urine samples from the original urine samples (control) and the adsorption experiment (filtrate) were pipetted into 500 mL volumetric flasks, acidified with 5 mL of 4M H_2SO_4 then topped with DI water to the 500 mL mark. 25 mL of each of the prepared samples were transferred into clean autoclave bottles. Subsequent procedures already described in this sub-section (addition of persulfate, autoclaving, color development) were then followed, and the absorbance reading obtained from the spectrophotometer used to calculate the concentration of the urine samples from the calibration curves.

3.2 Optimising the Adsorption of Ammonium Nitrogen and Phosphorous from Human Urine on Pineapple Peel Biochar and Lateritic Soil

3.2.1 Central Composite Circumscribed Experimental Design

Response Surface Methodology (RSM) was used to optimize NH_4^+-N and P adsorption on PPB and LS, respectively, and investigate the interactive effects of contact time, adsorbent loading and agitation speed on the adsorption process. The optimisation was

conducted using "Design-Expert® software, version 12, Stat-Ease, Inc., Minneapolis, MN, USA, www.statease.com". Central composite circumscribed design was used since it is the most effective in estimation of model parameters in addition to being rotatable. It consists of three critical points notably; factorial (2^k), axial (2k) and center points (six replicates), where k is the number of independent variables. Repetition of center points provides better estimate of pure error. The total number of experimental runs is the summation of factorial points, axial and the six center points. In this study, k = 3 (contact time, agitation speed and adsorbent loading) resulting into 8 factorial points and 6 axial points. The total experimental run (n) is the summation of factorial points, axial points and the centre points. Hence n = 8+6+6=20. The selected independent variables are coded according to Equation 3.3 given as:

$$x_i = \frac{X_i - X_o}{\Delta X} \tag{3.3}$$

Where:

x_i = the coded variable,

X_i = the un-coded value of the i^{th} independent variable,

X_o = the value of X_i at the center point of the investigation area,

ΔX = the step change.

Each variable was studied at 5 levels coded as -1.682, -1, 0, 1, +1.682, where (-1) is low level, (+1) is high level, (0) is the center point, ±1.682 are codes for points defined by the design expert software to be below and above the respective designated low and high levels in each factor studied. The parameters and levels for the experimental design used in this study are summarized and presented in Table 3.1.

Table 3.1: Parameters and Levels for the Experimental Design

Independent variable	Symbol	Coded factor levels				
		-1.682	-1	0	1	1.682
Contact time (min)	x_1	20	30	45	60	70
Agitation Speed(rpm)	x_2	39	80	140	200	241
Adsorbent loading(g)	x_3	0.03	0.1	0.2	0.3	0.37

3.2.2 Statistical Analysis

The RSM model correlates the dependent variables to the independent variables considered through second-order polynomial response equation given as in Equtaion 3.4

$$Y = \beta_o + \beta_1 x_1 + \beta_2 x_2 + \beta_3 x_3 + \beta_{12} x_1 x_2 + \beta_{13} x_1 x_3 + \beta_{23} x_2 x_3 + \beta_{11} x_1^2 + \beta_{22} x_2^2 + \beta_{33} x_3^2 + \varepsilon \quad (3.4)$$

Where:

Y = the predicted response

β_o = the value of the fixed response at the center point of the design

β_i, β_{ii},*and* β_{ij} = the linear, quadratic and interaction effect regression terms, respectively

ε = the random error

The analysis of variance (ANOVA) was conducted to study the significance of the quadratic model, while the value of the coefficient of determination (R^2) was used to determine the reliability of the quadratic model in fitting the experimental data and accurately predicting the output.

3.2.3 Graphical Plots and Numerical Optimisation

The 3D response surfaces were then drawn to visualize the individual and the interactive effects of the independent variables on the adsorption of phosphorous. The 3D plots are provided in the Figure D1, and E1 in Appendix IV, and V, respectively. To perform numerical optimization for the adsorption of NH_4^+-N and P on PPB and LS, respectively, the desirability function approach was followed. The desirability is a dimensionless entity that represents the closeness of a response to its ideal value and usually ranges from 0 to 1 with d = 0 being unacceptable, and d = 1 indicating that the model response is equal to that of the target value (Li et al., 2007; Myers et al., 2004). The RSM was set-up with the goal being to optimise adsorption so that the model could determine the values of the input variables that yield the highest adsorption capacity of NH_4^+-N and P on PPB and LS, respectively.

3.3 Determining the Thermal Degradation and Kinetic Behaviour of Pyrolyzed Human Faeces, Sawdust Char and their Blend

3.3.1 Sample Preparation and Characterization

Faecal matter was collected from a dry toilet and dried in a greenhouse under air for one week attaining constant moisture content. Sawdust was obtained from saw millers and similarly dried in a greenhouse for a week attaining constant moisture content. Both the dried human faeces and sawdust were then pyrolyzed in an electric muffle furnace FUW232PB (Toyo Seisakusho Kaisha, Ltd) at 350°C for 2 hours under a vacuum. The resulting char was crushed and particles with $\leq$ 300 μm sieved and stored in air tight plastic containers for further analysis. In addition, the two samples (pyrolyzed human faeces (hereon denoted as faecal char), and sawdust char) were blended in the weight ratio of 50:50 wt. %, hereon referred to as blend. Previous studies on production of briquettes from faecal char and sawdust char reported that equal weights (50:50 wt. %) produced briquettes of desirable heating values comparable to the fuel wood (Kabok et al., 2018; Atwijukye et al., 2018; Ward et al., 2014), and thus informed the ratio adopted

in this study. The morphological features of faecal char and sawdust char were observed using a LEO-1530 scanning electron microscope (SEM) operated at 1 kV. Fourier Transform Infrared (FTIR) Spectra of the samples were recorded on a spectrometer in the range 4000 – 650 cm^{-1}. An oxygen bomb calorimeter (Yoshinda 1013J) was used to determine the gross calorific values of the samples, while the proximate parameters (fixed carbon, volatile matter, moisture content, and ash content) were determined according to ASTM D1762-84 standard test method for chemical analysis of wood charcoal (American Society for Testing and Materials, 1984). Elemental analysis (C, H, N, and O) of faecal char and sawdust char was undertaken using Elemental Analyzer (AAS iCE 3300).

3.3.2 Thermogravimetric Analysis

The combustion characteristics and kinetic behavior of faecal char, sawdust char, and blend were investigated using a thermogravimetric analyzer (TA Instruments TGA-Q500) under non-isothermal conditions. For each TGA run, about 10 mg of sample was placed in an Aluminium crucible and heated from 30 to 800 °C under flowing air (60 mL/min), at heating rates of 5, 10, 20, and 40 °C/min. In addition, the effect of sample atmosphere on decomposition was also tested by running the three samples under N_2 at a heating rate of 5 °C/min.

3.3.3 Kinetic Methods

Kinetic analysis can give insights into the reaction mechanism of a given process. The rate of a chemical reaction $\frac{d\alpha}{dt}$ is described by the general kinetic rate equation as presented in Equation 3.5 given as:

$$\frac{d\alpha}{dt} = k(T).f(\alpha) \tag{3.5}$$

Where:

t = time

T = the absolute temperature

K= the rate constant

α = the conversion

The degree of conversion, $0 \leq \alpha \leq 1$, which is a measure of the extent of the reaction can be defined as in Equation 3.6

$$\alpha = \frac{m_o - m_t}{m_o - m_f} \tag{3.6}$$

Where:

m_o = the initial sample weight

m_t = the sample weight at time, t

m_f = the final sample weight

The rate constant is generally expressed by the Arrhenius equation (Equation 3.7)

$$k(T) = A \,.\, \exp\left(\frac{-E_a}{RT}\right) \tag{3.7}$$

Where:

A= the pre-exponential factor (/s),

E_a= the activation energy (kJ/mol),

T = the temperature (K),

R= the universal gas constant (8.314 J/mol·K).

Substituting the Arrhenius expression into Equation 3.5 gives the standard kinetic equation under isothermal or non-isothermal conditions shown in Equation 3.8

$$\frac{d\alpha}{dt} = \beta \frac{d\alpha}{dT} = A \,.\exp\left(\frac{-E_a}{RT}\right).\, f(\alpha) \tag{3.8}$$

Where:

β = the heating rate $\left(\frac{dT}{dt}\right)$(K time^{-1})

Integrated function of (3.8) yields Equation 3.9

$$g(\alpha) = \int_0^{\alpha} \frac{d\alpha}{f(\alpha)} = \frac{A}{\beta} \int_{T_0}^{T} \exp\left(\frac{-E_a}{RT}\right) dT \tag{3.9}$$

Where:

$g(\alpha)$ = the integral kinetic function or integral reaction model when its form is mathematically defined

In this study, the activation energies, E_a, were estimated using the iso-conversional methods of Kissinger-Akahira-Sunose (KAS) and Flynn-Wall-Ozawa (FWO).

3.3.3.1 Kissinger-Akahira-Sunose Method

The approximation of Equation 3.9 by Coats & Redfern (1964) give rise to the Equation 3.10 applied by the Kissinger-Akahira-Sunose method (KAS) (Kissinger, 1957; Akahira, T .; Sunose, 1971).

$$\ln\left(\frac{\beta}{T^2}\right) = \ln\left[\frac{A_\alpha \,.\, R}{E_\alpha \,.\, g(\alpha)}\right] - \frac{E_\alpha}{RT} \tag{3.10}$$

At a constant α, the apparent E_α can be estimated from the slope *(-Eα/R)* of the straight line obtained by plotting $ln(\beta/T^2)$ versus *1/T*.

3.3.3.2 Flynn-Wall-Ozawa Method

The Flynn-Wall-Ozawa (FWO) method is a model-free method developed by Flynn (1966) as well as Ozawa (1965). It uses Doyle's equation (Equation 3.11) for the approximation of the temperature integral in Equation 3.9 (Doyle, 1965).

$$\ln \beta = \ln \frac{AE_\alpha}{Rg(\alpha)} - 5.331 - 1.052 \frac{E_\alpha}{RT} \quad (3.11)$$

At a fixed value of α, plotting $ln\beta$ versus $1/T$ gave a straight line. The activation energy was determined from the slope $-1.052E\alpha/R$ over a series of α.

3.4 Evaluating Emission Properties of Briquettes Densified from Pyrolyzed Human Faeces, Sawdust Char and their Blend

3.4.1 Sample Collection

Human faeces was obtained from a dry toilet and dried in a greenhouse for 7 days attaining constant moisture content, while sawdust was obtained from saw millers and also dried in a greenhouse for 7 days attaining constant moisture content. The charcoal used in this study was produced in a tradition kiln as is the practice in African countries. The charcoal was from acacia tree of species (*Acacia nilotica)* which is among the preferred tree species for firewood in dryland areas in Kenya (Oduor et al., 2019). Molasses used as a binder originated from a sugar processing factory.

3.4.2 Sample Preparation and Characterization

Both the dried human faeces and sawdust were pyrolyzed in an electric muffle furnace FUW232PB (Toyo Seisakusho Kaisha, Ltd) at 350 °C for 2 hours under a vacuum. The resulting char was crushed and particles with ≤ 300 μm sieved and stored in air tight

plastic containers. Analysis of Elements (C, H, N, S, and O) of faecal char and sawdust char was undertaken using elemental analyzer (AAS iCE 3300).

3.4.3 Briquettes Production

An electronic weighing machine was used to obtain equal weights (450 g each) of both faecal char and sawdust char and then mixed homogeneously in 50:50 wt. % ratio. 100 g of cane molasses representing 10 wt. % of the overall weight was added to the charred samples and mixed homogeneously to stick the particles together. A cylindrical plastic mould of internal diameter 23 mm and height of 100 mm and a cylindrical wooden die of diameter 22 mm were used to compress the materials (15 g) fed into the mould upon application of 5 MPa pressure from a hydraulic press. With the applied pressure and the diameter of the dies, cylindrical briquettes of diameter 22mm and height of 60 mm were ejected from the mould and dried in an oven at 104 ±1°C for 24 hours to a constant weight.

3.4.4 Characterization of Briquettes and Charcoal

An oxygen bomb calorimeter (Yoshinda 1013J) was used to determine the gross calorific values of the produced briquettes, and charcoal, while the proximate parameters (fixed carbon, volatile matter, moisture content, and ash content) were determined according to ASTM D1762-84 standard test method for chemical analysis of wood charcoal (ASTM, 1984) as detailed in the following sections:

3.4.4.1 Moisture Content Determination

A sample of material was weighed and put in the oven at 104 ±1°C for 24 hours after which it was removed and weighed again. The difference in weight divided by the dry weight of the material gives the moisture content as per the gravimetric method.

3.4.4.2 Ash Content Determination

A specimen of the dry briquettes was ground, weighed and then placed in a crucible and heated gradually in furnace at controlled temperatures to about 600 °C. The sample was burned until all the carbon was consumed and the residual ash attained constant weight.

3.4.4.3 Volatile Matter Determination

1.0g of oven-dried specimen was weighed and then placed in platinum crucible with a tight- fitting lid and heated in a furnace at 930 – 970 °C for about 7 minutes while occasionally stirring with a wire. After cooling in a desiccator the weight of the residue was taken. The loss in weight was then recorded as the weight of volatile matter in the sample.

3.4.4.4 Fixed Carbon Determination

Fixed carbon was determined using the data previously obtained in the proximate analysis as shown in Equation 3.12:

$$\% FC = 100 - (\% Ash + \% VM) \quad (3.12)$$

Where:

FC = fixed carbon

VM = the volatile matter

3.4.5 Monitoring the Emission Levels in Combustion of Charcoal and Co-combustion of Charcoal with Faecal Char-Sawdust Char Briquettes

The concentration of CO, CO_2, H_2S and NO emitted from charcoal was measured by burning 450 g of the charcoal in a small-sized common energy saving cook stove called Kenya Ceramic Jiko (KCJ) as practiced by households. Co-combustion was done by

burning equal amount (225 g) of charcoal and briquettes in the cook stove which amounted to a total weight of 450 g of fuel filled in the cook stove. A conical shaped chimney/stack made of aluminium metal of 1.3 m height was fabricated such that the larger diameter could fit the top of the cook stove to minimise escape of gases before sampling, while the top of the chimney was left open to allow gases to escape. A circular opening of 1.0 cm diameter was made on the chimney to act as a sampling pot for the gases. The height from the cook stove to the sampling pot was 100 cm. E8500P industrial integrated emissions system combustion gas analyser was used to monitor the gas concentrations and gas temperatures with the sensor positioned at the sampling pot. A schematic diagram showing the experimental set-up is presented in Figure 3.1.

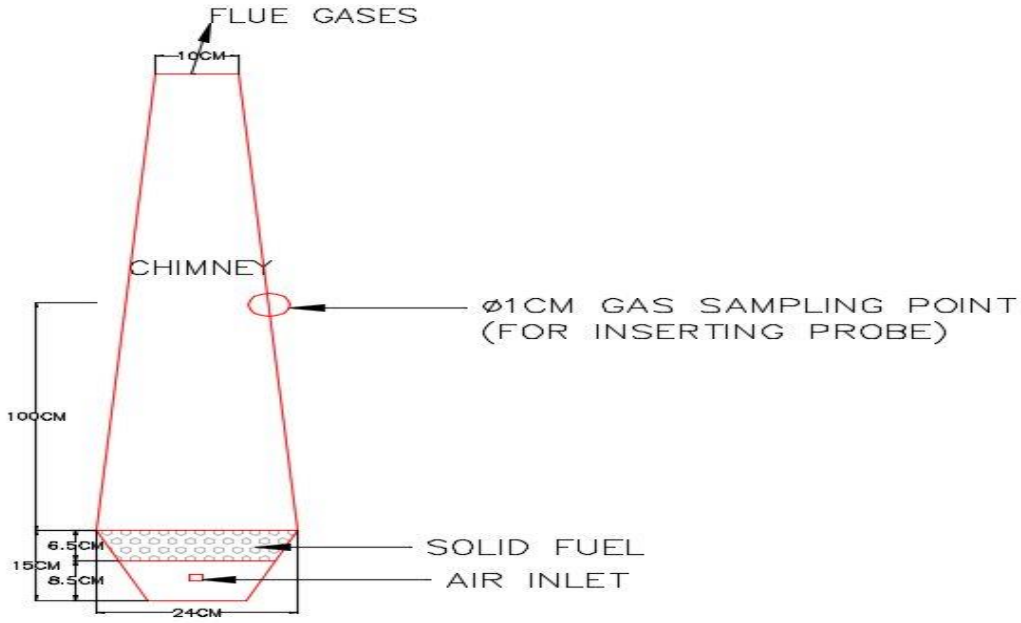

Figure 3.1: Schematic Diagram of the Combustion System

CHAPTER FOUR

RESULTS AND DISCUSSION

4.1 Behaviour and Capacity of Pineapple Peel Biochar and Lateritic Soil in Adsorbing Ammonium Nitrogen and Phosphorous from Human Urine

4.1.1 Composition and Structures of Lateritic Soil and Pineapple Peel Biochar

The semi-quantitative energy dispersive spectroscopy (EDS) analysis of lateritic soil (LS) reveals a chemical composition of O = 45.2 wt.%, Si = 32.8 wt.%, Al = 14.95 wt.%, Na = 1.1 wt.%, Ca = 3.4 wt.%, Mg = 0.5 wt.%, K = 2.45 wt.%, Fe = 1.05 wt.%, and S = 1.4 wt.% as shown in Figure A4 (a-c) in the Appendix I. From maps of the elemental distribution shown in Figure A3 in the Appendix A, structural heterogeneity could be observed, which a good indicator of phase mixtures is. Using the atomic weights of the elements, the oxides SiO_2, and Al_2O_3, could be identified as the dominant phases. The dominance of these oxides in LS has also been reported by Kamtchueng et al. (2015) and State et al. (2018). For pineapple peel biochar (PPB), the EDS maps shown in Figure A5 in the appendix A, confirm the uniform distribution of C = 87.6 wt.%, O = 8.3 wt.%, Si = 2.1 wt.%, Al = 1.0 wt.%, Mg = 0.3 wt.%, Ca = 0.3 wt.%, Na = 0.2 wt.%, and Fe = 0.2 wt.%. This finding is in good accord with what has been observed by Fu et al. (2016) and Shakya and Agarwal (2019).

To identify the phases, X-ray diffraction patterns were collected on sample powders at ambient conditions. The XRD patterns of LS and PPB samples are shown in Figures 4.1a and 4.1b, respectively. The LS powder consisted of several phases, also seen by EDS analysis in Figure A4 (a-c). These phases were identified as quartz ((SiO_2)-ICSD16331) with main peaks at 2θ = 20.6, 26.7, 36.5, and 50, kaolinite (($Al_2Si_2O_5(OH)_4$-ICSD30966) with main peaks at 2θ = 12.2, 21.5, 38.5, 45.8, 55.5, and 62.1, goethite-aluminian (($Fe_{0.83}Al_{0.17}$)O(OH)-ICSD109411) with main peaks at 2θ = 18,

21.3, 26.5, 33, and 37, and illite ((K($Al_4Si_2O_9(OH)_3$-ICSD90144) with main peaks at 2θ = 12.4, 21.6, 24.8, 38, and 55.8.

The XRD pattern of PPB (Figure 4.1b) shows an amorphous structure. In the XRD pattern, sharp peaks found at 2θ = 29.4, 35.9, 39.4, 43.2, and 47.8, and at 2θ = 14.5, 25.6, 29, 37.9, 39.4, 40.9, and 47.4, are attributable to calcite ($CaCO_3$-ICSD18164), and scapolite (Na, Ca)$_4$ (Al, Si)$_{12}O_{24}$(Cl, CO_3, SO_4)-ICSD7102), respectively, as impurity phases.

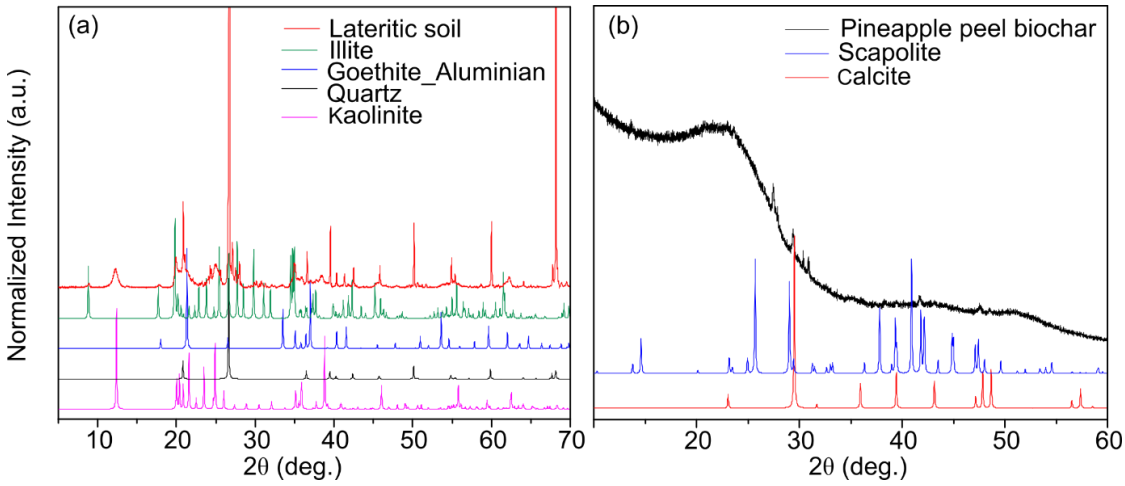

Figure 4.1: XRD Powder Patterns of (a) Lateritic Soil, and (b) Pineapple Peel Biochar

The morphology and particle sizes of LS and PPB from SEM are shown in Figures 4.2a, and 4.2b respectively. The PPB consists of microparticles with elongated honeycomb shapes that are uniform and highly porous. LS on the other hand, consist of nanoparticles which aggregate into different morphologies attributable to the presence of different structural phases.

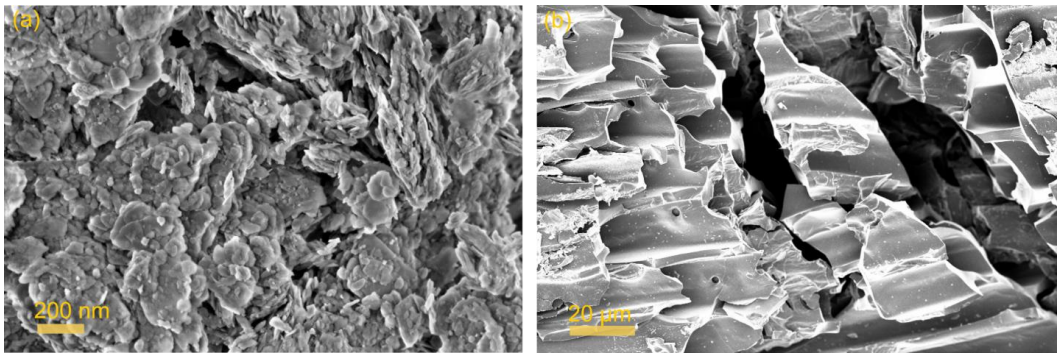

Figure 4.2: SEM Images of (a) Lateritic Soil, and (b) Pineapple Peel Biochar

The pore volume, the Brunauer-Emmett-Teller (BET) surface area (S_{BET}), and the average pore diameter of the two samples are presented in Table 4.1. Fittings of the BET equation to the adsorption isotherms of nitrogen at 77 K give the estimated surface areas of 140 m^2/g, and 44 m^2/g for PPB and LS, respectively. Also, the average pore diameter of PPB obtained was 23 nm, which indicated that its surface was microporous, in line with SEM results.

Table 4.1: Nitrogen Sorption Properties of Lateritic Soil and Pineapple Peel Biochar

Sample	BET surface area, S_{BET} (m^2/g)	Total pore volume, V_{tot} (cm^3/g)	Average pore diameter (nm)
LS	44	0.122	11
PPB	140	0.082	23

The surface area and total pore volume values observed herein for LS are generally within range of those reported for similar materials. For instance, S_{BET} (m^2/g) and V_{tot} (cm^3/g) values of lateritic soil derived from different geographical regions were reported as 17.5 – 18.5 m^2/g and 0.02 – 0.05 cm^3/g, and 71 – 182 m^2/g and 0.07 – 0.35 cm^3/g (Maiti et al., 2012, 2013). In the case of biochars, a wide variation in the surface areas and total pore volume values across the literature has been reported making their comparisons difficult. The variations could be ascribed to the differences in pyrolysis

temperatures, which affects the physicochemical properties of biochars (Kim et al., 2012).

The FTIR spectra in Figure 4.3 show different functional groups of the samples. For LS, the sharp absorption band over the range 3698–3617 cm^{-1} are assignable to –OH group, and appears due to the presence of strongly bonded water molecules. While the band at 1630 cm^{-1} is due to H–O–H bending mode in the weakly surface adsorbed or trapped water molecules in the large cavities of the polymeric framework (Lemougna et al., 2014). The bands in the region between 1376 and 752 cm^{-1} are associated with Si–O–Al, Si–O–Fe, Si–O, Al–OH, and Fe–OH vibrations, and are typical of kaolinites (Kakali et al., 2001). The band at 687 cm^{-1} is due to Fe–OH vibration (Rocha et al., 1990). Similar types of bands have also been observed by Maiti et al.(2012).

For PPB, the broad peaks observed between 3400–3000 cm^{-1} could be attributed to the stretching mode of O–H, indicating the presence of water (Fu et al., 2016). The band around 2915 cm^{-1} is due to aliphatic C–H stretching vibrations in biopolymers (Cantrell et al., 2012), and corresponds to the presence of cellulose and hemicellulose (Usman et al., 2015). This may indicate incomplete carbonization (Shakya & Agarwal, 2019). The strong band at 1589 cm^{-1} is due to alkyl and alkene stretching groups (C–H, C=C, and C–C) (Kim et al., 2012). The weak bands in the region 872–752 cm^{-1} are credited to the bending of C–H groups of the aromatic rings (Fu et al., 2016).

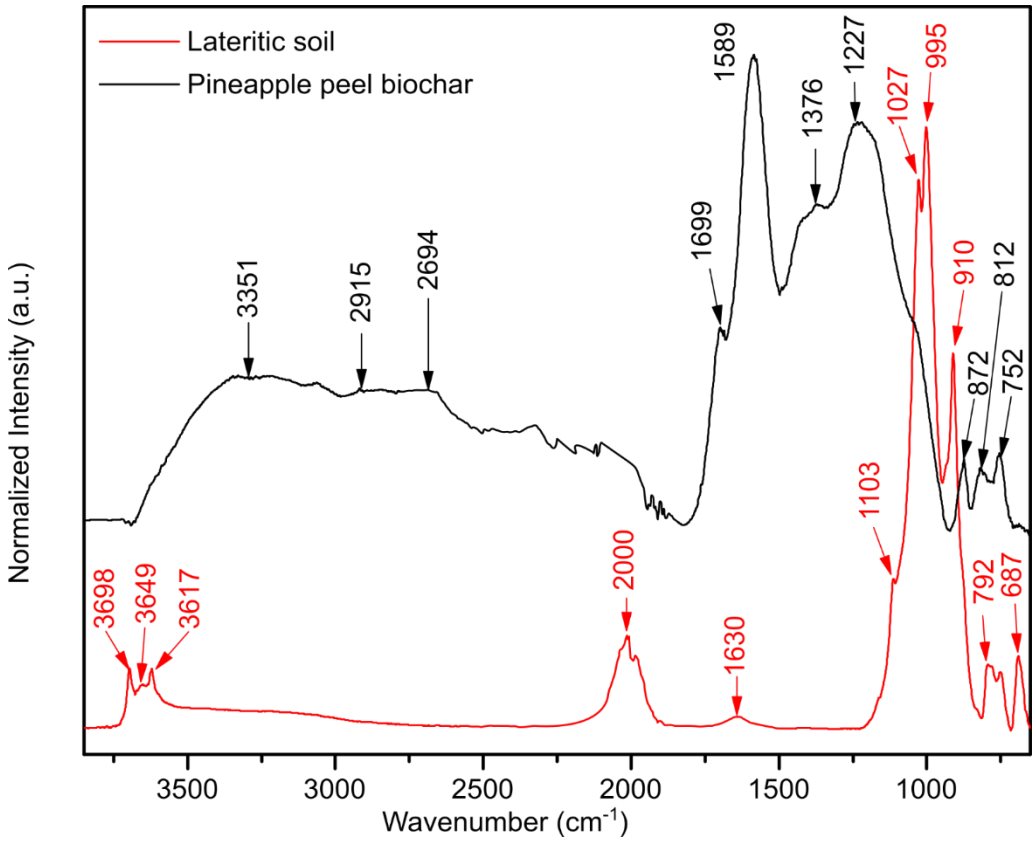

Figure 4.3: FTIR Spectra of Lateritic Soil, and Pineapple Peel Biochar

To understand the thermal stability of LS and PPB, thermogravimetric analysis (TGA) was done from room temperature to 800 °C. The TGA profile of LS (Figure 4.4) shows that the mass loss proceeds via three main steps. The first process < 100 °C corresponds to the elimination of water adsorbed at the surface (~1 wt.%) (Lemougna et al., 2014). The subsequent step in the range 100 °C ≤ T ≤ 350 °C is associated with pre-dehydroxylation and release of some organic matter. This is reflected by the DTG peak at 250 °C (Kakali et al., 2001). The presence of surface adsorbed water agrees well with the IR spectrum. Dehydroxylation of kaolinite through removal of the hydroxyl groups from Al–OH bonds started above 350 °C till ~600 °C (Kakali et al., 2001; Rocha & Klinowski, 1990). The total mass lost is approximately 10 wt.%, and is similar to what has been reported for similar materials (Lemougna et al., 2014).

In the case of PPB, gradual weight loss was observed with increasing pyrolysis temperature. The first mass loss step ≤ 100 °C corresponds to the release of physisorbed water molecules (~4 wt.%). The weight loss between 110 °C ≤ *T* ≤191 °C may be attributed to the removal of strongly bound water (Li et al., 2017). The mass decrease in the range 191 °C ≤ *T* ≤ 280 °C was assigned to degradation of hemicellulose, while thermal degradation of cellulose occurs between 281 °C and 380 °C (Lee et al., 2013). The breakdown of lignin and removal of hydrogen and oxygen (Deng et al., 2014) corresponds to the significant mass loss between 500 and 650 °C, accompanied by a DTG peak at 550 °C. The total weight loss was found to be ~23 wt.%. Similar finding have also been reported by Shakya and Agarwal (2019).

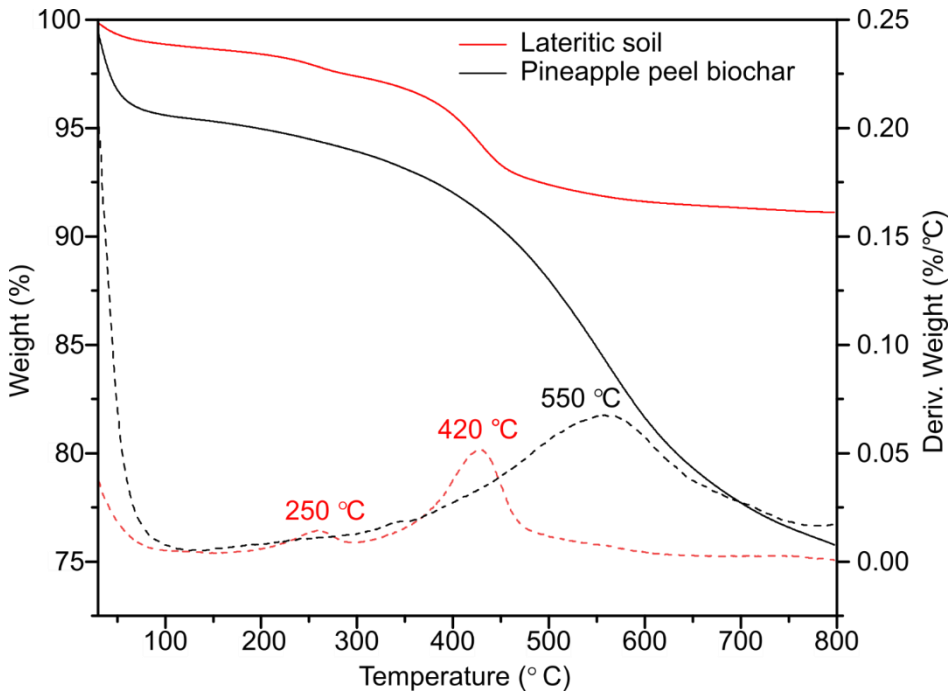

Figure 4.4: Thermogravimetric Analysis (TGA) Curves (solid lines) and DTG Curves (dashed lines) of Lateritic Soil and Pineapple Peel Biochar at a Heating Rate of 5 °C/min Under N2 Flow

In summary, PPB could be better suited for NH_4^+-N and P adsorption due to its large surface area and microporous nature as revealed by BET and SEM results. Also, this

material has a high amount of carbonates and organic matter as seen from TGA data. LS on the other hand, consist of a mixture of phases, and is more thermally stable according to EDS, XRD, and TGA results.

4.1.2 The Effect of Contact Time and the Initial Concentration on Adsorption of Ammonium Nitrogen from Human Urine on Lateritic Soil and Pineapple Peel Biochar

To evaluate the effect of contact time and the initial concentration of NH_4^+-N adsorption on LS and PPB, the experiments were carried out with varying initial NH_4^+-N concentrations (156.88, 161.36, 341.77, 398.92, 451.59, and 569.24 mg/L) at 21°C, pH = ~7.27 ± 0.202, dosage of 0.2 g in 25 mL of urine, and at varying contact time of 30, 60, 90, and 120 minutes, respectively. The effect of contact time of NH_4^+-N adsorption on both LS and PPB reveals that the uptake of NH_4^+-N was rapid initially but slowed with time gradually towards equilibrium (Figure 4.5).

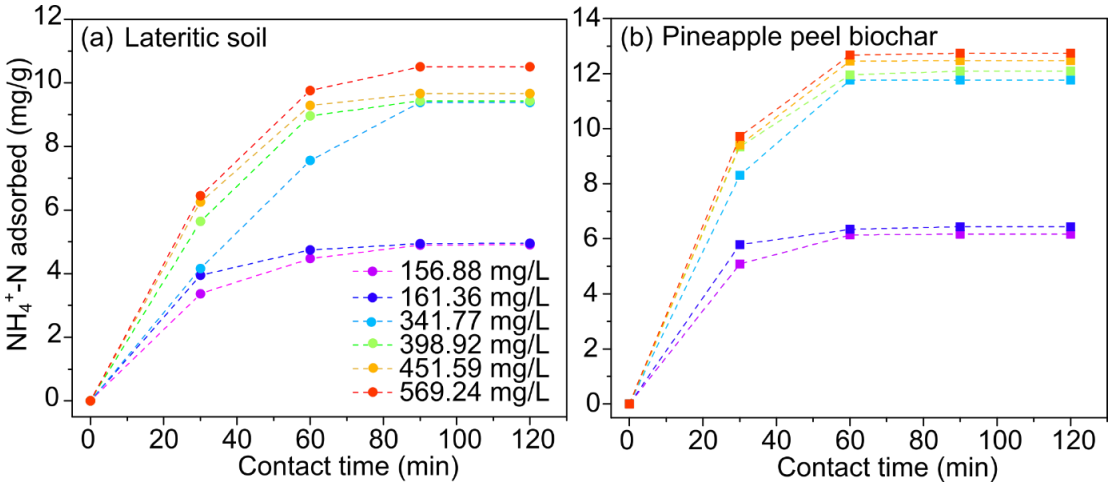

Figure 4.5: The Effect of Contact Time and the Initial Concentration on Adsorption of Ammonium Nitrogen from Human Urine on (a) Lateritic Soil, and (b) Pineapple Peel Biochar

For LS, rapid uptake occurred between 0 – 60 minutes and then slowed gradually between 60 – 90 minutes beyond which NH_4^+-N adsorbed was negligible. In the case of

PPB, rapid uptake occurred between 0 – 30 minutes and then slowed down gradually between 30 – 60 minutes beyond which NH_4^+-N adsorbed was negligible. The rapid uptake could be explained by the existence of high ionic gradient between the solution and the active adsorption sites at the beginning of adsorption resulting into rapid mass transfer of NH_4^+-N onto the adsorption sites. However, as the adsorption progressed, the ionic gradient reduced thereby slowing the transfer of ions. Eventually, the adsorption sites got saturated and could no longer adsorb more of the ions. Huang et al. (2010) using natural Chinese zeolite as adsorbent for removal of NH_4^+-N from aqueous solution observed a similar trend whereby the uptake of the NH_4^+-N ions was rapid within the first 60 minutes and then slowed down considerably, such that beyond 120 minutes the adsorption was almost negligible. These authors attributed this behaviour to the quick utilization of the most readily available active adsorption sites of the zeolite resulting into fast diffusion and attainment of equilibrium rapidly. Guo et al. (2019) in their study on removal of cadmium ions (Cd^{2+}) from aqueous solution using activated carbon also observed an initial rapid uptake of the ions and slowing down of the adsorption towards equilibrium. The authors attributed this phenomenon to the availability of large number of empty adsorption sites at the initial stage with the remaining adsorption sites being difficult to occupy as a result of the repulsive forces from the already occupied sites nearby. According to Inyinbor et al. (2016), the initial rapid adsorption of solutes may be attributed to the contacts of the solute molecules with the easily available surface of the adsorption sites, while subsequent gradual adsorption attributed to the slow uptake of the molecules into the pores of the adsorbents.

The increasing amount of NH_4^+-N adsorbed with increase in initial concentration alludes to more ions being progressively available to attach themselves on the adsorption sites. This finding corroborates those published in literature. For instance, Kizito et al. (2015) observed that as the initial NH_4^+-N concentration in pure NH_4Cl solution and manure slurry increased from 250 – 1400 mg/L, the amount adsorbed at equilibrium by both wood and rice husks biochar increased significantly. Similarly, Sarkhot et al. (2013) using hardwood biochar for sorption of ammonium from dairy effluent and pure NH_4Cl

solution observed that the equilibrium adsorbed amount of ammonium increased significantly with increasing initial concentration from 0 – 1000 mg/L. Both Kizito et al. (2015), and Sarkhot et al. (2013) ascribed their observation to the dependence of the amount of solutes adsorbed on the mass flow of the ions to the active sites, which is in turn was driven by the solute concentration. Thus, at low concentration, there is equally low flow of ions resulting into many active sites on the adsorbent being unoccupied.

In all the conditions investigated (varying the initial concentrations and the contact time), both LS and PPB adsorbed NH_4^+-N from urine. The capability of biochars to adsorb NH_4^+-N has been attributed to the presence of acidic functional groups containing oxygen and hydrogen, which makes the surface to be negatively charged thereby electrostatically attracting the NH_4^+-N (Ahmad et al., 2014; Sumaraj & Padhye, 2017; Hu et al., 2020). Based on the FTIR results, LS contained the functional groups having oxygen and hydrogen, which could have made its surface to be negatively charge thereby attracting the NH_4^+-N. Also, studies on zeolites have shown that the presence of aluminium and silicon elements makes zeolites to have high cation exchange capacity and high NH_4^+-N selective properties (Kithome et al., 1998). The EDS, and XRD results revealed that LS was dominantly composed of aluminium and silicon and this could have contributed to its high adsorption capacity of 10.73 mg/g, which is relatively higher than for most of the biochars reported.

Overall, the quantity of NH_4^+-N adsorbed at equilibrium by PPB was observed to be higher than for LS at all concentrations. For instance, the quantity adsorbed at equilibrium for initial NH_4^+-N concentration of 569.24. 451.59, 398.92, 341.77, 161.36, and 156.88 mg/L were 12.75, 12.47, 12.09,11.77, 6.44, 6.16 mg/g for PPB, while for LS it was 10.51, 9.66, 9.43, 9.38, 4.95, and 4.9 mg/g, respectively. The higher uptake of NH_4^+-N by PPB than LS could be attributed to the availability of larger surface area for adsorption in addition to being more porous as revealed by the BET and SEM results (Table 4.1). This could also have led to PPB reaching equilibrium much faster than the LS (Figure 4.6). It can therefore be deduced that other than having high cation exchange

capacity, the surface morphology of a material plays a significant role in enhancing its adsorption capacity.

4.1.3 Adsorption Isotherms for the Adsorption of Ammonium Nitrogen from Human Urine on the Lateritic Soil and Pineapple Peel Biochar

The graphical plots of Langmuir, Freundlich, and D-R isotherm models of NH_4^+-N adsorption on LS and PPB are shown in Figure 4.6.

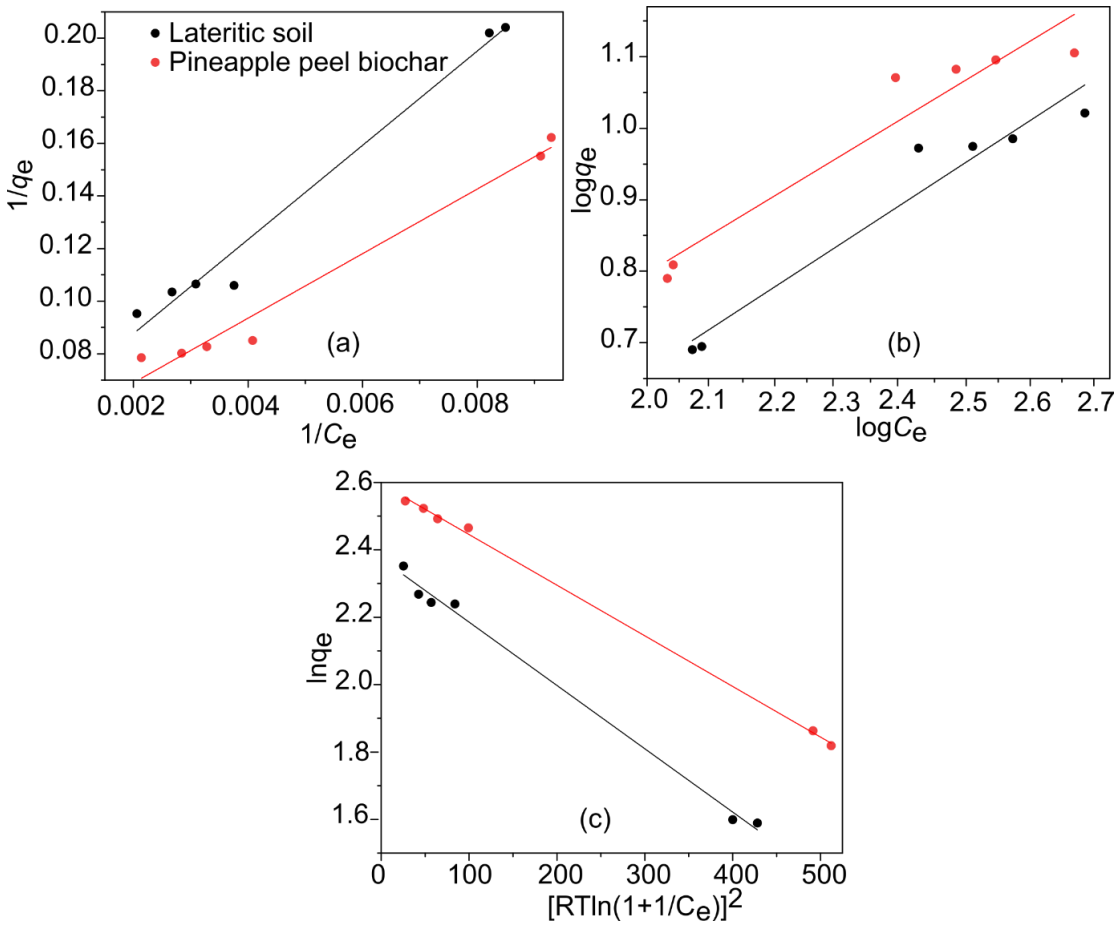

Figure 4.6: (a) Langmuir, (b) Freundlich, and (c) D-R Isotherm Model Fits of Lateritic Soil and Pineapple Peel Biochar

The equilibrium adsorption data obtained for NH_4^+-N adsorption on LS was best fitted by the D-R model (R^2 = 0.999) compared to Langmuir (R^2 = 0.977), and Freundlich models (R^2 = 0.928) as presented in Table 4.2. This implies that the adsorption was mainly due to pore volume filling as opposed to multilayer adsorption on the pore walls (Inglezakis, 2007; Alberti et al., 2012).

Table 4.2: Adsorption Isotherm Model Parameters for Adsorption of Ammonium Nitrogen from Human Urine on Lateritic Soil and Pineapple Peel Biochar

Isotherm	Parameter	Pineapple peel biochar	Lateritic soil
Langmuir	q_{max}(mg/g)	22.727	19.231
	K_L	0.004	0.003
	R_L	0.329	0.377
	R^2	0.977	0.983
Freundlich	K_f	0.520	0.316
	R^2	0.928	0.946
	1/n	0.540	0.581
Dubinin-Radushkevich (D-R)	q_o(mg/g)	13.40	10.73
	K_{DR}	0.0015	0.0019
	E(kJ/mol)	1.826×10^{-2}	1.622×10^{-2}
	R^2	0.999	0.995

The mean surface adsorption energies calculated from the D-R model presented in Table 4.2 also indicate that NH_4^+-N was bound on the active adsorption sites of LS by weak electrostatic (Van der Waal) forces since the value was below 8 kJ/mol (Hu & Zhang, 2019). This becomes ideal in agricultural production since the adsorbed ions can easily dissolve in soil solution and readily be utilized by plants. Based on the XRD and SEM analyses, LS exhibited a mixture of phases, suggesting the possibility that the active adsorption sites could have varying adsorption energy potential or affinity, a property which makes the D-R model the best in describing NH_4^+-N adsorption on LS. This is because the D-R model does not solely consider homogeneity or constant adsorption potential of the adsorption surface (Kaur et al., 2015). The D-R model therefore displayed a more general applicability in comparison to Langmuir, and Freundlich models, as it gave the best fit to the data. Although most studies have investigated the

use of zeolite as a geological material for adsorption of NH_4^+-N, there are no reports on the adsorption capacity of NH_4^+-N on LS that could be used to compare the value of 10.73 mg/g obtained herein.

PPB also exhibited an adsorption trend similar to LS. The correlation coefficients (R^2) were 0.999, 0.977, and 0.928 for the D-R, Langmuir, and Freundlich models, respectively. Therefore, the description of the behaviour of NH_4^+-N adsorption on PPB is similar to that of LS. The PPB exhibited phase mixtures although it was dominantly composed of carbon as revealed by XRD data. The phase impurities could have resulted into its heterogeneity, a property that made D-R model best in describing NH_4^+-N adsorption on its active sites. These finding agree well with the study by Halim et al. (2017). These authors observed that the D-R model best described the behaviour of NH_4^+-N adsorption on spent mushroom substrate biochar, and that the NH_4^+-N ions were attracted onto the surface of the adsorbent by weak electrostatic forces. Zhu et al. (2012) reported in their study of NH_4^+-N removal from aqueous solution using activated carbon from rice husks that D-R model best described the adsorption process although ion exchange was the major mechanism of adsorption. A similar study on NH_4^+-N adsorption on biochar derived from different feedstocks (maize stover, sugarcane pith, pine wood and grape pip) concluded that NH_4^+-N adsorption occurred on heterogeneous surfaces through weak electrostatic attraction (Aghoghovwia et al. 2020). A comparison of the maximum adsorption capacity of NH_4^+-N (13.40 mg/g) on PPB obtained herein with those reported for biochars from different sources are presented in Table 4.3.

Table 4.3: Capacities of Various Biochars in Adsorbing Ammonium Nitrogen

Adsorbents	Isotherm model	Adsorption capacity - q_{max} (mg/g)	Reference
Rice husk	Langmuir	44.64	(Kizito et al., 2015)
Maize straw	Langmuir	15.46	(Gai et al., 2014)
Milled bamboo	Langmuir	22.90	(Qin et al., 2019)
Rice husk	D-R	6.80	(Zhu et al., 2012)
Spent mushroom substrate	D-R	12.6	(Halim et al., 2017)
Rice husk	D-R	6.12	(Mathurasa et al., 2018)
Pineapple peel	D-R	13.40	This study

The differences in adsorption capacities presented in Table 4.2 could have resulted from different experimental conditions such as initial concentrations, biochar modification, and different pyrolysis temperature as well as solution pH. However, most of the studies indicate that biochar has a great potential for NH_4^+-N recovery.

4.1.4 The Effect of Contact Time and the Initial Concentration on Adsorption of Phosphorous from Human Urine on Lateritic Soil and Pineapple Peel Biochar

The effect of contact time and the initial concentration of P in urine on the amount of adsorbed P on LS and PPB are presented in Figure 4.7a and 4.7b, respectively.

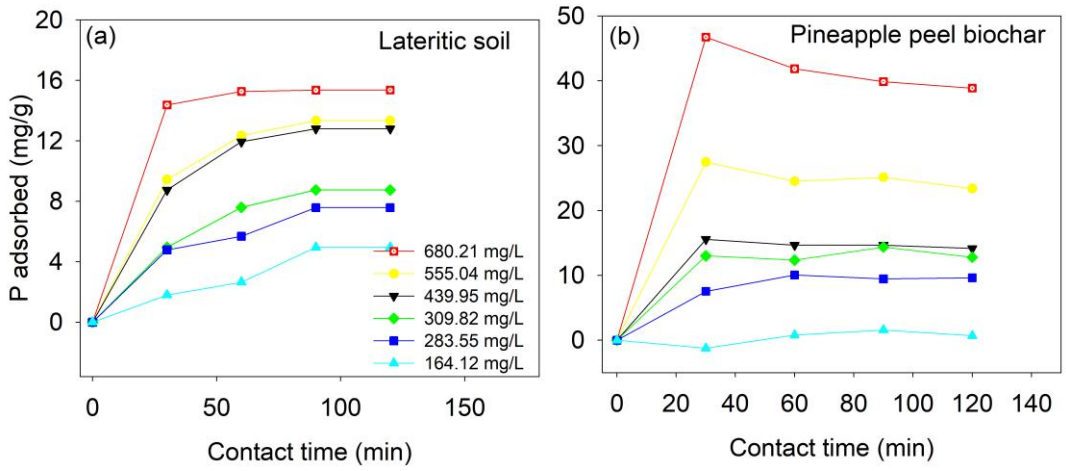

Figure 4.7: The Effect of Contact Time and the Initial Concentration of Phosphorous Adsorption on (a) Lateritic Soil and (b) Pineapple Peel Biochar

As illustrated in Figure 4.7a, it is evident that the adsorption of P on LS mainly occurred in three stages. The adsorption of P was rapid within the first 30 minutes of contact time. This is attributable to a large number of vacant adsorption sites available. What follows is a gradual decline in the sorption rate between 30 – 90 minutes, which could be due to the adsorption sites being gradually occupied as the adsorption process continued. In the final step, the adsorption of solutes tends towards constant values beyond 90 minutes, suggesting saturation of the available sorption sites. Ragheb (2013) observed a similar trend when slag and fly ash were used to remove phosphate from aqueous solution. According to the author a rapid uptake occurred in the first 30 minutes of contact period but the amount of the adsorbed phosphates beyond 60 minutes remained constant. The ionic gradient influences adsorption such that the high difference in phosphate concentration between the solution and the adsorbents at the onset of adsorption process resulted into a higher rate of diffusion of the solutes through the pores of the adsorbent to the internal adsorption sites. However, the diffusion of the solute ions into the bulk of the adsorbent reduces towards equilibrium. In a study by Bhattacharjee et al. (2021) using LS as an adsorbent for the removal of P from sewage effluent, an initial rapid solute uptake was observed, followed by a gradual decline and

finally a steady state condition where negligible uptake of the solutes occurred. These authors attributed the initial rapid mass transfer of the phosphates to the adsorption sites to a high ionic gradient. Moreover, the slow rate of phosphate sorption after equilibrium could have also resulted from an increase in the total negative charge on the LS surface causing the repulsion of the anionic phosphates in the solution. Özacar (2003) reported that the adsorption of P onto calcined alunite increased with time but remained constant after 120 minutes. The author attributed the single, smooth, and continuous time profile curve of P uptake to the possible monolayer adsorption on the surface of the adsorbent.

The increasing amount of P adsorbed on LS with increase in the initial concentration could be due to more ions being progressively available to attach themselves on to the adsorption sites. Also, the higher ionic gradient between the adsorption surface and the solution at higher concentrations could lead to higher mass transfer of phosphate ions to the adsorption surface and consequently higher uptake of P. Similar results have been reported by Ramakrishnaiah (2012) in a study of phosphate adsorption on low-cost adsorbents. The author remarked that higher mass flow of ions to the adsorption sites occurs at elevated solute concentrations than at low concentrations. Wei et al. (2008) also found that phosphorous adsorption capacity of acid mine drainage sludge ranged from 9.89 to 31.97 mg/g when the concentration of municipal wastewater effluent was increased from 0.21 to 13.61 mg/L. The authors argued that increasing the concentration of the anionic phosphate ions in the solution enhanced the electrostatic attraction between the ions and the positively charged surfaces of sludge particles.

On the other hand, Figure 4.7b shows that PPB adsorbed P in human urine but released it into the solution gradually thereby not reaching equilibrium. The phenomenon of non-modified biochar leaching phosphorous into aqueous solution has been previously reported. For instance, Yao et al. (2012) reported that non-modified sugarcane bagasse carbonized at 300 and 600 °C adsorbed and released phosphorous into the aqueous solution thereby not reaching equilibrium. Also, a study by Wunderlich (2015) observed that non-modified biochar could not adsorb phosphorous at all from human urine but instead leached the inherent P it into the solution. Nevertheless, the capacity of PPB to

adsorb P from human urine could be attributed to the presence of calcium oxides which has been reported to have capacity to remove phosphates from human urine through formation of amorphous calcium phosphates (Randall et al., 2016). However, Randall et al. (2016) observed that calcium oxides are highly soluble in urine, which could have resulted into the dissolution of the formed complexes as evidenced in this study making equilibrium not to be attained. Attempt to increase the capability of the negatively charged biochars to adsorb the anionic phosphates has resulted in a concept of modification of biochar surfaces using metal cations with magnesium oxides being the most widely reported compound for the modification (Li et al., 2017; Xu et al., 2019). Yao et al. (2013) in their attempt to study the correlation between P removal rates and metal element (Mg, Ca, K, Fe, Zn, Cu, and Al) contents of 25 biochars, reported a varying correlation, with Mg having the highest correlation (77.9%) compared to Ca (36.4%), K (25.1%), Cu (10.6%), Fe (8.5%), Al (1.3%) and Zn (1.1%). Other studies (Liu et al., 2019; Luo et al., 2019) have similarly reported that the presence of positively charged MgO nanocomposites in the biochar matrix is the major mechanism of P removal from aqueous solutions through electrostatic attraction to form magnesium-phosphate complexes ($MgHPO_4$ and $Mg(H_2PO_4)_2$) on the surface.

4.1.5 Adsorption Isotherms for the Adsorption of Phosphorous from Human Urine on the Lateritic Soil

The adsorption isotherms of the Langmuir, Freundlich and D-R models describing the behaviour of P adsorption on LS are presented in Figure 4.8, while the isotherm parameters are summarized in Table 4.6. Lateritic soil was chosen for equilibrium studies due to its potential to hold phosphorous unlike pineapple peel biochar that shows a tendency to release phosphorous in urine solution.

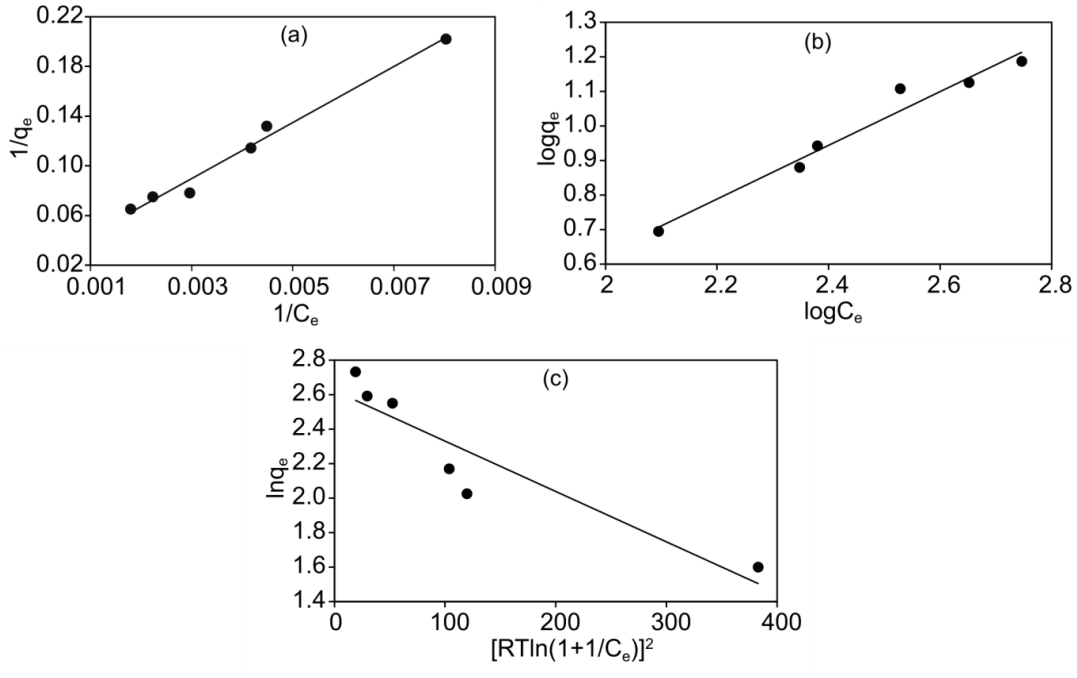

Figure 4.8: (a) Langmuir, (b) Freundlich, and (c) D-R Isotherm Model Fits of Lateritic Soil

The correlation coefficients (R^2) for Langmuir, Freundlich, and D-R models were 0.984, 0.966, and 0.858, respectively as presented in Table 4.6. On the basis of the R^2 values, both Langmuir and Freundlich isotherm models yielded satisfactory fit to the experimental data but Langmuir model gave the best fit. Therefore, it can be interpreted that the available adsorption sites for P on LS have the same adsorption energy and that the process is reversible. In essence, the sorption mechanism is controlled by the surface area and chemical properties of the soil. Other studies (Bhattacharjee et al., 2021; Fulazzaky et al., 2014) have also reported the Langmuir model to best describe P adsorption on LS with Al and Fe cations considered to be responsible for the removal of P from aqueous phase through electrostatic attraction to form complexes. The calculated mean surface adsorption energy (E = 1.313 $\times 10^{-2}$ kJ/mol) from the D-R model presented in Table 4.6 shows that P was bound on the LS surface by weak electrostatic (Van der Waal) forces since the value was below 8 kJ/mol (Hu & Zhang, 2019).

Table 4.4: Langmuir, Freundlich, and D-R Isotherm Parameters for the Adsorption of Phosphorous on Lateritic Soil

Isotherm parameters	
Langmuir	
q_{max} (mg/g)	45.25
K_L	0.001
R_L	0.6
R^2	0.984
Freundlich	
K_f	0.119
1/n	0.778
R^2	0.966
Dubinin-Radushkevich (D-R)	
q_o (mg/g)	13.75
K_{DR}	0.0029
E (kJ/mol)	1.313×10^{-2}
R^2	0.858

The adsorption capacities of different adsorbents are highly dependent on the operating temperatures, material surface area, and initial solution concentrations (Liang Zhang et al., 2011)**.** As shown in Table 4.7, it is evident that LS used in this study can adsorb a maximum of 45.25 mg/g P from human urine, which is in the typical range for many adsorbents; 9.8 mg/g for bentonites, 4.3 mg/g for wood aspen fibres, 41.97 mg/g for calcined alunite, and 36 mg/g for Fe-Mn binary oxide among others.

Table 4.5: Comparison of Phosphorous Adsorption Maxima, q_{max} (mg/g) of Lateritic Soil with other Adsorbents

Adsorbent	**Solution**	**q_{max} (mg/g)**	**Reference**
Lateritic soil	Aqueous solution	31.25	(Hue & Tung, 2018)
Lateritic soil	Human urine	45.25	This study
Calcined alunite	Aqueous solution	41.97	(Özacar, 2003)
Bentonites	Aqueous solution	9.80	(R. Zhu et al., 2009)
Wood aspen fibres	Aqueous solution	4.30	(Eberhardt et al., 2006)
Fe –Mn binary oxide	Aqueous solution	36.00	(Gaosheng Zhang et al., 2009)

4.2 Optimised Adsorption of Ammonium Nitrogen and Phosphorous from Human Urine on Pineapple Peel Biochar and Lateritic Soil

4.2.1 Response Surface Methodology Experiment for Optimised Adsorption of Ammonium Nitrogen from Human Urine on Pineapple Peel Biochar

The response surface methodology (RSM) was carried out using "Design-Expert® software, version 12, Stat-Ease, Inc., Minneapolis, MN, USA, www.statease.com" to optimise the adsorption of NH_4^+-N on pineapple peel biochar (PPB) and to investigate interactive effect of contact time, agitation speed and adsorbent loading. Based on the results from the adsorption isotherm studies, pineapple peel biochar was selected for optimization studies due to its high monolayer maximum adsorption capacity (22.727 mg/g) compared with lateritic soil (19.231 mg/g). The optimisation modeling was performed at 21 °C, and pH of 7.2. The relationship between the response of adsorbed NH_4^+-N and the three influencing variables; contact time, agitation speed, and adsorbent loadings was analysed based on the central composite circumscribed design with each variable studied at 5 levels.

The estimated second-order quadratic response model equation in coded form that was used to explain the adsorption behavior of NH_4^+-N is presented in Equation 4.1 given as:

$$Y = 11.07 + 2.09x_1 + 0.1134x_2 - 12.16x_3 - 1.21x_1x_2 - 1.31x_1x_3 - 0.5544x_2x_3 + 0.6586x_1^2 + 0.0891x_2^2 + 8.87x_3^2 \quad (4.1)$$

Where:

Y (mg/g) = the amount of the adsorbed NH_4^+-N

x_1, x_2, and x_3 = the coded terms for contact time, agitation speed, and adsorbent loading, respectively

The predicted amount of the adsorbed NH_4^+-N for each run presented in Table 4.4 was obtained by solving Equation 4.1.

Table 4.6: Ammonium Nitrogen Adsorption Results Based on the Response Surface Methodology and the Central Composite Circumscribed Experimental Design

Run	Coded Values			Actual Values			Ammonium Nitrogen response	
	x_1	x_2	x_3	Contact time (min)	Speed (rpm)	Loading (g)	Actual (mg/g)	Predicted (mg/g)
1	-1.682	0	0	20	140	0.20	9.66	9.71
2	0	0	0	45	140	0.20	11.07	11.12
3	0	-1.682	0	45	39	0.20	11.21	11.27
4	0	0	1.682	45	140	0.37	15.45	15.68
5	0	0	-1.682	45	140	0.03	57.22	56.55
6	1.682	0	0	70	140	0.20	16.53	16.62
7	0	0	0	45	140	0.20	11.07	11.12
8	1	-1	-1	60	80	0.10	36.42	36.84
9	-1	1	1	30	200	0.30	8.68	8.76
10	-1	-1	1	30	80	0.30	6.91	6.91
11	1	-1	1	60	80	0.30	11.25	11.44
12	-1	-1	-1	30	80	0.10	27.45	27.48
13	1	1	1	60	200	0.30	7.56	7.62
14	0	1.682	0	45	241	0.20	11.77	11.83
15	0	0	0	45	140	0.20	11.07	11.12
16	0	0	0	45	140	0.20	11.07	11.12
17	1	1	-1	60	200	0.10	35.58	35.65
18	0	0	0	45	140	0.20	11.07	11.12
19	0	0	0	45	140	0.20	11.07	11.12
20	-1	1	-1	30	200	0.10	30.82	31.97

As shown in Table 4.4, a wide range of adsorbed amount of NH_4^+-N on PPB from a minimum of 7.62 mg/g to a maximum of 56.55 mg/g occurred for the predicted responses, indicating a strong correlation between the adsorption of NH_4^+-N and the contact time, speed and loading.

4.2.2 ANOVA Analysis and Reliability of the Response Surface Methodology Model for Optimised Adsorption of Ammonium Nitrogen from Human Urine on Pineapple Peel Biochar

An ANOVA was conducted to study the significance of the quadratic model, while the value of the coefficient of determination (R^2) was used to determine the reliability of the quadratic model in fitting the experimental data and accurately predicting the output. The quadratic model had R^2 value of 0.999 implying that approximately 99.9% of the variance in the experimental data is attributed to the variables investigated. The quadratic model was therefore adequate in predicting the amount of adsorbed P under

the given experimental conditions since nearly all the variations could be accounted for by the quadratic model. Moreover, there was no difference between the R^2 (0.999) and adjusted R^2_{adj} (0.999) suggesting that the predicted values (response) matched well with the observed ones, implying that the regression model had an excellent stability (Myers et al., 2004). To verify the adequacy of the model, the experiment was conducted at the optimal conditions described of 60 minutes contact time, 80 rpm agitation speed, and adsorbent loading of 0.1g, yielding an adsorption capacity of NH_4^+-N of 36.42 mg/g, which agreed well with the predicted adsorption capacity of 36.84 mg/g. The ANOVA results for the response surface quadratic model for the adsorption of P are summarized and presented in Table 4.5.

Table 4.7: ANOVA for Response Surface Quadratic Model for Optimised Adsorption of Ammonium Nitrogen from Human Urine on Pineapple Peel Biochar

Source	F-value	p-value	
Model	3175.47	< 0.0001	significant
x_1-contact time	522.27	< 0.0001	significant
x_2-agitation speed	1.54	0.2423	not significant
x_3-adsorbent loading	17753.93	< 0.0001	significant
x_1x_2	102.59	< 0.0001	significant
x_1x_3	121.21	< 0.0001	significant
x_2x_3	21.61	0.0009	significant
x_1^2	54.92	< 0.0001	significant
x_2^2	1.01	0.3397	not significant
x_3^2	9972.89	< 0.0001	significant

R^2, R^2_{adj} (coefficient of determination) of the model is 0.999, 0.999, respectively.

The probability p-value of < 0.0001 indicates that there was less than 0.01% chance that the output response (adsorbed NH_4^+-N) is due to noise and therefore the quadratic model was statistically significant at 95% confidence level. Among the three factors, contact time, agitation speed, and adsorbent loading optimised for achieving optimal adsorption of NH_4^+-N on PPB, increasing the agitation speed did not significantly ($P > 0.05$) increase the uptake of NH_4^+-N. This is further depicted by the 3D surfaces in Figures

D1a and D1b presented in Appendix IV which shows no gradual change in the amount of NH_4^+-N with increase in agitation speed. Theoretically, it is expected that increasing speed results into increased collision of active sites with the solutes thereby increasing the amount of solutes adsorbed. However, from the findings, it can be stated that increasing the agitation speed beyond the optimum level does not increase the amount of NH_4^+-N adsorbed on PPB. This concurs with a study by Zahoor (2011) who observed that the adsorption of insecticide (imidacloprid) on activated carbon increased with the agitation speed from 200 upto 300 rpm beyond which negligible adsorption occurred. The author argued that increasing turbulence decreases the boundary layer thickness surrounding the adsorbent particles leading to an increase in the accessibility of the available adsorption site. However, negligible increase in the adsorption beyond 300 rpm implies that for any adsorption process, there is an optimum speed to achieve optimal adsorption, and thus should be investigated for every adsorbent.

On the other hand, increasing the contact time beyond 30 minutes significantly ($P<0.05$) increased the amount of NH_4^+-N adsorbed on PPB, an observation which indicates that equilibrium conditions had not been attained at 30 minutes since no further adsorption occurs when all active adsorption sites are occupied. Since adsorption occurs on adsorbent surfaces or pores, the removal of solutes in aqueous phase will generally be affected by the adsorbent dosage. In this study, increasing the adsorbent dosage beyond 0.1g significantly ($P<0.05$) reduced the amount of NH_4^+-N adsorbed which is also depicted by the 3D surfaces presented as Figures D1a and D1c in the Appendix IV. This is in line with studies by Pillai et al. (2014) and Sica et al. (2014) who observed that increasing the adsorbent loadings resulted into a decrease in the amount of solutes adsorbed. These authors explained that increase in adsorbent loadings results in the agglomeration of particles thereby reducing the amount of surface available for attachment, which consequently results into low amounts solutes adsorbed at equilibrium. Based on these observations, it is worth pointing out that to achieve an optimal removal of solutes in any given fixed volume of a solution, the adsorption

experiments should be carried out at optimum contact time, agitation speed and adsorbent dosage.

4.2.3 Response Surface Methodology Experiment for Optimised Adsorption of Phosphorous from Human Urine on Lateritic Soil

Data analysis using the Response Surface Methodology (RSM) was undertaken using "Design-Expert® software, version 12, Stat-Ease, Inc., Minneapolis, MN, USA, www.statease.com" to optimise the adsorption of P on LS and to investigate interactive effect of contact time, agitation speed and adsorbent loading. The optimisation modelling was performed at 21 °C, pH of 7.83 and initial P concentration of 470.03 mg/L. The relationship between the response of adsorbed P and the three influencing variables, contact time, agitation speed, and adsorbent loadings considered in this study was analysed based on the central composite circumscribed design with each variable studied at 5 levels.

The estimated second-order quadratic response model equation in coded form was used to explain the adsorption behavior of P on LS is presented in Equation 4.2 given as:

$$Y = 10.36 + 0.1707x_1 - 14.64x_2 - 33.27x_3 + 2.44x_1x_2 + 1.51x_1x_3 + 17.0x_2x_3 + 5.12x_1^2 + 4.74x_2^2 + 23.89x_3^2 \quad (4.2)$$

Where:

Y = the amount of the adsorbed P (mg/g)

x_1, x_2, and x_3 = the coded terms for contact time, agitation speed, and adsorbent loading, respectively.

The predicted amount of the adsorbed P for each run presented in Table 4.8 was obtained by solving Equation 4.2.

Table 4.8: Phosphorous Adsorption Results Based on the Response Surface Methodology and the Central Composite Circumscribed Experimental Design

	Coded values			Actual values			Adsorbed phosphorous	
Run	x_1	x_2	x_3	Contact time (min)	Speed (rpm)	Loading (g)	Actual (mg/g)	Predicted (mg/g)
1	1.682	0	0	70	140	0.20	33.17	25.13
2	0	0	0	45	140	0.20	10.15	10.36
3	0	0	-1.682	45	140	0.03	144.49	133.89
4	1	-1	-1	30	80	0.10	112.93	112.80
5	0	-1.682	0	45	39	0.20	43.10	48.39
6	0	0	0	45	140	0.20	10.15	10.36
7	0	0	0	45	140	0.20	10.15	10.36
8	1	-1	-1	60	80	0.10	96.64	105.26
9	-1.682	0	0	20	140	0.20	23.92	24.56
10	1	-1	1	60	80	0.30	15.01	7.72
11	-1	1	-1	30	200	0.10	32.11	44.6
12	1	1	1	60	200	0.30	6.94	17.31
13	0	0	0	45	140	0.20	10.15	10.36
14	-1	1	1	30	200	0.30	12.47	9.08
15	0	0	0	45	140	0.20	10.15	10.36
16	0	0	0	45	140	0.20	10.15	10.36
17	1	1	-1	60	200	0.10	40.78	46.84
18	0	1.682	0	45	241	0.20	11.81	11.69
19	0	0	-1.682	45	140	0.37	18.78	21.98
20	-1	-1	1	30	80	0.30	10.07	9.24

As shown in Table 4.8, a wide range of adsorbed amount of P on LS from a minimum of 7.72 mg/g to a maximum of 133.89 mg/g occurred for the predicted responses, indicating a strong correlation between the adsorption of P and the contact time, speed, and loading.

4.2.4 ANOVA Analysis and Reliability of the Response Surface Methodology Model for Optimised Adsorption of Phosphorous from Human Urine on Lateritic Soil

An ANOVA was conducted to study the significance of the quadratic model, while the value of the coefficient of determination (R^2) was used to determine the reliability of the quadratic model in fitting the experimental data and accurately predicting the output. The quadratic model had R^2 value of 0.972 implying that approximately 97.2% of the variance in the experimental data is attributed to the variables investigated. The quadratic model was therefore adequate in predicting the amount of adsorbed P under the given experimental conditions since only 2.84 % of the total variations could not be

accounted for by the quadratic model. Moreover, the difference between the R^2 (0.972) and adjusted R^2_{adj} (0.956) was < 0.2 suggesting that the predicted values (response) matched well with the observed ones, implying that the regression model had an excellent stability (Myers et al., 2004a). To verify the adequacy of the model, the experiment was conducted at the optimal conditions described, yielding an adsorption capacity of P of 112.23 mg/g, which agreed well with the predicted adsorption capacity of P. The ANOVA results for the response surface quadratic model for the adsorption of P are summarized and presented in Table 4.9.

Table 4.9: ANOVA for Response Surface Quadratic Model for Optimised Adsorption of Phosphorous from Human Urine on Lateritic Soil

Source	F-value	p-value	
Model	37.97	< 0.0001	Significant
x_1-contact time	0.0047	0.9466	Not significant
x_2-agitation speed	34.71	0.0002	Significant
x_3-adsorbent loading	179.21	< 0.0001	Significant
x_1x_2	0.5624	0.4706	Not significant
x_1x_3	0.2148	0.6530	Not significant
x_2x_3	27.41	0.0004	Significant
x_1^2	4.48	0.0604	Not significant
x_2^2	3.83	0.0788	Not significant
x_3^2	97.50	< 0.0001	Significant

R^2, R^2_{adj} (coefficient of determination) of the model is 0.972, 0.956, respectively.

The results show that the quadratic model is statistically significant at 95% confidence level, with F-value of 37.97 and very low p-value of < 0.0001, i.e., there is less than 0.01% chance that the output response is due to noise. Among the three factors, contact time, agitation speed, and adsorbent loading optimised for achieving optimal adsorption of P on LS, increasing the contact time did not significantly (P > 0.05) increase the uptake of P. This implies that once the equilibrium is reached, no further adsorption can occur since all the active sites are occupied.

On the other hand, increasing the agitation speed beyond 80 rpm showed a gradual decline in the amount of the adsorbed P as depicted in the 3D graphs presented in Figures E1a, and E1c in the appendix. We can draw parallels with a study by Geethakarthi and Phanikumar (2011) where the adsorption of reactive dyes on activated carbon was seen to decline with increase in the agitation speed beyond 120 rpm. The desorption or detachment of the adsorbed molecules at higher speed suggest that there is an optimal agitation speed or turbulence for any adsorption process. However, increasing the agitation speed gradually upto the optimum generally leads to a gradual increase in the amount of solutes adsorbed. For instance, Zahoor (2011) observed that the adsorption of imidacloprid on activated carbon increased with the agitation speed from 200 upto 300 rpm beyond which no significant increase in the adsorption occurred. The author argued that increasing turbulence decreases the boundary layer thickness surrounding the adsorbent particles leading to an increase in the accessibility of the available adsorption site. However, insignificant increase in the adsorption beyond 300 rpm implies that for any adsorption process, there is an optimum speed to achieve optimal adsorption, and thus should be investigated for every adsorbent.

The removal of solutes in aqueous phase will generally be affected by the adsorbent dosage since the adsorbents provide attachment sites. In this study, adsorbent dosage beyond 0.1g led to a decline in the amount of the adsorbed P as shown by the 3D graphs in Figure E1a and E1b in the appendix V. This is line with the work by Drenkova-Tuhtan et al. (2017), which reported a decrease in the removal of phosphates with increase in the adsorbent dose beyond the optimum dosage. The authors credited this observation to agglomeration of particles at higher dosage thereby reducing the accessibility of the active adsorption sites. In contrast, Xiong et al. (2011) reported that phosphate removal from aqueous solution increased with the amount of powdered freshwater mussel shells, an observation they attributed to an increase in the available surface area for attachment of phosphates. Based on the above discussion, it is worth pointing out that to achieve an optimal removal of solutes in any given fixed volume of a

solution, the adsorption experiments should be carried out at optimum contact time, agitation speed and adsorbent dosage.

4.3 Thermal Degradation and Kinetic Behaviour of Pyrolyzed Human Faeces, Sawdust Char and their Blend

4.3.1 Morphological, Physicochemical Properties, and Thermal Behaviors of Faecal Char, Sawdust Char, and their Blend

The comparative results of proximate analysis (volatile matter, fixed carbon, moisture content, and ash content), ultimate analysis (C, H, N, and O) and heating values of faecal char and sawdust char are listed in Table 4.10. The volatile matter in faecal char compares well to sawdust char hence good for combustion processes, although the latter biomass has noticeably more ash content, ~8 %, which may affect its burning rate. This value is however below those reported in the literature, i.e., 13% to 51.2% (Hafford et al., 2018; Krueger et al., 2020). High ash content may pose several issues such as poor combustion, excess processing costs, disposal problem, and reduced energy conversion (Sait et al., 2012). The predicted gross calorific values for faecal char and sawdust char were 24.5 MJ/kg, and 26.3 MJ/kg, respectively, which are comparable to those of natural coals (8 – 27 MJ/kg), wood (19 – 25 MJ/kg), and charcoal (29 – 33 MJ/kg) (Patel et al., 2007; Ruiz-Aquino et al., 2019). The carbon content in faecal char, 55.3%, is comparable to 58.3% and 56.1% in human faeces pyrolyzed at 200 and 300 °C, respectively (Afolabi et al., 2017; Ward et al., 2014). Also, the 78.2% carbon content in sawdust char is in complete agreement with 78.7% in hazelnut shells pyrolyzed at 350 °C (Bonelli et al., 2003).

Table 4.10: Proximate and Ultimate Analysis of Faecal Char and Sawdust Char

Analysis	Faecal Char	Sawdust Char
Proximate analysis (wt. %)		
Volatile matter	25.9	36.4
Fixed carbon	63.3	57.8
Moisture content	2.16	2.13
Ash content	8.62	2.64
Ultimate analysis (wt. %)		
C	55.3	78.2
H	5.8	4.6
N	3.1	1.1
O[a]	35.8	16.1
Gross calorific value (MJ/kg)	24.5	26.3

[a] Estimated as a difference

The morphological SEM image shown in Figure 4.9a reveals faecal char surface as fibrous with very few pores, which may be due to dehydration and decomposition of volatile matter (Liang et al., 2016). On the other hand, sawdust exhibits highly macroporous tubular shapes, attributable to the presence of plant cells (Figure 4.9b). The tubes are perforated, an indication that they were partially oxidised (Krueger et al., 2020). These observations correlate fairly well with previous reports on faecal char, and sawdust char (Chowdhury et al., 2016; Krueger et al., 2020).

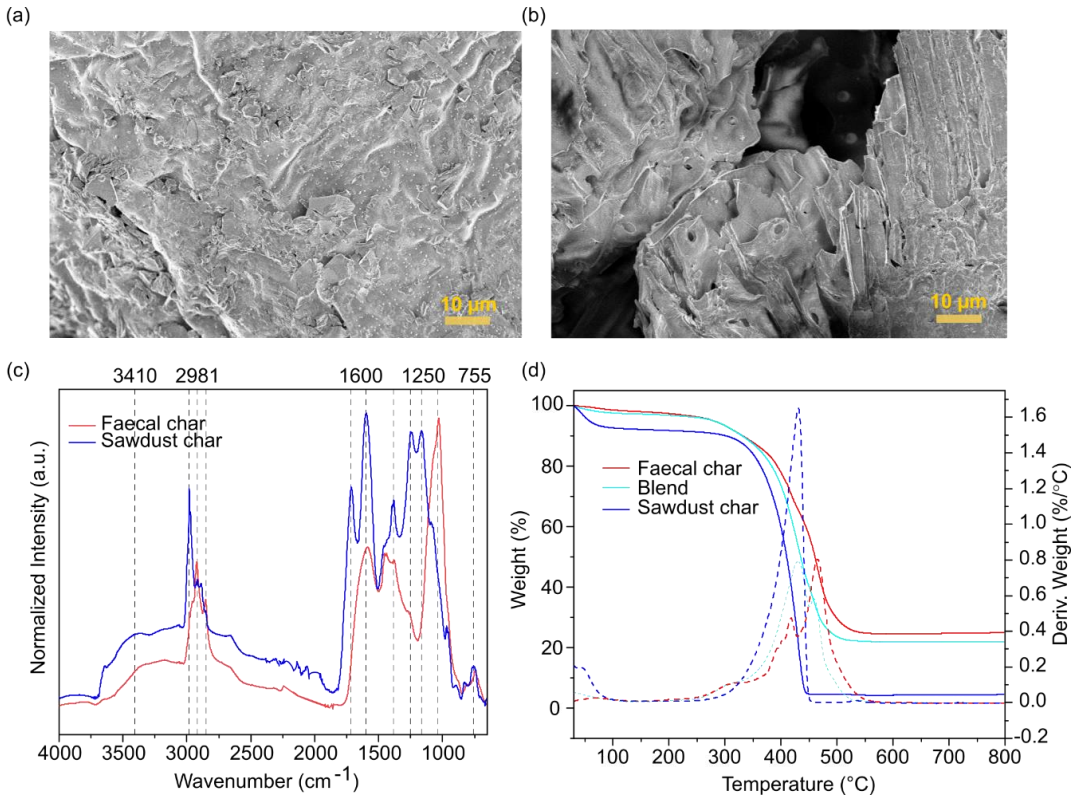

Figure 4.9: Physical Properties of Faecal Char, Sawdust Char, and Blend; (a) and (b) SEM Images of Faecal Char and Sawdust Char, Respectively, (c) FTIR Spectra, and (d) TGA(solid lines) and DTG (dash lines) Profiles at a Heating Rate of 5 °C/min from 30 to 800 °C Under Air

The main characteristic FTIR functional groups of faecal char, and sawdust char are shown in Figure 4.9c. There are some similarities between the spectra of these samples, and are mostly composed of hemicellulose, cellulose and lignin albeit with minor differences. Bands commonly associated with hemicellulose and cellulose are observed in the region between 3400 and 3000 cm^{-1} corresponding to –OH stretching due to moisture, while the peaks between 2922 and 2851 cm^{-1} may be assigned to aliphatic C–H stretching (Abdulrazzaq et al., 2014). The bands around 1700 cm^{-1} are typical of C=O stretching vibrations of unconjugated hemicellulose (de Figueredo et al., 2017), while the sharp band around 2981 cm^{-1} is due to the asymmetric stretching of CH_2 and CH of cellulose (Lun et al., 2017). The absorption bands in the region between 1600 and 1540

cm^{-1} are due to C=C skeletal stretching of the aromatic compounds (Keiluweit et al., 2010). The bands around 1026 cm^{-1} are associated with symmetric C–O stretching of cellulose, hemicellulose, and lignin (Liu et al., 2015). The bands in the region 850 – 755 cm^{-1} are credited to the out of plane deformation modes of aromatic C–H (Y. Liu et al., 2015). Some differences in the two samples are also noticeable. Specifically, the relative intensities of bands around 1600 and 1540 cm^{-1} are greater for sawdust char than for faecal char, attributable to high carbon content in the aromatic rings (Bonelli et al., 2003). A sharp C–O stretching band, and of high intensity is seen for faecal char around 1034 cm^{-1}, and is typical of carbohydrates or hemicellulose and cellulose (Afolabi et al., 2017). These results share a number of similarities with those observed for biochars derived from human faeces, grass, rice husk, and wood (Keiluweit et al., 2010; Abdulrazzaq et al., 2014; Afolabi et al., 2017).

The thermogravimetric analysis (TGA) and corresponding differential thermogravimetric (DTG) results shown in Figure 4.9d readily relates the weight loss to a given thermal breakdown temperature. To have a better insight into the mechanisms of the decomposition, a deconvolution of DTG values into individual peaks was performed. The decomposition process can be explained by three main components, (i) moisture release, (ii) liberation of hemicellulose and cellulose, and (iii) decomposition of lignin. According to Fig. 4.9d the TGA curves of the three samples followed the usual shape for biomass materials. In all the samples, most of the weight loss occurred between 250 and 550 °C, the temperature range typically associated with hemicellulose (220 – 315 °C), cellulose (315 – 420 °C), and lignin (420 – 550 °C) decomposition. Their characteristic temperatures are marked by peaks of the DTG curves. In most TGA studies, authors often neglect the first stage (<100 °C) because of very low moisture content. The faecal char, and sawdust char exhibited dissimilar TGA degradation curves, while their blend displayed a TGA profile very analogous to that of the faecal char. The blend, however, showed a slightly higher mass loss than the faecal char, which is an indication of synergistic interaction between sawdust char and faecal char. The decomposition process of sawdust shows very high mass loss due to high reactivity, while that of faecal char

and blend is lower, and is attributed to low volatile content and high ash content, in line with the proximate analysis. A slight weight loss due to moisture release is observed before reaching 100 °C for sawdust char, but the main thermal decomposition results in one major peak around 410 °C, corresponding to the simultaneous decomposition of hemicellulose and cellulose, whereas the existence of multi-component steps seen for faecal char and blend between 250 and 550 °C is credited to the co-operative release of hemicellulose, cellulose, and lignin. Raveendran et al. (1996) demonstrated that small amounts of volatiles from lignin component may also be given off in the second stage. It is here further observed that, the decomposition patterns of each sample involved multi-step reaction. This phenomenon can be explained by the complex nature of the samples since degradation patterns indicate overlapping zones of hemicellulose, cellulose, and lignin. These results corroborate FTIR data and are also concurrent with degradation of other biomasses found in the literature (Grønli et al., 2002; Shaaban et al., 2013; Abdulrazzaq et al., 2014).

4.3.2 Type of Purge Gas on Thermal Decomposition

Comparison of the TGA curves under air and nitrogen as the purge gases show noticeable difference between the two gases for each sample (Figure 4.10).

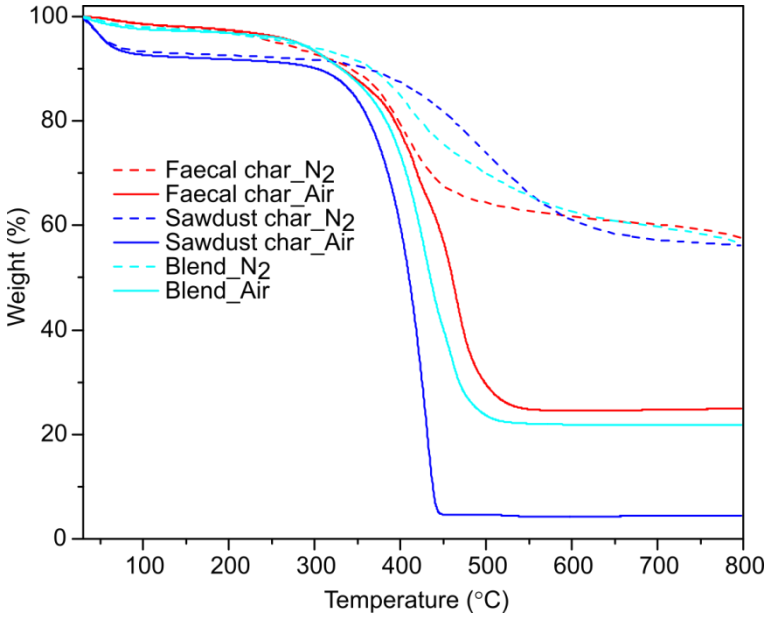

Figure 4.10: Thermal Behavior at a Heating Rate of 5 °C/min under Flowing N_2 and Air from 30 to 800 °C

When the samples are heated under air, a higher weight loss is seen than when heated under nitrogen. This could be due to chemical reactions occurring between oxygen and the volatiles present in the biomass. The reaction would result in more volatiles being liberated and therefore a larger amount of mass loss when using air as the purge gas. This lends support to previous works by Ma et al. (2018), and Chandrasekaran & Hopke (2012) on the thermal degradation of palm oil waste, and switch grass, respectively.

4.3.3 Effect of Variations of Heating Rate on Thermal Decomposition Properties

It is apparent that the thermal degradation process is dependent on the heating rate under air, i.e., when the heating rates were increased from 5 °C/min to 40 °C/min, the thermal decomposition process was slower (Figure 4.11). This is consistent with the work by (Heydari et al., 2015) on the thermal decomposition of lignite coal, and further supports the idea that a higher heating rate has a shorter decomposition time and the temperature needed for the sample to reach the same conversion will be higher. Thus, TGA and DTG curves are shifted towards higher temperature. Also, some individual small DTG peaks

at lower heating rates overlapped to form broader peaks at higher heating rates thereby degrading simultaneously. As discussed by Gai et al. (2013), a short reaction time is required at higher heating rates, therefore the temperature needed for the sample to decompose is also higher. Other researchers have attributed this phenomenon to less heat transfer among sample particle with increasing heating rate due to minimal time available for volatilization to occur (Chen et al., 2017; Zhang et al., 2019). Sittisun et al., (2015) noted that the reduced residence time at higher heating rate may be insufficient for heat transfer to permeate into the center of the tested sample thereby delaying the thermal decomposition process.

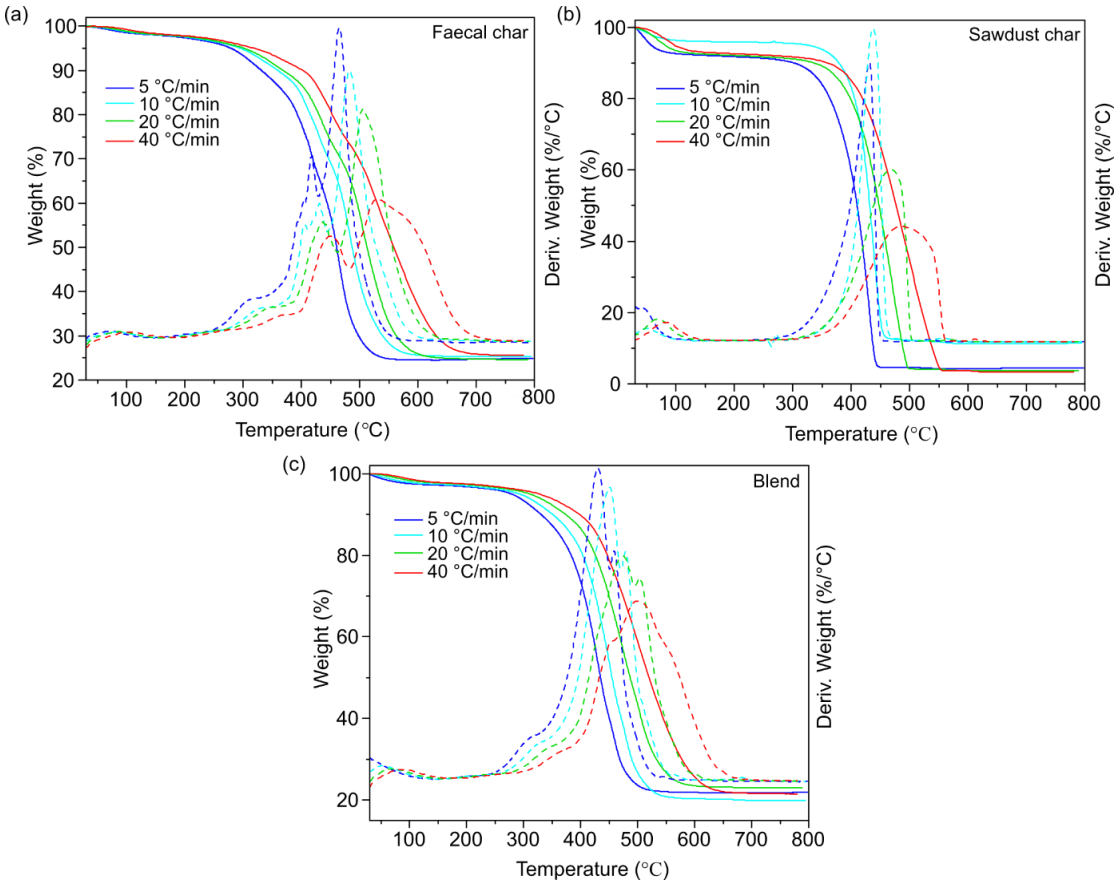

Figure 4.11: TGA (solid lines) and DTG (dash lines) Profiles of (a) Faecal Char, (b) Sawdust Char, and (c) Blend under Air with the Ramp Rates of 5, 10, 20, and 40 °C/min

4.3.4 Conversion Rate

The conversion curves shown in Figure 4.12 exhibit a theoretical temperature hysteresis, which is manifested as a curve shifting to a higher temperature region with increase in the heating rate without changing the thermal profile. This is an indication that during a thermal decomposition process, the overall reaction rate is only dependent on temperature (Lopez-Velazquez et al., 2013). Hence, combustion characteristic parameters shifted to higher values with elevated heating rates.

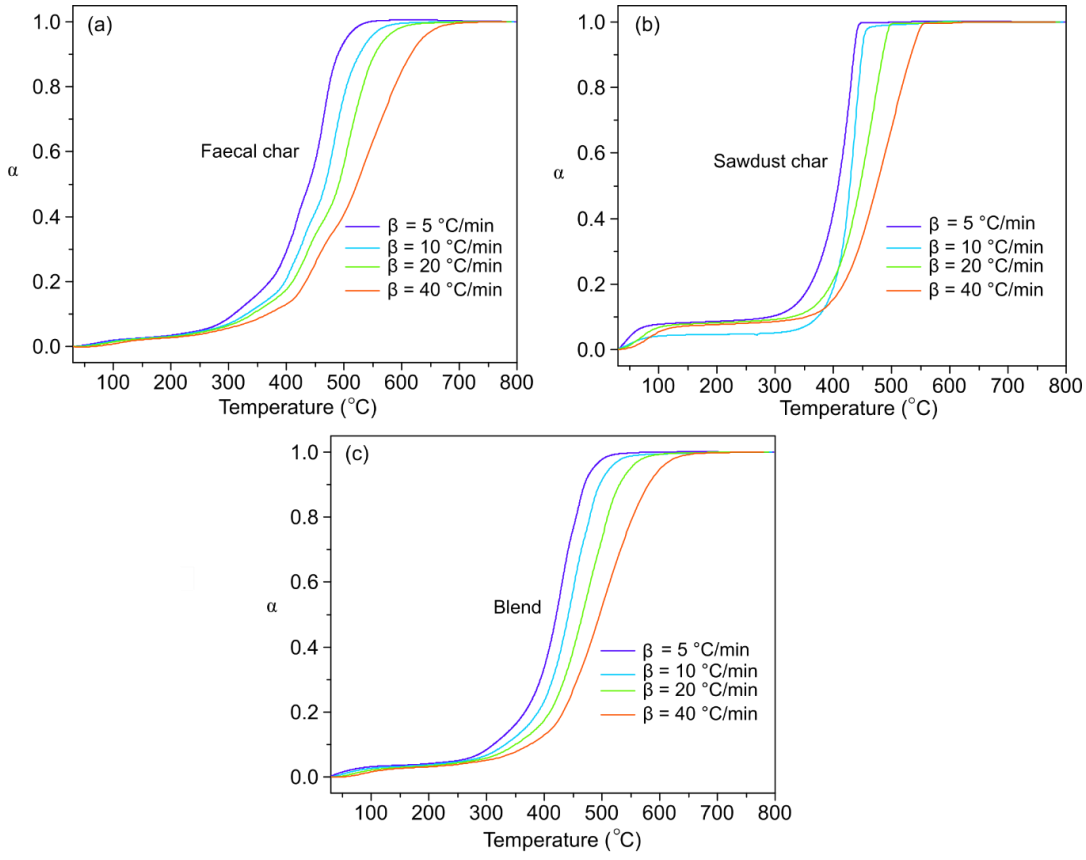

Figure 4.12: Conversion Curve of the Entire Reaction (a) Faecal Char, (b) Sawdust Char, and (c) Blend at Different Heating Rates (β)

4.3.5 Decomposition Kinetics

A number of successive and/or parallel reactions occur during the thermal breakdown of biomass making it a complicated process. Two iso-conversional methods, KAS, and FWO were employed to determine the decomposition kinetics during active decomposition step in the range $0.2 \leq \alpha \leq 0.9$ at four different heating rates (β), 5, 10, 20, and 40 °C/min (Figure 4.13).

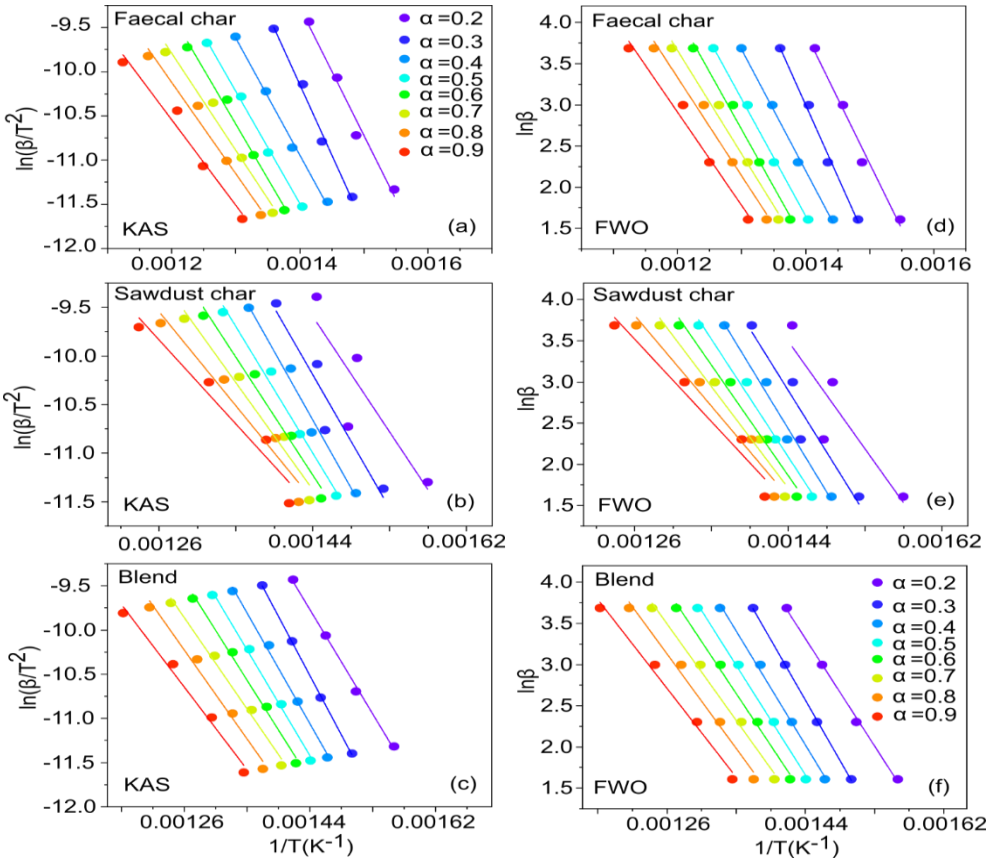

Figure 4.13: KAS (a-c) and FWO (d-f) Plots of Faecal Char, Sawdust Char, and Blend at Different Values of Conversion (α).

The activation energies (E_α) were extracted from the slopes of iso-conversional lines, -(E_α/R) in the KAS, and -1.052(E_α/R) in the FWO methods. The calculated E_α together with regression coefficients (R^2) for each α are summarized in Tables 4.15 and 4.16. The

two models agreed well with the experimental data over $0.2 \leq \alpha \leq 0.9$, for faecal char, and blend. However, for sawdust char the models could only fit 76.3% of the data at α = 0.2, and over 91% of the data at $\alpha > 0.2$. Sawdust char contained a significant amount of physisorbed moisture (~8 wt. %) as seen from the TGA results. Therefore, the energy absorbed at α = 0.2 was partly used for water release, whereas only decomposition of volatile matter occurred at $\alpha > 0.2$. Similarly, Chandrasekaran and Hopke (2012) observed in their study of kinetics of thermal decomposition of switch grass pellets, that iso-conversional model gave a good fit to the experimental data between a conversion range of 0 – 70%, beyond which the model deviated significantly from the experimental data. These authors, however, utilized a single step global reaction model to determine the kinetics rather than a multi-step reaction model.

Table 4.11: Activation Energies (Eα (kJ/mol)) Estimated for Faecal Char, Sawdust Char, and Blend using KAS Method at Different α

α	Faecal char		Sawdust char		Blend	
	E_α (kJ/mol)	R^2	E_α (kJ/mol)	R^2	E_α (kJ/mol)	R^2
0.2	120.5	0.979	109.8	0.763	109.2	0.998
0.3	132.6	0.992	127.0	0.914	123.8	0.999
0.4	110.2	0.996	129.9	0.979	115.8	0.996
0.5	105.6	0.997	120.2	0.987	110.7	0.996
0.6	102.9	0.991	111.9	0.980	104.2	0.994
0.7	91.3	0.979	101.7	0.968	95.6	0.991
0.8	85.9	0.979	89.5	0.951	93.1	0.986
0.9	80.4	0.973	80.0	0.942	86.4	0.986

Table 4.12: Activation Energies (Eα (kJ/mol)) Estimated for Faecal Char, Sawdust Char and Blend using FWO Method at Different α

α	Faecal char		Sawdust char		Blend	
	E_α (kJ/mol)	R^2	E_α (kJ/mol)	R^2	E_α (kJ/mol)	R^2
0.2	125.2	0.982	114.8	0.796	114.4	0.998
0.3	137.2	0.994	131.6	0.926	128.7	0.999
0.4	116.3	0.997	134.6	0.982	121.4	0.997
0.5	112.2	0.998	125.5	0.989	116.8	0.997
0.6	110	0.993	117.9	0.984	110.8	0.995
0.7	99.2	0.985	108.3	0.975	102.8	0.993
0.8	94.3	0.985	96.9	0.962	100.7	0.989
0.9	89.5	0.981	88.0	0.957	94.7	0.990

The trend of the lines presented in Figure 4.13, could be divided into two stages: α = 0.2 – 0.6, and α = 0.7 – 0.9 based on their parallelism. Thus, a two-step kinetic mechanism is applied to describe the thermal degradation of all the samples. Activation energy is considered as the minimum energy required to start a reaction, therefore higher activation energy values means that a reaction is more difficult to start. Between α = 0.2 – 0.6, the average activation energies, using KAS method were 114.4, 119.8 and 112.7 kJ/mol for faecal char, sawdust char, and blend, respectively. These values represent activation energies associated with the decomposition of hemicellulose and cellulose. On the other hand, the average activation energies during lignin decomposition, i.e., between α = 0.7 – 0.9, were 85.9, 90.4 and 91.7 kJ/mol for faecal char, sawdust char and the blend, respectively. Similar values were also found for average activation energies estimated using FWO method at the same α (Table 4.16). Such that, the average activation energies of faecal char were 120.2 kJ/mol between α = 0.2 – 0.6, whereas sawdust char, and blend had average activation energies of 124.9 and 118.4 kJ/mol, respectively. The activation energies between α = 0.7 – 0.9, were 94.3, 97.7 and 99.4 kJ/mol for faecal char, sawdust char, and blend, respectively. Evidently, the activation energy of the samples decreased in the second reaction step (α = 0.7 – 0.9). This remarkable difference can be rationalized by assuming that thermal decomposition starts with slower reactions and is independent of the heating rates. Overall, the two iso-

conversional methods yielded similar average activation energies and regression coefficients.

Independent of the method used, and for all the samples, the average E_α values were determined to be in the range of 105 – 135 kJ/mol, and 80 –105 kJ/mol for stages I (α = 0.2 – 0.6), and II (α = 0.7 – 0.9), respectively. These values align well with those in the literature for similar biomass materials. For instance, Grønli et al. (2002) contended that for both hard and soft woods, the *E* values ranged between 98 – 256 kJ/mol for hemicellulose and cellulose, and 46 kJ/mol for lignin. In their analysis of sewage sludge, and animal manure, Sanchez et al. (Sanchez et al., 2009) reported activation energy values of 146.4, and 143.3 kJ/mol, respectively. Yacob et al. (2018) concluded that *E* values for hemicellulose and cellulose components in dried human faeces ranged between 80 – 238 kJ/mol, while Urban and Antal (1982) identified average *E* values between 130 – 250 kJ/mol for the two components in undigested sludge. These authors, however, argued that the activation energies of human faeces are likely to be higher due to the presence of micro-organisms. Herein, human faeces were pyrolyzed to eliminate the effect of micro-organisms on the activation energies.

On the basis of the TGA data, the thermal degradation presented a multi-stage intricate reaction phenomenon in which a series of simultaneous complex reactions occurred. The decomposition of hemicellulose, cellulose, and lignin components ensued over a wide temperature range, 200 – 550 °C at 5 °C/min, with corresponding prominent FTIR bands in the range between 3400 – 755 cm^{-1}. The thermal reactivity of the samples was influenced by the heating rate. When two iso-conversional methods were used for kinetic analysis, an alteration in the activation energy with conversion degree was noticed for all the samples. Concerning the determination of activation energies, the degradation regions were split into two stages. The average activation energy for stage-I during active decomposition was found to be in the range of 105 – 135 kJ/mol, while stage-II had average activation energy between 80 – 105 kJ/mol from both KAS and FWO models. We accentuate that, the activation energy values varied greatly with α, particularly in stage-I (α = 0.2 – 0.6) than in stage-II (α = 0.7 – 0.9). This variation is a

signature of heterogeneous nature of solid wastes, which leads to a complex mechanism involving parallel, competitive, and complex reaction schemes. The higher E_α value in the region $0.2 \leq \alpha \leq 0.6$ means that on average more energy is required in the combustion process of hemicellulose and cellulose than for lignin.

Noteworthy, is that quantitative analysis of TG–MS and FTIR of gaseous products evolved during the pyrolysis of sewage sludge (Hernández et al., 2017), and agricultural residues (corn brakes, wheat straw, and hazelnut shell) (Manić et al., 2019) have been published by other researchers, but were not performed in the current study. Nevertheless, we can draw comparisons with the previous findings provided in the literature. For instance thermal decomposition of human faeces occur between 200 and 650 °C, and leads to the emission of H_2O, CH_4, C_2H_6, CO_2, and CO (Yacob et al., 2018). Most of these gaseous species, especially the latter two are mainly dominant below 350 °C, and may have been eliminated during pyrolysis in this study. These gases are evolved due to the decomposition of bound water, hemicellulose, cellulose, and lignin, and could be beneficial in distinguishing the thermal decomposition stages during combustion.

4.4 Emission Properties of Briquettes Densified from Pyrolyzed Human Faeces, Sawdust Char and their Blend

4.4.1 Proximate Analysis Results and Heating Values of Briquettes and Charcoal

The major parameters; volatile matter (VM) , fixed carbon (FC), ash content (ASH), moisture content (MC), and gross calorific value (GCV) used to assess the quality of solid fuels depicts that charcoal made from acacia tree can liberate more heat, and produce less ash making it a better fuel compared to the briquettes produced in this study (Table 4.13).

Table 4.13: Proximate Analysis Results and Heating Values of Briquettes and Charcoal

Fuel Source	Proximate Analysis				Heating Value (MJ/kg)
	VM	**FC**	**ASH**	**MC**	**GCV**
Briquette	16.9±0.1	62.7±0.4	12.3±0.5	7.1 ±0.6	19.8±0.1
Charcoal	14.4±0.3	76.2±0.1	4.2±0.2	5.2±0.2	25.7±0.2

The higher gross calorific value of charcoal could be due to its higher fixed carbon content (Bulmau et al., 2010). Moreover, biomass fuels with low ash content have higher calorific values since the amount of heat absorbed by the inorganic fraction in ash is reduced (Hafford et al., 2018). Other studies (Carnaje et al., 2018; Saeed et al., 2021) have reported that solid fuels with lower moisture content have larger voids/pores which allow easy diffusion of oxygen from air to sustain better combustion in solid fuels consequently releasing more heat. Nevertheless, despite the briquettes having lower fixed carbon content, high moisture content, and higher ash content which lowers the calorific value of solid fuels, the reported value of 19.8 MJ/kg is comparable to 19–25 MJ/kg of wood fuel (Bulmau et al., 2010) and hence it can still provide net benefit during combustion.

Solid fuels of higher volatile matter content ignites faster (Kabok et al., 2018) and therefore, they are desirable. However, higher moisture reduces the speed of ignition of briquettes thereby necessitating pre-drying before combustion or co-combustion of briquettes with charcoal particles or wooden sticks so as to initiate the combustion process (Ngusale et al., 2014). Pre-drying may however not be practical during rainy seasons. The higher moisture content in the briquettes produced in this study could have been contributed by molasses due to its hygroscopic nature as a result of the fructose content (Davis, 1995; Palmonari et al., 2020).

4.4.2 Elemental Composition of Human Faecal Char, Sawdust Char, and Molasses

Table 4.14 presents the elemental composition of the main materials (faecal char and sawdust char) used in the briquette production. Properties of cane molasses reported in previous studies are also presented.

Table 4.14: Elemental Composition of Human Faecal Char, Sawdust Char, and Molasses

Feedstock	Pyrolysis Temp (°C)	%C	%H	%N	%S	%O	References
Human faeces	350	55.3	5.8	3.1	–	35.8	This study
Cyprus wood sawdust	350	78.2	4.6	1.1	–	16.1	This study
Cane molasses		37.9	5.2	0.5	1.4	42.6	(Dirbeba et al., 2021)
Cane molasses		47.40	7.87	2.63	0.33	41.97	(Zhai et al., 2018)

Pyrolysis of biomass materials increases their carbon content (Li et al., 2017) which consequently increases their calorific values (Bulmau et al., 2010). Faecal char had lower carbon content than sawdust char and therefore blending the two materials could produce a solid fuel with higher calorific value than faecal char. The nitrogen content in faecal char was also observed to be higher compared to sawdust char, a property that can be attributed to the presence of proteins in faeces that constitute the larger fraction of nitrogenous compounds in faecal mass (Rose et al., 2015). Nitrogen content in human faeces can however be significantly reduced by increasing pyrolysis temperature which consequently results in the degradation of proteins (Spitzer et al., 2018). It was also noted that sulphur content in faecal char and sawdust char are negligible which makes them safe in terms of sulphur emission during combustion. Although the study did not characterize molasses, other researchers (Zhai et al., 2018; Dirbeba et al., 2021) have reported that molasses contains sulphur and therefore it could be a contributor of sulphur containing gases during combustion of briquettes produced in this study.

4.4.3 Concentration of Flue Gases from Combustion of Charcoal and Co-combustion of Charcoal with Faecal Char-Sawdust Char Briquettes

The profile of flue gases emitted against combustion time presented in Figure 4.14, shows a rise in amount of flue gases liberate upto a peak followed by a gradual decline. The sudden rise in the amount of gases after the declining phase in both set-ups is as a result of the shaking of the cook stove so as to shed off the incombustible ash fraction that accumulated on the surface of the solid fuel during combustion, consequently allowing more heat and gases to be liberated. It was also observed that there was no emission of NO during combustion of charcoal. In addition, whereas H_2S emission profile showed short lived peaks during charcoal combustion, there was continuous liberation of the gas throughout the co-combustion of charcoal with briquettes.

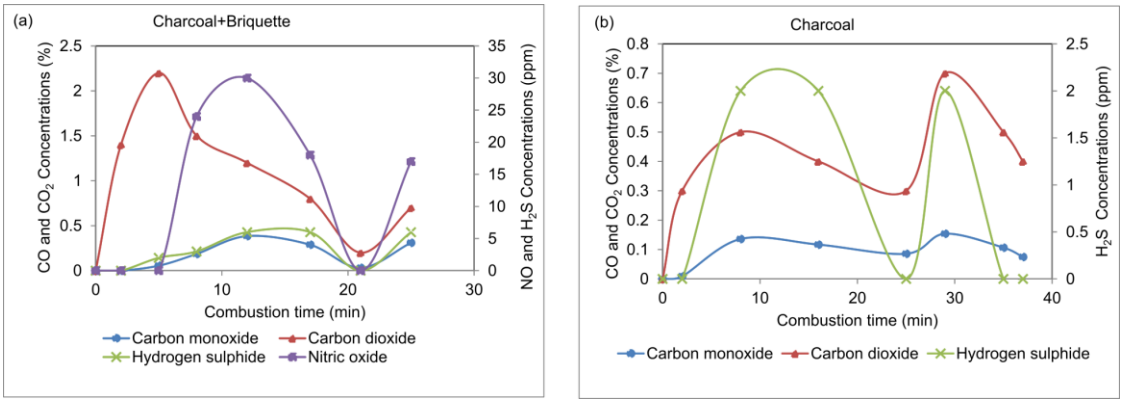

Figure 4.14: (a) Emissions from Co-combustion of Charcoal with Faecal Char-Sawdust Char Briquettes, and (b) Emissions from Combustion of Charcoal

CO_2 results from complete combustion of fuel and therefore it is not regarded as a pollutant while CO which is a product of incomplete combustion, is toxic to human health (EPA, 2002; Townsend & Maynard, 2002). The amount of CO and CO_2 released during combustion is influenced by a range of factors. For instance, Kim et al. (2021) in their attempt to compare emission from different briquettes attributed the lower CO and CO_2 emission from combustion of briquettes densified from spent coffee grounds to their less carbon content (46.1–54.9 wt. %) compared to the anthracite briquettes (75.23

wt. %). High moisture content in biomass fuel also reduces oxidation reactions during combustion hence significantly increasing CO emission while CO_2 emission slightly declines due to the reduced dry biomass per kg of the fuel (Bhattacharya et al., 2002). Thus, the higher moisture content of the briquettes could have contributed to the higher CO emission during co-combustion with charcoal. Both combustion of the charcoal and co-combustion of charcoal with briquettes caused CO concentrations above the critical limit of 35 ppm allowed for human exposure for one hour (EPA, 2002). It can be recommended that proper ventilation is necessary when the fuels are used for indoor heating to enhance oxidation of the carbon content in fuel.

Liberation of H_2S during fuel combustion has been reported to be as a result of reduction of SO_2 that is formed due to oxidation of compounds containing sulphur in the fuel. For instance, Shirai et al. (2013) observed that during coal combustion in a furnace, SO_2 released reacts with H_2 to form H_2S and H_2O as shown by the reaction Equation 4.3 given as:

$$SO_2 + 3H_2 = H_2S + 2H_2O \tag{4.3}$$

Study by Ryason & Harkins (1967), also reported that the SO_2 in flue gases released during coal combustion in a furnace reacts with carbon monoxide to form CO_2 and elemental sulphur as depicted in Equation 4.4

$$2CO + SO_2 = 2CO_2 + \frac{1}{2}S \tag{4.4}$$

Based on WHO short term (30 minutes), H_2S odour guidelines (WHO, 1981), it can be stated that combustion of faecal char-sawdust char briquettes could cause more discomfort throughout the combustion duration by liberating offensive odours since H_2S concentration was > 0.005 ppm. Moreover, the briquettes could cause other health effects such as coughs, throat irritation and low oxygen uptake as had been reported by

Bhambhani & Singh (1991) since the emission was above 2.5 ppm. Apart from health effects, H_2S poses a challenge of corrosion of metal wares (Malone Rubright et al., 2017).

Nitric oxides (NO) are mainly formed during combustion of solid fuels as a result of oxidation of the organic nitrogen (fuel-N) that they contain (Aho et al., 1995; Zevenhoven & Kilpinen, 2001). Prompt NO and thermal NO may also form from atmospheric molecular nitrogen (N_2) during combustion. However according to Hayhurst & Lawrence (1996), formation of prompt NO which normally result from reaction between N_2 and hydrogen radicals from the fuel is small. The formation of thermal NO on the other hand occurs at very high temperatures (≥1300 °C), since thermal dissociation of N_2 to N radicals is needed to start NO formation (Saastamoinen & Leino, 2019). The highest temperature (475 °C) attained during the co-combustion of briquettes with charcoal in this study could not result in the release of thermal NO. The briquettes therefore released NO majorly as a result of oxidation of the organic nitrogen contained in the faecal char. According to NIOSH exposure limits, it can be reported that no immediate health hazard due to NO can be posed by combusting the briquettes produced in this study since the peak emission of 30 ppm recorded was < 100 ppm (Schieb, 1976). It is also worth noting that although oxygen was measured in the flue gases, oxidation of NO to NO_2 gas was not observed. Formation of NO_2 requires reaction between hydrogen peroxide radical (HO_2) and NO which can only occur when in the cooler zones of the flame or when rapid cooling of the flame occurs (Aho et al., 1995; Glarborg et al., 2018; Zevenhoven & Kilpinen, 2001). Furthermore, NO_2 rapidly decomposes back to NO if it moves to the hot parts of the flame (Aho et al., 1995). Cooling process does not exist in a furnace or in the experimental set-up adopted in this study and thus possibly the reason as to why NO_2 wasn't detected. NO_2 is therefore mostly formed under normal ambient conditions in the atmosphere (Saastamoinen & Leino, 2019)

A summary of the comparison of flue gases quality during combustion of charcoal and in co-combustion of charcoal with briquettes against the permissible short term exposure

limit guidelines set by the Environmental Protection Agency (EPA), World Health Organization (WHO), and National Institute for Occupational Safety and Health (NIOSH) is presented in Table 4.15.

Table 4.15: Comparison of Flue Gases Quality during Combustion of Fuels

Chemical species	Maximum limit of Conc. (ppm)	Short term duration of exposure (min)	Charcoal	Charcoal + Briquettes	Standards	References
CO	35	60	90 –1539	316 –3845	EPA	(EPA, 2002)
NO	>100	30	0	0 –30	NIOSH	(Schieb, 1976)
H_2S	>0.005	30	0 –2	0 – 6	WHO	(WHO, 1981)

Total duration of monitoring combustion of charcoal, and co-combustion of charcoal with briquettes was 37, and 25 min, respectively.

4.4.4 Variation of Flue Gases Temperatures with Combustion Time

The thermal profile depicted during combustion of charcoal and co-combustion of charcoal with briquettes is presented in Figure 4.15.

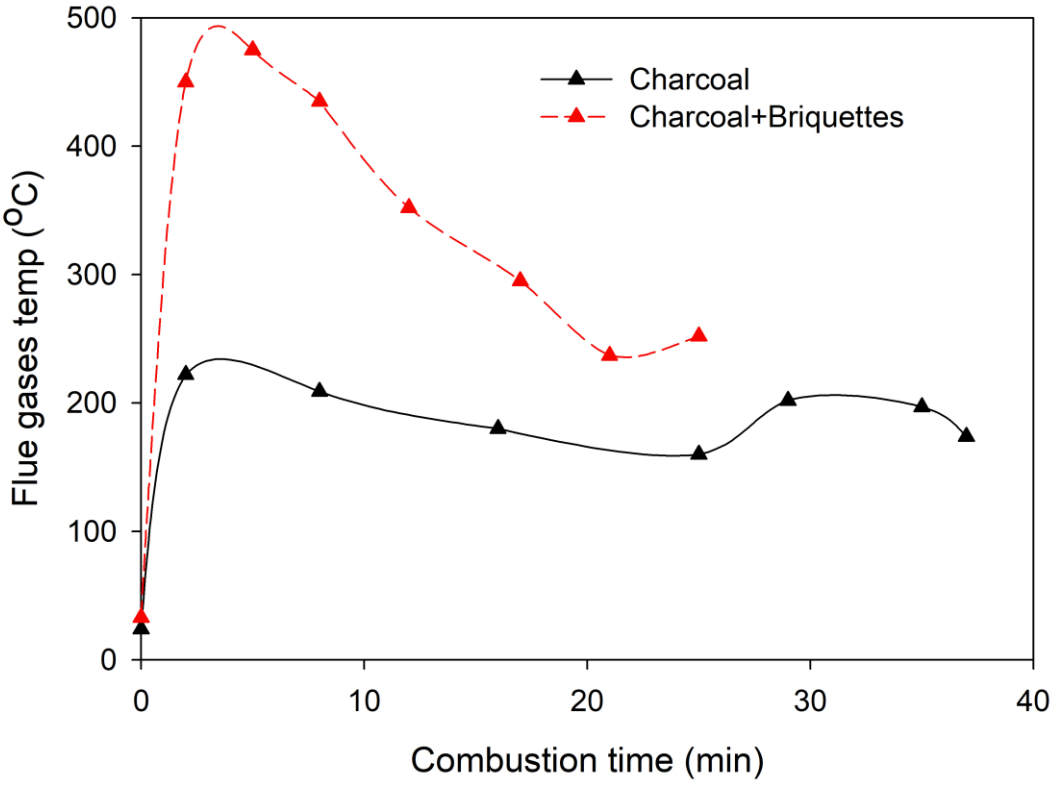

Figure 4.15: Variation of Flue Gases Temperatures with Combustion Time

It can be seen from Figure 4.15 that after ignition, a sudden rise in temperature of flue gases occurs for both combustion set ups followed by a sharp decline in temperature and finally a gradual temperature loss as combustion proceeds towards the end. Al-Shemmeri et al.(2015) made similar observation in a study on combustion of various biomass fuels in a small-scale biomass combustor. The authors attributed the sudden rise in temperature of flue gases upto a peak to the combustion of volatile gases, which is immediately followed by a reduction in the calorific content of the fuel resulting to the sharp decline in the flue gases temperature since they are carriers of the significant proportion of the heat liberated during combustion. The authors further explained that the gradual decline in temperature of flue gases after the combustion of volatile gases as the fuel diminishes is associated with oxidation of char which is a slow process

compared to rate of combustion of volatile gases, resulting in longer periods of combustion before the formation of ash. Other studies (Borowski et al., 2017; Pilusa et al., 2013) with similar thermal profile obtained during combustion of briquettes ascribed the variations in the heat content of the flue gases during combustion of the fuels to heterogeneous complex reactions occurring during combustion of biomass materials. It was also evident that the peak temperature (475 °C) of flue gases liberated during co-combustion of briquettes with charcoal was higher compared to 222 °C attained during combustion of charcoal. This is an indication that synergistic complex thermochemical interactions occur during biomass co-combustion. Statistical test of the means of the temperatures of the flue gases liberated using notched box plot (Figure 4.16a) showed that there existed significant ($P<0.05$) differences during combustion in both set-ups which depicts that co-combustion of briquettes with charcoal enhanced the amount of heat released.

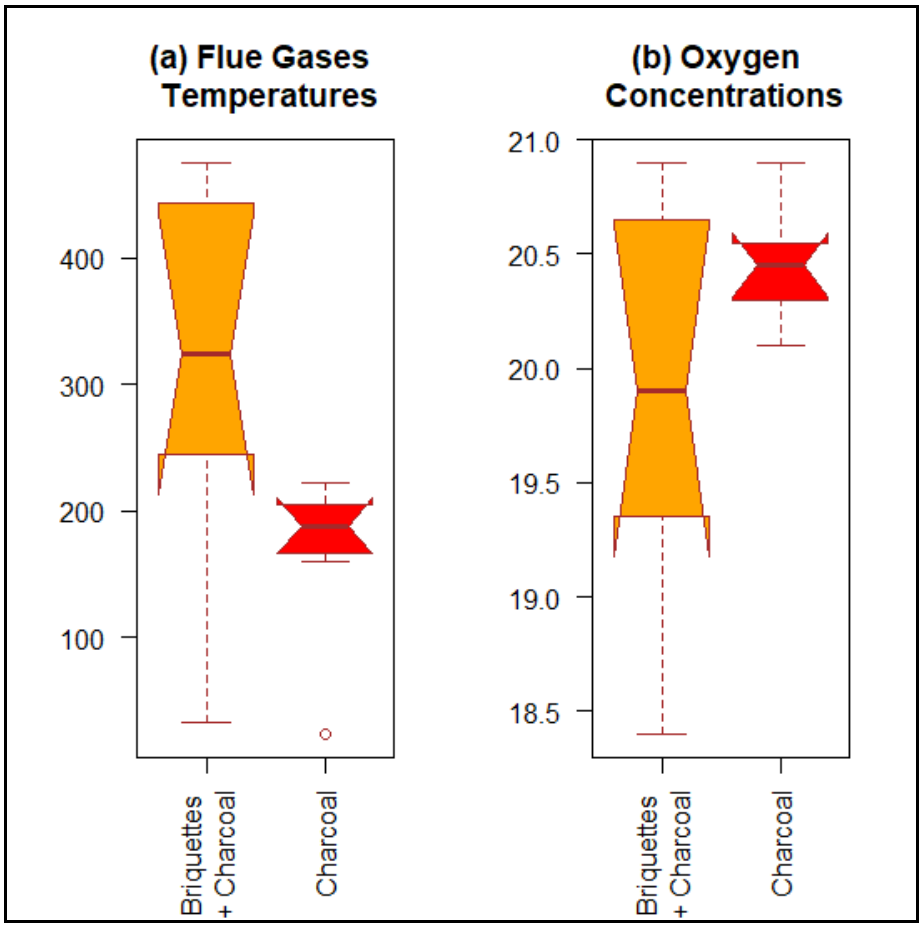

Figure 4.16: Notched Box Plots of (a) Flue Gases Temperatures During Co-combustion of Briquettes with Charcoal and Combustion of Charcoal, (b) Oxygen Concentrations During Co-combustion of Briquettes with Charcoal and Combustion of Charcoal.

4.4.5 Variation of Oxygen Concentration with Combustion Temperatures of Flue Gases

Variation of oxygen concentration with combustion temperatures of flue gases is presented in Figure 4.17.

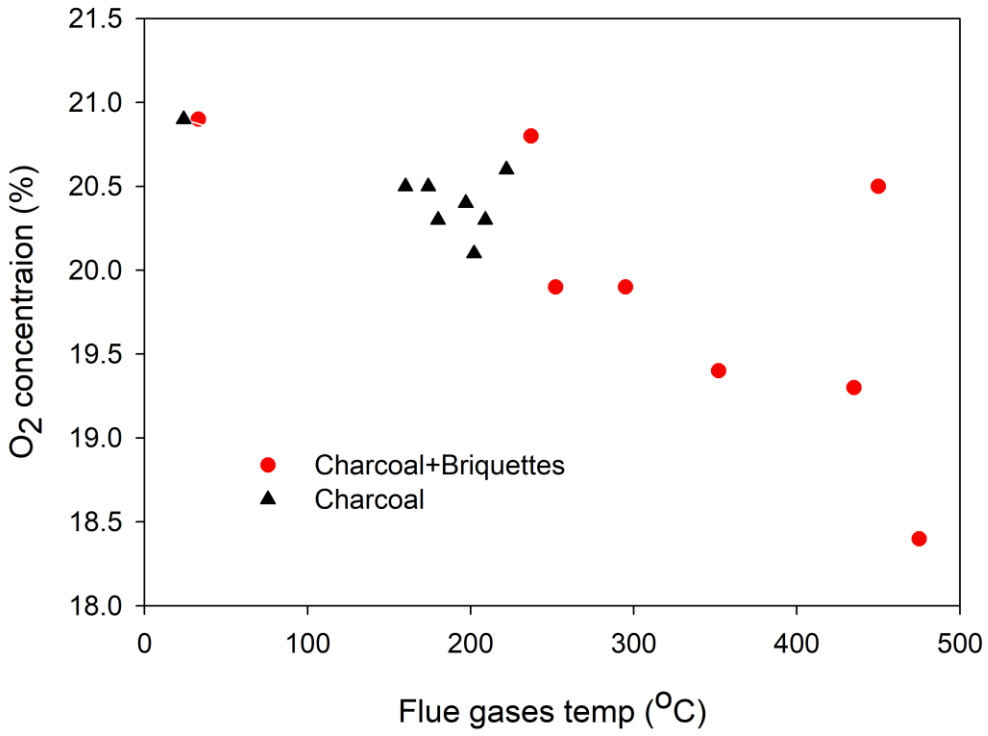

Figure 4.17: Variation of Flue Gases Temperatures with Oxygen Concentrations

From the Figure 4.17, a decline in O_2 concentration in the flue gases occurred with increase in temperature. Oxidation of hydrocarbons to form gases is an exothermic process (Ren et al., 2019) therefore, higher oxygen consumption resulted in higher heat energy content liberated and which are consequently carried by the flue gases in the chimney. Similar observation was reported from combustion of eco-fuel briquettes (Pilusa et al., 2013). An increase in O_2 concentration in flue gases is expected as the fuel combustion nears completion since most hydrocarbons will have been oxidised. Statistically, the means of the oxygen concentrations in the flue gases at different temperatures in both set-ups were not significantly ($P>0.05$) different as depicted by the notched box plot (Figure 4.16b). This suggests that co-combustion of briquettes with charcoal is beneficial in the provision of higher heat energy than combustion of charcoal without consuming significantly higher amounts of oxygen.

CHAPTER FIVE

CONCLUSIONS AND RECOMMENDATIONS

5.1 Conclusions

Based on the results and findings presented in this thesis, the following conclusions can be made:

i. Pineapple peel biochar can effectively recover ammonium nitrogen from human urine with an adsorption capacity of 13.40 mg/g, but it exhibits a tendency of adsorbing phosphorous from human urine and gradually releasing it into the solution thereby not attaining equilibrium. On the other hand, lateritic soil can effectively adsorb both ammonium nitrogen and phosphorous from human urine, with an adsorption capacity of 10.73 and 45.25 mg/g, respectively.

ii. Response surface methodology can be used to effectively optimize the amount of ammonium nitrogen adsorbed on pineapple peel biochar from human urine to 34.42 mg/g, and phosphorous adsorbed on lateritic soil from human urine to 112.80 mg/g, with contact time, adsorbent loading and agitation speed significantly ($P<0.05$) influencing the adsorption process.

iii. Human faecal char have higher thermal stability and ash content (~ 23 wt.%) than sawdust char and their blend, with sawdust char being the most reactive and thus having lower ash content (~ 6 wt.%). Also the activation energies of the different organic components (hemicellulose, cellulose and lignin) in all the samples were different, an indication of parallel, competitive and complex reaction schemes during thermal decomposition of biomass materials.

iv. Briquettes densified from pyrolyzed human faeces, sawdust char and molasses does not cause respiratory irritation and other associated health impacts of nitric oxides since the amount of nitric oxides liberated was below

dangerous exposure limit of 100 ppm, while it can cause odor discomfort since the hydrogen sulphide liberated was above exposure limit of 0.005 ppm. Also, the carbon monoxide released was above the exposure limit of 35 ppm an indication that combustion of the briquettes should be done in a well ventilated room.

v. Emission of nitric oxides (NO) during combustion of briquettes densified from human faecal char, sawdust char, and molasses is below the dangerous exposure limit of 100 ppm set by the National Institute for Occupational Safety and Health, while the carbon monoxide (CO), and hydrogen sulphide (H_2S) is above short term exposure limits of 35 ppm, and 0.005 ppm, respectively, as set by Environmental Protection Agency, and World Health Organisation, respectively.

5.2 Recommendations

Based on the results presented in this thesis, the following recommendations can be made:

5.2.1 Recommendations for Application

i. Pineapple peel biochar and lateritic soils should be enriched with ammonium nitrogen and phosphorous from human urine to produce slow release fertilizers or a medium for crop production so as to manage the pineapple peel wastes in the environment and also to utilize lateritc soils for agricultural production.

ii. Pyrolyzed human faeces should be blended with pyrolyzed sawdust to lower the input energy require to initiate its thermal decomposition and also lower its ash content.

iii. Utilization of binders with no sulphur content is recommended for production of briquettes from human faecal char and sawdust char so as to avoid emission of sulphur containing gases during combustion.

iv. Combustion of solid fuels for domestic cooking and heating should be conducted in a well-ventilated room to reduce the amount of carbon monoxide released by enhancing complete oxidation of carbon content.

5.2.2 Recommendations for Further Research

i. Pot experiments should be conducted on the studied materials when enriched with human urine to monitor their effectiveness in releasing the adsorbed nutrients for crop use and their influence on the physicochemical properties of the soil.
ii. Thermogravimetric analysis studies should focus on the effect of blending ratio of faecal char with other carbonized waste streams to determine their effect on reduction of ash content.
iii. Alternative binders (organic, inorganic or composite) with minimal effect on increasing moisture content of briquettes upon heating should be research on to ease their ignition without need to co-combust with charcoal particles or sticks or to pre-dry them.
iv. Level of emission of CO, NO and H_2S during combustion of briquettes should be compared when different binder materials are used.

REFERENCES

Abdulrazzaq, H., Jol, H., Husni, A., & Abu-Bakr, R. (2014). Characterization and Stabilisation of Biochars Obtained from Empty Fruit Bunch, Wood, and Rice Husk. *BioResources*, *9*(2), 2888–2898. https://doi.org/10.15376/biores.9.2.2888-2898

Afolabi, O. O. D., Sohail, M., & Thomas, C. L. P. (2017). Characterization of solid fuel chars recovered from microwave hydrothermal carbonization of human biowaste. *Energy*, *134*, 74–89. https://doi.org/10.1016/j.energy.2017.06.010

Aghoghovwia, M. P., Hardie, A. G., & Rozanov, A. B. (2020). Characterisation, adsorption and desorption of ammonium and nitrate of biochar derived from different feedstocks. *Environmental Technology (United Kingdom)*, *0*(0), 1–14. https://doi.org/10.1080/09593330.2020.1804466

Aguko Kabok, P., Nyaanga, D. M., Mbugua, J. M., & Eppinga, R. (2018). Effect of Shapes, Binders and Densities of Faecal Matter - Sawdust Briquettes on Ignition and Burning Times. *Journal of Petroleum & Environmental Biotechnology*, *09*(02). https://doi.org/10.4172/2157-7463.1000370

Ahmad, M., Rajapaksha, A. U., Lim, J. E., Zhang, M., Bolan, N., Mohan, D., Vithanage, M., Lee, S. S., & Ok, Y. S. (2014). Biochar as a sorbent for contaminant management in soil and water: A review. *Chemosphere*, *99*, 19–33. https://doi.org/10.1016/j.chemosphere.2013.10.071

Aho, M. J., Paakkinen, K. M., Pirkonen, P. M., Kilpinen, P., & Hupa, M. (1995). The effects of pressure, oxygen partial pressure, and temperature on the formation of N2O, NO, and NO2 from pulverized coal. *Combustion and Flame*, *102*(3), 387–400. https://doi.org/10.1016/0010-2180(95)00019-3

Akahira, T .; Sunose, T. (1971). Method of determining activation deteriorationconstant of electrical insulating materials. *Research Report Chiba Institute of Technology*

(Science Technology), *16*, 22–31.

Akowuah, J. O., Kemausuor, F., & Mitchual, S. J. (2012). Physico-chemical characteristics and market.pdf. *International Journal of Energy and Environmental Engineering*, *3*(20), 1–6.

Al-Shemmeri, T. T., Yedla, R., & Wardle, D. (2015). Thermal characteristics of various biomass fuels in a small-scale biomass combustor. *Applied Thermal Engineering*, *85*, 243–251. https://doi.org/10.1016/j.applthermaleng.2015.03.055

Alberti, G., Amendola, V., Pesavento, M., & Biesuz, R. (2012). Beyond the synthesis of novel solid phases: Review on modelling of sorption phenomena. *Coordination Chemistry Reviews*, *256*(1–2), 28–45. https://doi.org/10.1016/j.ccr.2011.08.022

Alhashimi, H. A., & Aktas, C. B. (2017). Life cycle environmental and economic performance of biochar compared with activated carbon: A meta-analysis. *Resources, Conservation and Recycling*, *118*, 13–26. https://doi.org/10.1016/j.resconrec.2016.11.016

Ali, I., Asim, M., & Khan, T. A. (2012). Low cost adsorbents for the removal of organic pollutants from wastewater. *Journal of Environmental Management*, *113*, 170–183. https://doi.org/10.1016/j.jenvman.2012.08.028

Altun, N. E., Hicyilmaz, C., & Kök, M. V. (2001). Effect of different binders on the combustion properties of lignite - Part I. Effect on thermal properties. *Journal of Thermal Analysis and Calorimetry*, *65*(3), 787–795. https://doi.org/10.1023/A:1011915829632

American Society for Testing and Materials. (1984). Standard test method for chemical analysis of wood charcoal - designation: D1762 - 84 (Reapproved 2007). *Annual Book of ASTM Standards*, *84*(2), 292–293. https://doi.org/10.1520/D1762-84R07.2

Antonini, S., Nguyen, P. T., Arnold, U., Eichert, T., & Clemens, J. (2012). Solar thermal evaporation of human urine for nitrogen and phosphorus recovery in Vietnam. *Science of the Total Environment*, *414*, 592–599.

Aransiola, E. F., Oyewusi, T. F., Osunbitan, J. A., & Ogunjimi, L. A. O. (2019). Effect of binder type, binder concentration and compacting pressure on some physical properties of carbonized corncob briquette. *Energy Reports*, *5*, 909–918. https://doi.org/10.1016/j.egyr.2019.07.011

Asamoah, B., Nikiema, J., Gebrezgabher, S., Odonkor, E., & Njenga, M. (2016). *RESOURCE RECOVERY & REUSE SERIES 7 Fuel Briquettes*. International Water Management Institute.

Atwijukye, O., Kulabako, R., Niwagaba, C., & Sugden, S. (2018). Low cost faecal sludge dewatering and carbonisation for production of fuel briquettes. *41st WEDC International Conference*, *Srep 2014*, 1–7.

Avelar, N. V., Rezende, A. A. P., Carneiro, A. de C. O., & Silva, C. M. (2016). Evaluation of briquettes made from textile industry solid waste. *Renewable Energy*, *91*, 417–424. https://doi.org/10.1016/j.renene.2016.01.075

Ayawei, N., Ebelegi, A. N., & Wankasi, D. (2017). Modelling and Interpretation of Adsorption Isotherms. *Journal of Chemistry*, *2017*. https://doi.org/10.1155/2017/3039817

Bai, X., Li, Z., Zhang, Y., Ni, J., Wang, X., & Zhou, X. (2018). Recovery of Ammonium in Urine by Biochar Derived from Faecal Sludge and its Application as Soil Conditioner. *Waste and Biomass Valorization*, *9*(9), 1619–1628. https://doi.org/10.1007/s12649-017-9906-0

Ban, Z. S., & Dave, G. (2004). Laboratory studies on recovery of n and p from human urine through struvite crystallisation and zeolite adsorption. *Environmental Technology (United Kingdom)*, *25*(1), 111–121. https://doi.org/10.1080/09593330409355443b

Bassan, M., Koné, D., Mbéguéré, M., Holliger, C., & Strande, L. (2015). Success and failure assessment methodology for wastewater and faecal sludge treatment projects in low-income countries. *Journal of Environmental Planning and Management*, *58*(10), 1690–1710. https://doi.org/10.1080/09640568.2014.943343

Behrendt, J., Arevalo, E., Gulyas, H., Niederste-Hollenberg, J., Niemiec, A., Zhou, J., & Otterpohl, R. (2002). Production of value added products from separately collected urine. *Water Science and Technology*, *46*(6–7), 341–346. https://doi.org/10.2166/wst.2002.0698

Beler-Baykal, B., Bayram, S., Akkaymak, E., & Cinar, S. (2004). Removal of ammonium from human urine through ion exchange with clinoptilolite and its recovery for further reuse. *Water Science and Technology*, *50*(6), 149–156. https://doi.org/10.2166/wst.2004.0371

Bezerra, M. A., Santelli, R. E., Oliveira, E. P., Villar, L. S., & Escaleira, L. A. (2008). Response surface methodology (RSM) as a tool for optimization in analytical chemistry. *Talanta*, *76*(5), 965–977. https://doi.org/10.1016/j.talanta.2008.05.019

Bhambhani, Y., & Singh, M. (1991). Physiological effects of hydrogen sulfide inhalation during exercise in healthy men. *Journal of Applied Physiology*, *71*(5), 1872–1877.

Bhattacharjee, A., Jana, B. B., Mandal, S. K., Lahiri, S., & Bhakta, J. N. (2021). Assessing phosphorus removal potential of laterite soil for water treatment and eco-technological application. *Ecological Engineering*, *166*(April), 106245. https://doi.org/10.1016/j.ecoleng.2021.106245

Bhattacharya, S. C., Albina, D. O., & Khaing, A. M. (2002). Effects of selected parameters on performance and emission of biomass- red cookstoves. *Biomass and Bioenergy*, *23*(2002), 387 – 395.

Bischel, H. N., Özel Duygan, B. D., Strande, L., McArdell, C. S., Udert, K. M., & Kohn, T. (2015). Pathogens and pharmaceuticals in source-separated urine in eThekwini, South Africa. *Water Research*, *85*, 57–65. https://doi.org/10.1016/j.watres.2015.08.022

Bonelli, P. R., Cerrella, E. G., & Cukierman, A. L. (2003). Slow pyrolysis of nutshells: Characterization of derived chars and of process kinetics. *Energy Sources*, *25*(8), 767–778. https://doi.org/10.1080/00908310390207819

Bonvin, C., Etter, B., Udert, K. M., Frossard, E., Nanzer, S., Tamburini, F., & Oberson, A. (2015). Plant uptake of phosphorus and nitrogen recycled from synthetic source-separated urine. *Ambio*, *44*(2), 217–227. https://doi.org/10.1007/s13280-014-0616-6

Borowski, G., Stępniewski, W., & Wójcik-Oliveira, K. (2017). Effect of starch binder on charcoal briquette properties. *International Agrophysics*, *31*(4), 571–574. https://doi.org/10.1515/intag-2016-0077

Bu, Q., Lei, H., Wang, L., Wei, Y., Zhu, L., Zhang, X., Liu, Y., Yadavalli, G., & Tang, J. (2014). Bio-based phenols and fuel production from catalytic microwave pyrolysis of lignin by activated carbons. *Bioresource Technology*, *162*, 142–147. https://doi.org/10.1016/j.biortech.2014.03.103

Bulmau, C., Mărculescu, C., Badea, A., & Apostol, T. (2010). Pyrolysis parameters influencing the bio-char generation from wooden biomass. *UPB Scientific Bulletin, Series C: Electrical Engineering*, *72*(1), 29–38.

Cantrell, K. B., Hunt, P. G., Uchimiya, M., Novak, J. M., & Ro, K. S. (2012). Impact of pyrolysis temperature and manure source on physicochemical characteristics of biochar. *Bioresource Technology*, *107*, 419–428. https://doi.org/10.1016/j.biortech.2011.11.084

Carnaje, N. P., Talagon, R. B., Peralta, J. P., Shah, K., & Paz-Ferreiro, J. (2018). Development and characterisation of charcoal briquettes from water hyacinth (Eichhornia crassipes)-molasses blend. *PLoS ONE*, *13*(11), 1–14. https://doi.org/10.1371/journal.pone.0207135

Ceylan, Z., & Sungur, B. (2020). Estimation of coal elemental composition from proximate analysis using machine learning techniques. *Energy Sources, Part A: Recovery, Utilization and Environmental Effects*, *42*(20), 2576–2592. https://doi.org/10.1080/15567036.2020.1790696

Chandrasekaran, S. R., & Hopke, P. K. (2012). Bioresource Technology Kinetics of switch grass pellet thermal decomposition under inert and oxidizing atmospheres. *Bioresource Technology*, *125*, 52–58. https://doi.org/10.1016/j.biortech.2012.08.061

Chen, H. L., Haack, V. S., Janecky, C. W., Vollendorf, N. W., & Marlett, J. A. (1998). Mechanisms by which wheat bran and oat bran increase stool weight in humans. *American Journal of Clinical Nutrition*, *68*(3), 711–719. https://doi.org/10.1093/ajcn/68.3.711

Chen, J., Liu, J., He, Y., Huang, L., Sun, S., Sun, J., Chang, K. L., Kuo, J., Huang, S., & Ning, X. (2017). Investigation of co-combustion characteristics of sewage sludge and coffee grounds mixtures using thermogravimetric analysis coupled to artificial neural networks modeling. *Bioresource Technology*, *225*, 234–245. https://doi.org/10.1016/j.biortech.2016.11.069

Cheng, J. J., Schuster-Wallace, C. J., Watt, S., Newbold, B. K., & Mente, A. (2012). An

ecological quantification of the relationships between water, sanitation and infant, child, and maternal mortality. *Environmental Health: A Global Access Science Source*, *11*(1). https://doi.org/10.1186/1476-069X-11-4

Chowdhury, Z. Z., Ziaul Karim, M., Ashraf, M. A., & Khalid, K. (2016). Influence of carbonization temperature on physicochemical properties of biochar derived from slow pyrolysis of durian wood (Durio zibethinus) sawdust. *BioResources*, *11*(2), 3356–3372. https://doi.org/10.15376/biores.11.2.3356-3372

Clark, W. F., Sontrop, J. M., Macnab, J. J., Suri, R. S., Moist, L., Salvadori, M., & Garg, A. X. (2011). Urine volume and change in estimated GFR in a community-based cohort study. *Clinical Journal of the American Society of Nephrology*, *6*(11), 2634–2641. https://doi.org/10.2215/CJN.01990211

Coats, A. W., & Redfern, J. P. (1964). Kinetic parameters from thermogravimetric data. *Nature*, *201*(4914), 68–69.

Collins, J., & Lewis, D. (2000). *Hydrogen Sulfide : Evaluation Of Current California Air Quality Standards With Respect To Protection Of Children A . Extended abstract*.

Davies, R. (2013). Ignition and Burning Rate of Water Hyacinth Briquettes. *Journal of Scientific Research and Reports*, *2*(1), 111–120. https://doi.org/10.9734/jsrr/2013/1964

Davis, E. A. (1995). Functionality of sugars: Physicochemical interactions in foods. *American Journal of Clinical Nutrition*, *62*(1 SUPPL.), 170–177. https://doi.org/10.1093/ajcn/62.1.170S

de Figueredo, N. A., da Costa, L. M., Melo, L. C. A., Siebeneichlerd, E. A., & Tronto, J. (2017). Characterization of biochars from different sources and evaluation of release of nutrients and contaminants. *Revista Ciencia Agronomica*, *48*(3), 395–

403. https://doi.org/10.5935/1806-6690.20170046

De Gisi, S., Lofrano, G., Grassi, M., & Notarnicola, M. (2016). Characteristics and adsorption capacities of low-cost sorbents for wastewater treatment: A review. *Sustainable Materials and Technologies*, *9*, 10–40. https://doi.org/10.1016/j.susmat.2016.06.002

Deng, H., Yu, H., Chen, M., & Ge, C. (2014). Sorption of atrazine in tropical soil by biochar prepared from cassava waste. *BioResources*, *9*(4), 6627–6643. https://doi.org/10.15376/biores.9.4.6627-6643

Diener, S., Semiyaga, S., Niwagaba, C. B., Muspratt, A. M., Gning, J. B., Mbéguéré, M., Ennin, J. E., Zurbrugg, C., & Strande, L. (2014). A value proposition: Resource recovery from faecal sludge - Can it be the driver for improved sanitation? *Resources, Conservation and Recycling*, *88*, 32–38. https://doi.org/10.1016/j.resconrec.2014.04.005

Dirbeba, M. J., Brink, A., Lindberg, D., Hupa, M., & Hupa, L. (2021). Thermal Conversion Characteristics of Molasses. *ACS Omega*, *6*(33), 21631–21645. https://doi.org/10.1021/acsomega.1c03024

Doyle, C. (1965). Series approximations to the equation of thermogravimetric data. *Nature*, *207*, 1–2.

Drenkova-Tuhtan, A., Schneider, M., Franzreb, M., Meyer, C., Gellermann, C., Sextl, G., Mandel, K., & Steinmetz, H. (2017). Pilot-scale removal and recovery of dissolved phosphate from secondary wastewater effluents with reusable ZnFeZr adsorbent @ Fe3O4/SiO2 particles with magnetic harvesting. *Water Research*, *109*, 77–87. https://doi.org/10.1016/j.watres.2016.11.039

Dutta, P., Mandal, S., & Kumar, A. (2018). Comparative study: FPA based response surface methodology & ANOVA for the parameter optimization in process control.

Advances in Modelling and Analysis C, *73*(1), 23–27. https://doi.org/10.18280/ama_c.730104

Eberhardt, T. L., Min, S. H., & Han, J. S. (2006). Phosphate removal by refined aspen wood fiber treated with carboxymethyl cellulose and ferrous chloride. *Bioresource Technology*, *97*(18), 2371–2376. https://doi.org/10.1016/j.biortech.2005.10.040

Ehujuo, N., Ehujuo, *, Okeke, N. N., & Akaolisa, O. C. (2017). Geotechnical Properties of Lateritic Soils Derived from Various Geologic Formations in Okigwe Area, Southeastern Nigeria. *Geotechnical Properties Of… Futo Journal Series (FUTOJNLS)*, *3*(2), 178–189. www.futojnls.org

Elehinafe, F. B., Okedere, O. B., Fakinle, B. S., & Sonibare, J. A. (2017). Assessment of sawdust of different wood species in Southwestern Nigeria as source of energy. *Energy Sources, Part A: Recovery, Utilization and Environmental Effects*, *39*(18), 1901–1905. https://doi.org/10.1080/15567036.2017.1384869

EPA. (1971). *Air quality criteria for nitrogen oxides*.

EPA. (2002). *Air Quality Criteria for Particulate Matter*. *3*, 255–258.

Esrey, S. A., Gough, J., Rapaport, D., Sawyer, R., Simpson-Hébert, M., Vargas, J., & Winblad, U. (1998). Ecological Sanitataion. *Swedish International Development Cooperation Agency*, 1–100.

Etter, B., Tilley, E., Khadka, R., & Udert, K. M. (2011). Low-cost struvite production using source-separated urine in Nepal. *Water Research*, *45*(2), 852–862. https://doi.org/10.1016/j.watres.2010.10.007

Falemara, B. C., Joshua, V. I., Aina, O. O., & Nuhu, R. D. (2018). Performance evaluation of the physical and combustion properties of briquettes produced from agro-wastes and wood residues. *Recycling*, *3*(3), 1–13.

https://doi.org/10.3390/recycling3030037

Farrow, T. S., Sun, C., & Snape, C. E. (2013). Impact of biomass char on coal char burn-out under air and oxy-fuel conditions. *Fuel*, *114*, 128–134. https://doi.org/10.1016/j.fuel.2012.07.073

Feachem, R., Bradley, D., Garelick, H., & Mara, D. (1984). Sanitation and Disease - Health Aspects of Excreta and Waste-water Management. *JAWRA Journal of the American Water Resources Association*, *20*(5), 803–803. https://doi.org/10.1111/j.1752-1688.1984.tb04765.x

Fidalgo, B., Chilmeran, M., Somorin, T., Sowale, A., Kolios, A., Parker, A., Williams, L., Collins, M., McAdam, E. J., & Tyrrel, S. (2019). Non-isothermal thermogravimetric kinetic analysis of the thermochemical conversion of human faeces. *Renewable Energy*, *132*, 1177–1184. https://doi.org/10.1016/j.renene.2018.08.090

Finnish Standards SFS 3026. (1986). Finnish standard for determination of total phosphorus in water. Digestion with peroxodisulfate. In *Finnish Standards Association, Helsinki, Finland.*

Flynn, J. H.; Wall, L. A. (1966). A quick, direct method for the determination of activation energy from thermogravimetric data. *Journal of Polymer Science Part B: Polymer Letters*, *4*(5), 323–328. https://doi.org/10.1098/rstb.1988.0133

Foo, K. Y., & Hameed, B. H. (2010). Insights into the modeling of adsorption isotherm systems. *Chemical Engineering Journal*, *156*(1), 2–10. https://doi.org/10.1016/j.cej.2009.09.013

Foo, K. Y., & Hameed, B. H. (2012). Porous structure and adsorptive properties of pineapple peel based activated carbons prepared via microwave assisted KOH and K2CO 3 activation. *Microporous and Mesoporous Materials*, *148*(1), 191–195.

https://doi.org/10.1016/j.micromeso.2011.08.005

Frame, M. H., & Schandl, C. A. (2015). A case example of asphyxia due to occupational exposure to airborne chemicals and review of workplace fatalities. *Journal of Forensic Sciences*, *60*(2), 521–524. https://doi.org/10.1111/1556-4029.12695

Fu, B., Ge, C., Yue, L., Luo, J., Feng, D., Deng, H., & Yu, H. (2016). Characterization of Biochar Derived from Pineapple Peel Waste and Its Application for Sorption of Oxytetracycline from Aqueous Solution. *BioResources*, *11*(4). https://doi.org/10.15376/biores.11.4.9017-9035

Fulazzaky, M. A., Khamidun, M. H., Din, M. F. M., & Yusoff, A. R. M. (2014). Adsorption of phosphate from domestic wastewater treatment plant effluent onto the laterites in a hydrodynamic column. *Chemical Engineering Journal*, *258*, 10–17. https://doi.org/10.1016/j.cej.2014.07.092

G.Manić, N., Ž.Janković, B., D.Stojiljković, D., V.Jovanović, V., & Radojević, M. B. (2019). Tga-Dsc-Ms Analysis of Pyrolysis Process. *Thermal Science*, *23*, 1457–1472.

Gai, C., Dong, Y., & Zhang, T. (2013). The kinetic analysis of the pyrolysis of agricultural residue under non-isothermal conditions. *Bioresource Technology*, *127*, 298–305. https://doi.org/10.1016/j.biortech.2012.09.089

Gai, X., Wang, H., Liu, J., Zhai, L., Liu, S., Ren, T., & Liu, H. (2014). Effects of feedstock and pyrolysis temperature on biochar adsorption of ammonium and nitrate. *PLoS ONE*, *9*(12), 1–19. https://doi.org/10.1371/journal.pone.0113888

Ganrot, Z., Dave, G., & Nilsson, E. (2007a). Recovery of N and P from human urine by freezing, struvite precipitation and adsorption to zeolite and active carbon. *Bioresource Technology*, *98*(16), 3112–3121. https://doi.org/10.1016/j.biortech.2006.10.038

Ganrot, Z., Dave, G., & Nilsson, E. (2007b). Recovery of N and P from human urine by freezing, struvite precipitation and adsorption to zeolite and active carbon. *Bioresource Technology*, *98*(16), 3112–3121. https://doi.org/10.1016/j.biortech.2006.10.038

Geethakarthi, A., & Phanikumar, B. R. (2011). Adsorption of reactive dyes from aqueous solutions by tannery sludge developed activated carbon: Kinetic and equilibrium studies. *International Journal of Environmental Science and Technology*, *8*(3), 561–570.

Githeko., C. N. &. (2013). Effect of Binder Types and Amount on. *International Journal of Engineering Research and Science and Technology*, *2*(1), 12–20.

Glarborg, P., Miller, J. A., Ruscic, B., & Klippenstein, S. J. (2018). Modeling nitrogen chemistry in combustion. *Progress in Energy and Combustion Science*, *67*, 31–68. https://doi.org/10.1016/j.pecs.2018.01.002

Glocheux, Y., Pasarín, M. M., Albadarin, A. B., Allen, S. J., & Walker, G. M. (2013). Removal of arsenic from groundwater by adsorption onto an acidified laterite by-product. *Chemical Engineering Journal*, *228*, 565–574. https://doi.org/10.1016/j.cej.2013.05.043

Gold, M., Niang, S., Niwagaba, C. B., Eder, G., Muspratt, A. M., Diop, S. P., & Strande, L. (2014). Results from FaME (Faecal Management Enterprises) – can dried faecal sludge fuel the sanitation service chain? *37th WEDC International Conference, December*, 1–6. http://wedc.lboro.ac.uk/resources/conference/37/Gold-2026.pdf

Grønli, M. G., Várhegyi, G., & Di Blasi, C. (2002). Thermogravimetric analysis and devolatilization kinetics of wood. *Industrial and Engineering Chemistry Research*, *41*(17), 4201–4208. https://doi.org/10.1021/ie0201157

Grover, P. D., & Mishra, S. K. (1996). Biomass Briquetting : Technology and

Pratices.Regional wood energy development program in Asia, field document no. 46. Bangkok, Thailand: Food and Agriculture Organization of the United Nations; *Regional Wood Energy Development Programme in Asia*, *46*, 1–48.

Guo, J., Song, Y., Ji, X., Ji, L., Cai, L., Wang, Y., Zhang, H., & Song, W. (2019). Preparation and characterization of nanoporous activated carbon derived from prawn shell and its application for removal of heavy metal ions. *Materials*, *12*(2). https://doi.org/10.3390/ma12020241

Gwara, S., Wale, E., Odindo, A., & Buckley, C. (2021). Attitudes and perceptions on the agricultural use of human excreta and human excreta derived materials: A scoping review. *Agriculture (Switzerland)*, *11*(2), 1–30. https://doi.org/10.3390/agriculture11020153

Habib, U., Habib, M., & Khan, A. U. (2014). Factors influencing the performance of coal briquettes. *Walailak Journal of Science and Technology*, *11*(1), 1–6. https://doi.org/10.2004/wjst.v11i1.417

Hafford, L. M., Ward, B. J., Weimer, A. W., & Linden, K. (2018). Fecal sludge as a fuel: Characterization, cofire limits, and evaluation of quality improvement measures. *Water Science and Technology*, *78*(12), 2437–2448. https://doi.org/10.2166/wst.2019.005

Hale, S. E., Alling, V., Martinsen, V., Mulder, J., Breedveld, G. D., & Cornelissen, G. (2013). The sorption and desorption of phosphate-P, ammonium-N and nitrate-N in cacao shell and corn cob biochars. *Chemosphere*, *91*(11), 1612–1619. https://doi.org/10.1016/j.chemosphere.2012.12.057

Halim, S. F., Yong, S. K., & Tay, C. C. (2017). Ammonia nitrogen adsorption using spent mushroom substrate biochar (Smsb). *Pertanika Journal of Science and Technology*, *25*(S7), 9–20.

Hameed, B. H., & El-Khaiary, M. I. (2008). Malachite green adsorption by rattan sawdust: Isotherm, kinetic and mechanism modeling. *Journal of Hazardous Materials*, *159*(2–3), 574–579. https://doi.org/10.1016/j.jhazmat.2008.02.054

Harder, R., Wielemaker, R., Larsen, T. A., Zeeman, G., & Öberg, G. (2019). Recycling nutrients contained in human excreta to agriculture: Pathways, processes, and products. *Critical Reviews in Environmental Science and Technology*, *49*(8), 695–743. https://doi.org/10.1080/10643389.2018.1558889

Hayhurst, A. N., & Lawrence, A. D. (1996). The amounts of NOx and N2O formed in a fluidized bed combustor during the burning of coal volatiles and also of char. *Combustion and Flame*, *105*(3), 341–357. https://doi.org/10.1016/0010-2180(95)00215-4

He, C., Giannis, A., & Wang, J. Y. (2013). Conversion of sewage sludge to clean solid fuel using hydrothermal carbonization: Hydrochar fuel characteristics and combustion behavior. *Applied Energy*, *111*, 257–266. https://doi.org/10.1016/j.apenergy.2013.04.084

He, X., Liu, Z., Niu, W., Yang, L., Zhou, T., Qin, D., Niu, Z., & Yuan, Q. (2018). Effects of pyrolysis temperature on the physicochemical properties of gas and biochar obtained from pyrolysis of crop residues. *Energy*, *143*, 746–756. https://doi.org/10.1016/j.energy.2017.11.062

Hernández, A. B., Okonta, F., & Freeman, N. (2017). Thermal decomposition of sewage sludge under N2, CO2 and air: Gas characterization and kinetic analysis. *Journal of Environmental Management*, *196*, 560–568. https://doi.org/10.1016/j.jenvman.2017.03.036

Heydari, M., Rahman, M., & Gupta, R. (2015). Kinetic study and thermal decomposition behavior of lignite coal. *International Journal of Chemical Engineering*, *2015*. https://doi.org/10.1155/2015/481739

Hikal, W. M., Mahmoud, A. A., Said-Al Ahl, H. A. H., Bratovcic, A., Tkachenko, K. G., Kačániová, M., & Rodriguez, R. M. (2021). Pineapple (<i>Ananas comosus</i> L. Merr.), Waste Streams, Characterisation and Valorisation: An Overview. *Open Journal of Ecology*, *11*(09), 610–634. https://doi.org/10.4236/oje.2021.119039

Höglund, C., Vinneras, B., Stenström, T. A., & Jönsson, H. (2000). Variation of chemical and microbial parameters in collection and storage tanks for source separated human urine. *Journal of Environmental Science and Health - Part A Toxic/Hazardous Substances and Environmental Engineering*, *35*(8), 1463–1475. https://doi.org/10.1080/10934520009377047

Hossain, M. F. (2016). World pineapple production: An overview. *African Journal of Food, Agriculture, Nutrition and Development*, *16*(4), 11443–11456. https://doi.org/10.18697/ajfand.76.15620

Hotta, S., & Funamizu, N. (2008). Evolution of ammonification potential in storage process of urine with fecal contamination. *Bioresource Technology*, *99*(1), 13–17. https://doi.org/10.1016/j.biortech.2006.12.001

Hu, Q., & Zhang, Z. (2019). Application of Dubinin–Radushkevich isotherm model at the solid/solution interface: A theoretical analysis. *Journal of Molecular Liquids*, *277*, 646–648. https://doi.org/10.1016/j.molliq.2019.01.005

Hu, X., Zhang, X., Ngo, H. H., Guo, W., Wen, H., Li, C., Zhang, Y., & Ma, C. (2020). Comparison study on the ammonium adsorption of the biochars derived from different kinds of fruit peel. *Science of the Total Environment*, *707*, 135544. https://doi.org/10.1016/j.scitotenv.2019.135544

Huang, H., Xiao, X., Yan, B., & Yang, L. (2010). Ammonium removal from aqueous solutions by using natural Chinese (Chende) zeolite as adsorbent. *Journal of Hazardous Materials*. https://doi.org/10.1016/j.jhazmat.2009.09.156

Hue, N. T., & Tung, N. H. (2018). Study on simultaneous adsorption of phosphate and fluoride from water environment by modified laterite ore from Northern Vietnam. *Green Processing and Synthesis*, *7*(2), 89–99. https://doi.org/10.1515/gps-2016-0136

Inglezakis, V. J. (2007). Solubility-normalized Dubinin-Astakhov adsorption isotherm for ion-exchange systems. *Microporous and Mesoporous Materials*, *103*(1–3), 72–81. https://doi.org/10.1016/j.micromeso.2007.01.039

Inyinbor, A. A., Adekola, F. A., & Olatunji, G. A. (2016). Kinetics, isotherms and thermodynamic modeling of liquid phase adsorption of Rhodamine B dye onto Raphia hookerie fruit epicarp. *Water Resources and Industry*, *15*, 14–27. https://doi.org/10.1016/j.wri.2016.06.001

Iriel, A., Bruneel, S. P., Schenone, N., & Cirelli, A. F. (2018). The removal of fluoride from aqueous solution by a lateritic soil adsorption: Kinetic and equilibrium studies. *Ecotoxicology and Environmental Safety*, *149*(November 2017), 166–172. https://doi.org/10.1016/j.ecoenv.2017.11.016

Jana, B. B., Rana, S., & Bag, S. K. (2012). Use of human urine in phytoplankton production as a tool for ecological sanitation. *Water Science and Technology*, *65*(8), 1350–1356. https://doi.org/10.2166/wst.2012.044

Kakali, G., Perraki, T., Tsivilis, S., & Badogiannis, E. (2001). Thermal treatment of kaolin: The effect of mineralogy on the pozzolanic activity. *Applied Clay Science*, *20*(1–2), 73–80. https://doi.org/10.1016/S0169-1317(01)00040-0

Kamtchueng, B. T., Onana, V. L., Fantong, W. Y., Ueda, A., Ntouala, R. F., Wongolo, M. H., Ndongo, G. B., Ze, A. N., Kamgang, V. K., & Ondoa, J. M. (2015). Geotechnical, chemical and mineralogical evaluation of lateritic soils in humid tropical area (Mfou, Central-Cameroon): Implications for road construction. *International Journal of Geo-Engineering*, *6*(1), 1–21.

https://doi.org/10.1186/s40703-014-0001-0

Kanbara, A., Miura, Y., Hyogo, H., Chayama, K., & Seyama, I. (2012). Effect of urine pH changed by dietary intervention on uric acid clearance mechanism of pH-dependent excretion of urinary uric acid. *Nutrition Journal*, *11*(1), 1–7. https://doi.org/10.1186/1475-2891-11-39

Karahalios, T., Berner, C., & Njenga, M. (2018). Human Waste-to-fuel Briquettes as a Sanitation and Energy Solution for Refugee Camps and Informal Urban Settlements. *Recovering Bioenergy in Sub-Saharan Africa: Gender Dimensions, Lessons and Challenges*, *December*, 96. https://www.researchgate.net/profile/Mary_Njenga/publication/329557889_Recovering_Bioenergy_in_Sub-Saharan_Africa_Gender_Dimensions_Lessons_and_Challenges/links/5c0f8b5e299bf139c74fe81e/Recovering-Bioenergy-in-Sub-Saharan-Africa-Gender-Dimensions-Lessons-

Karak, T., & Bhattacharyya, P. (2011). Human urine as a source of alternative natural fertilizer in agriculture: A flight of fancy or an achievable reality. *Resources, Conservation and Recycling*, *55*(4), 400–408. https://doi.org/10.1016/j.resconrec.2010.12.008

Kaur, S., Rani, S., Mahajan, R. K., Asif, M., & Gupta, V. K. (2015). Synthesis and adsorption properties of mesoporous material for the removal of dye safranin: Kinetics, equilibrium, and thermodynamics. *Journal of Industrial and Engineering Chemistry*, *22*, 19–27. https://doi.org/10.1016/j.jiec.2014.06.019

Kavvada, O., Tarpeh, W. A., Horvath, A., & Nelson, K. L. (2017). Life-cycle cost and environmental assessment of decentralized nitrogen recovery using ion exchange from source-separated urine through spatial modeling. *Environmental Science and Technology*, *51*(21), 12061–12071. https://doi.org/10.1021/acs.est.7b02244

Keiluweit, M., Nico, P. S., Johnson, M., & Kleber, M. (2010). Dynamic molecular

structure of plant biomass-derived black carbon (biochar). *Environmental Science and Technology*, *44*(4), 1247–1253. https://doi.org/10.1021/es9031419

Khamparia, S., & Jaspal, D. (2016). Investigation of adsorption of Rhodamine B onto a natural adsorbent Argemone mexicana. *Journal of Environmental Management*, *183*, 786–793. https://doi.org/10.1016/j.jenvman.2016.09.036

Kim, K. H., Kim, J. Y., Cho, T. S., & Choi, J. W. (2012). Influence of pyrolysis temperature on physicochemical properties of biochar obtained from the fast pyrolysis of pitch pine (Pinus rigida). *Bioresource Technology*, *118*, 158–162. https://doi.org/10.1016/j.biortech.2012.04.094

Kim, Y., Park, T., & Hong, D. (2021). Heating and emission characteristics of briquettes developed from spent coffee grounds. *Environmental Engineering Research*, *27*(4), 210063–0. https://doi.org/10.4491/eer.2021.063

Kirchmann, H., & Pettersson, S. (1994). Human urine - Chemical composition and fertilizer use efficiency. *Fertilizer Research*, *40*(2), 149–154. https://doi.org/10.1007/BF00750100

Kissinger, H. E. (1957). Reaction Kinetics in Differential Thermal Analysis. *Analytical Chemistry*, *29*(11), 1702–1706. https://doi.org/10.1021/ac60131a045

Kitano, M., Inoue, Y., Yamazaki, Y., Hayashi, F., Kanbara, S., Matsuishi, S., Yokoyama, T., Kim, S. W., Hara, M., & Hosono, H. (2012). Ammonia synthesis using a stable electride as an electron donor and reversible hydrogen store. *Nature Chemistry*, *4*(11), 934–940. https://doi.org/10.1038/nchem.1476

Kithome, M., Paul, J. W., Lavkulich, L. M., & Bomke, A. A. (1998). Kinetics of Ammonium Adsorption and Desorption by the Natural Zeolite Clinoptilolite. *Soil Science Society of America Journal*, *62*(3), 622–629. https://doi.org/10.2136/sssaj1998.03615995006200030011x

Kizito, S., Wu, S., Kipkemoi Kirui, W., Lei, M., Lu, Q., Bah, H., & Dong, R. (2015). Evaluation of slow pyrolyzed wood and rice husks biochar for adsorption of ammonium nitrogen from piggery manure anaerobic digestate slurry. *Science of the Total Environment, 505*, 102–112. https://doi.org/10.1016/j.scitotenv.2014.09.096

Krueger, B. C., Fowler, G. D., Templeton, M. R., & Moya, B. (2020). Resource recovery and biochar characteristics from full-scale faecal sludge treatment and co-treatment with agricultural waste. *Water Research*, *169*, 115253. https://doi.org/10.1016/j.watres.2019.115253

Ku, J. (1991). *Nitric oxide in workplace atmospheres*. *1989*. https://www.osha.gov/dts/sltc/methods/inorganic/id190/id190.pdf

Kumar, D., Singh, A., & Gaur, J. P. (2008). Mono-component versus binary isotherm models for Cu(II) and Pb(II) sorption from binary metal solution by the green alga Pithophora oedogonia. *Bioresource Technology*, *99*(17), 8280–8287. https://doi.org/10.1016/j.biortech.2008.03.008

Kuntke, P., Sleutels, T. H. J. A., Saakes, M., & Buisman, C. J. N. (2014). Hydrogen production and ammonium recovery from urine by a Microbial Electrolysis Cell. *International Journal of Hydrogen Energy*, *39*(10), 4771–4778. https://doi.org/10.1016/j.ijhydene.2013.10.089

Lam, S. S., Liew, R. K., Cheng, C. K., Rasit, N., Ooi, C. K., Ma, N. L., Ng, J. H., Lam, W. H., Chong, C. T., & Chase, H. A. (2018). Pyrolysis production of fruit peel biochar for potential use in treatment of palm oil mill effluent. *Journal of Environmental Management*, *213*, 400–408. https://doi.org/10.1016/j.jenvman.2018.02.092

Langergraber, G., & Muellegger, E. (2005). Ecological Sanitation - A way to solve global sanitation problems? *Environment International*, *31*(3), 433–444. https://doi.org/10.1016/j.envint.2004.08.006

Larsen, T. A., Alder, A. C., Eggen, R. L., Maurer, M., & Lienert, J. (2009). A new planning and design paradigm to achieve sustainable resource recovery from wastewater. *Environmental Science and Technology*, *43*(16), 6126–6130. https://doi.org/10.1021/es9010515

Ledezma, P., Kuntke, P., Buisman, C. J. N., Keller, J., & Freguia, S. (2015). Source-separated urine opens golden opportunities for microbial electrochemical technologies. *Trends in Biotechnology*, *33*(4), 214–220. https://doi.org/10.1016/j.tibtech.2015.01.007

Lee, Y., Park, J., Ryu, C., Gang, K. S., Yang, W., Park, Y. K., Jung, J., & Hyun, S. (2013). Comparison of biochar properties from biomass residues produced by slow pyrolysis at 500°C. *Bioresource Technology*, *148*, 196–201. https://doi.org/10.1016/j.biortech.2013.08.135

Lemougna, P. N., Madi, A. B., Kamseu, E., Melo, U. C., Delplancke, M. P., & Rahier, H. (2014a). Influence of the processing temperature on the compressive strength of Na activated lateritic soil for building applications. *Construction and Building Materials*, *65*, 60–66. https://doi.org/10.1016/j.conbuildmat.2014.04.100

Lemougna, P. N., Madi, A. B., Kamseu, E., Melo, U. C., Delplancke, M. P., & Rahier, H. (2014b). Influence of the processing temperature on the compressive strength of Na activated lateritic soil for building applications. *Construction and Building Materials*, *65*, 60–66. https://doi.org/10.1016/j.conbuildmat.2014.04.100

Li, B., Huang, H. M., Boiarkina, I., Yu, W., Huang, Y. F., Wang, G. Q., & Young, B. R. (2019). Phosphorus recovery through struvite crystallisation: Recent developments in the understanding of operational factors. *Journal of Environmental Management*, *248*(January), 109254. https://doi.org/10.1016/j.jenvman.2019.07.025

Li, H., Mahyoub, S. A. A., Liao, W., Xia, S., Zhao, H., Guo, M., & Ma, P. (2017). Effect of pyrolysis temperature on characteristics and aromatic contaminants adsorption

behavior of magnetic biochar derived from pyrolysis oil distillation residue. *Bioresource Technology*, *223*, 20–26. https://doi.org/10.1016/j.biortech.2016.10.033

Li, J., Ma, C., Ma, Y., Li, Y., Zhou, W., & Xu, P. (2007). Medium optimization by combination of response surface methodology and desirability function: An application in glutamine production. *Applied Microbiology and Biotechnology*, *74*(3), 563–571. https://doi.org/10.1007/s00253-006-0699-5

Li, R., Wang, J. J., Zhou, B., Zhang, Z., Liu, S., Lei, S., & Xiao, R. (2017). Simultaneous capture removal of phosphate, ammonium and organic substances by MgO impregnated biochar and its potential use in swine wastewater treatment. *Journal of Cleaner Production*, *147*, 96–107. https://doi.org/10.1016/j.jclepro.2017.01.069

Liang, H., Chen, L., Liu, G., & Zheng, H. (2016). *Surface morphology properties of biochars produced from different feedstocks*. *Iccte*, 1205–1208. https://doi.org/10.2991/iccte-16.2016.210

Lienert, J., Bürki, T., & Escher, B. I. (2007). Reducing micropollutants with source control: Substance flow analysis of 212 pharmaceuticals in faeces and urine. *Water Science and Technology*, *56*(5), 87–96. https://doi.org/10.2166/wst.2007.560

Lim, A. C. R., Chin, B. L. F., Jawad, Z. A., & Hii, K. L. (2016). Kinetic Analysis of Rice Husk Pyrolysis Using Kissinger-Akahira-Sunose (KAS) Method. *Procedia Engineering*, *148*, 1247–1251. https://doi.org/10.1016/j.proeng.2016.06.486

Lind, B. B., Ban, Z., & Bydén, S. (2000). Nutrient recovery from human urine by struvite crystallization with ammonia adsorption on zeolite and wollastonite. *Bioresource Technology*, *73*(2), 169–174. https://doi.org/10.1016/S0960-8524(99)90157-8

Liu, J., Jiang, J., Aihemaiti, A., Meng, Y., Yang, M., Xu, Y., Gao, Y., Zou, Q., & Chen, X. (2019). Removal of phosphate from aqueous solution using MgO-modified magnetic biochar derived from anaerobic digestion residue. *Journal of Environmental Management*, *250*(June), 109438. https://doi.org/10.1016/j.jenvman.2019.109438

Liu, Y., He, Z., & Uchimiya, M. (2015). Comparison of Biochar Formation from Various Agricultural By-Products Using FTIR Spectroscopy. *Modern Applied Science*, *9*(4), 246–253. https://doi.org/10.5539/mas.v9n4p246

Lopez-Velazquez, M. A., Santes, V., Balmaseda, J., & Torres-Garcia, E. (2013). Pyrolysis of orange waste: A thermo-kinetic study. *Journal of Analytical and Applied Pyrolysis*, *99*, 170–177. https://doi.org/10.1016/j.jaap.2012.09.016

Lun, L. W., Gunny, A. A. N., Kasim, F. H., & Arbain, D. (2017). Fourier transform infrared spectroscopy (FTIR) analysis of paddy straw pulp treated using deep eutectic solvent. *AIP Conference Proceedings*, *1835*(April 2017). https://doi.org/10.1063/1.4981871

Luo, L., Wang, G., Shi, G., Zhang, M., Zhang, J., He, J., Xiao, Y., Tian, D., Zhang, Y., Deng, S., Zhou, W., Lan, T., & Deng, O. (2019). The characterization of biochars derived from rice straw and swine manure, and their potential and risk in N and P removal from water. *Journal of Environmental Management*, *245*(January), 1–7. https://doi.org/10.1016/j.jenvman.2019.05.072

Ma, Z., Wang, J., Yang, Y., Zhang, Y., Zhao, C., Yu, Y., & Wang, S. (2018). Comparison of the thermal degradation behaviors and kinetics of palm oil waste under nitrogen and air atmosphere in TGA-FTIR with a complementary use of model-free and model-fitting approaches. In *Journal of Analytical and Applied Pyrolysis* (Vol. 134). Elsevier B.V. https://doi.org/10.1016/j.jaap.2018.04.002

Mahmoud, M. A. (2015). Kinetics and thermodynamics of aluminum oxide nanopowder

as adsorbent for Fe (III) from aqueous solution. *Beni-Suef University Journal of Basic and Applied Sciences*, *4*(2), 142–149. https://doi.org/10.1016/j.bjbas.2015.05.008

Maiti, A., Basu, J. K., & De, S. (2012). Experimental and kinetic modeling of As(V) and As(III) adsorption on treated laterite using synthetic and contaminated groundwater: Effects of phosphate, silicate and carbonate ions. *Chemical Engineering Journal*, *191*, 1–12. https://doi.org/10.1016/j.cej.2010.01.031

Maiti, A., Thakur, B. K., Basu, J. K., & De, S. (2013). Comparison of treated laterite as arsenic adsorbent from different locations and performance of best filter under field conditions. *Journal of Hazardous Materials*, *262*, 1176–1186. https://doi.org/10.1016/j.jhazmat.2012.06.036

Malone Rubright, S. L., Pearce, L. L., & Peterson, J. (2017). Environmental toxicology of hydrogen sulfide. *Nitric Oxide - Biology and Chemistry*, *71*(412), 1–13. https://doi.org/10.1016/j.niox.2017.09.011

Mambo, W. (2016). *Optimal compaction pressure, particle size and binder ratio for quality briquettes made from maize cobs*. http://ir.jkuat.ac.ke/handle/123456789/2387

Mansing R, P., & Rout, P. . (2013). Removal of phosphorus from sewage effluent by adsorption on Laterite. *International Journal of Engineering Research & Technology*, *2*(9), 551–559.

Martin, T. M. P., Esculier, F., Levavasseur, F., & Houot, S. (2020). Human urine-based fertilizers: A review. *Critical Reviews in Environmental Science and Technology*, *0*(0), 1–47. https://doi.org/10.1080/10643389.2020.1838214

Mathurasa, L., & Damrongsiri, S. (2018). Low cost and easy rice husk modification to efficiently enhance ammonium and nitrate adsorption. *International Journal of*

Recycling of Organic Waste in Agriculture, *7*(2), 143–151. https://doi.org/10.1007/s40093-018-0200-3

Matsui, Y., Nakao, S., Sakamoto, A., Taniguchi, T., Pan, L., Matsushita, T., & Shirasaki, N. (2015). Adsorption capacities of activated carbons for geosmin and 2-methylisoborneol vary with activated carbon particle size: Effects of adsorbent and adsorbate characteristics. *Water Research*, *85*, 95–102. https://doi.org/10.1016/j.watres.2015.08.017

Maurer, M., Pronk, W., & Larsen, T. A. (2006a). Treatment processes for source-separated urine. *Water Research*, *40*(17), 3151–3166. https://doi.org/10.1016/j.watres.2006.07.012

Maurer, M., Pronk, W., & Larsen, T. A. (2006b). Treatment processes for source-separated urine. In *Water Research* (Vol. 40, Issue 17, pp. 3151–3166). https://doi.org/10.1016/j.watres.2006.07.012

Mishra, R. K., & Mohanty, K. (2018). Pyrolysis kinetics and thermal behavior of waste sawdust biomass using thermogravimetric analysis. *Bioresource Technology*, *251*, 63–74. https://doi.org/10.1016/j.biortech.2017.12.029

Mitra, S., Thakur, L. S., Rathore, V. K., & Mondal, P. (2016). Removal of Pb(II) and Cr(VI) by laterite soil from synthetic waste water: single and bi-component adsorption approach. *Desalination and Water Treatment*, *57*(39), 18406–18416. https://doi.org/10.1080/19443994.2015.1088806

Mouni, L., Belkhiri, L., Bollinger, J. C., Bouzaza, A., Assadi, A., Tirri, A., Dahmoune, F., Madani, K., & Remini, H. (2018). Removal of Methylene Blue from aqueous solutions by adsorption on Kaolin: Kinetic and equilibrium studies. *Applied Clay Science*, *153*, 38–45. https://doi.org/10.1016/j.clay.2017.11.034

Muspratt, A. M., Nakato, T., Niwagaba, C., Dione, H., Kang, J., Stupin, L., Regulinski,

J., Mbéguéré, M., & Strande, L. (2014). Fuel potential of faecal sludge: Calorific value results from Uganda, Ghana and Senegal. *Journal of Water Sanitation and Hygiene for Development*, *4*(2), 223–230. https://doi.org/10.2166/washdev.2013.055

Myers, R. H., Montgomery, D. C., Geoffrey Vining, G., Borror, C. M., & Kowalski, S. M. (2004a). Response Surface Methodology: A Retrospective and Literature Survey. *Journal of Quality Technology*, *36*(1), 53–78. https://doi.org/10.1080/00224065.2004.11980252

Myers, R. H., Montgomery, D. C., Geoffrey Vining, G., Borror, C. M., & Kowalski, S. M. (2004b). Response Surface Methodology: A Retrospective and Literature Survey. In *Journal of Quality Technology* (Vol. 36, Issue 1, pp. 53–78). https://doi.org/10.1080/00224065.2004.11980252

Nellie Oduor, Emily Kitheka, Celestine Ingutia, Nathan Nyamai, James Kimwemwe, & Kevin Juma. (2019). Quality and Emission Analysis of Charcoal from Various Species of Wood Using Improved Carbonization Technologies in Kenya. *Journal of Environmental Science and Engineering A*, *8*(1). https://doi.org/10.17265/2162-5298/2019.01.002

Neset, T. S. S., & Cordell, D. (2012). Global phosphorus scarcity: Identifying synergies for a sustainable future. *Journal of the Science of Food and Agriculture*, *92*(1), 2–6. https://doi.org/10.1002/jsfa.4650

Ng, C. W. W., Akinniyi, D. B., Zhou, C., & Chiu, C. F. (2019). Comparisons of weathered lateritic, granitic and volcanic soils: Compressibility and shear strength. *Engineering Geology*, *249*, 235–240. https://doi.org/10.1016/j.enggeo.2018.12.029

Ngusale, G. K., Luo, Y., & Kiplagat, J. K. (2014). Briquette making in Kenya: Nairobi and peri-urban areas. *Renewable and Sustainable Energy Reviews*, *40*, 749–759. https://doi.org/10.1016/j.rser.2014.07.206

Nguyen-Viet, H., Zinsstag, J., Schertenleib, R., Zurbrügg, C., Obrist, B., Montangero, A., Surkinkul, N., Koné, D., Morel, A., Cissé, G., Koottatep, T., Bonfoh, B., & Tanner, M. (2009). Improving environmental sanitation, health, and well-being: A conceptual framework for integral interventions. *EcoHealth*, *6*(2), 180–191. https://doi.org/10.1007/s10393-009-0249-6

Nguyen, T. T. N., Némery, J., Gratiot, N., Strady, E., Tran, V. Q., Nguyen, A. T., Aimé, J., & Peyne, A. (2019). Nutrient dynamics and eutrophication assessment in the tropical river system of Saigon – Dongnai (southern Vietnam). *Science of the Total Environment*, *653*, 370–383. https://doi.org/10.1016/j.scitotenv.2018.10.319

Njenga, M., Karanja, N., Jamnadass, R., Kithinji, J., Sundberg, C., & Jirjis, R. (2013). Quality of cooking fuel briquettes produced locally from charcoal dust and sawdust in Kenya. *Journal of Biobased Materials and Bioenergy*, *7*(3), 315–322. https://doi.org/10.1166/jbmb.2013.1355

Nyberg, K. A., Ottoson, J. R., Vinnerås, B., & Albihn, A. (2014). Fate and survival of Salmonella Typhimurium and Escherichia coli O157:H7 in repacked soil lysimeters after application of cattle slurry and human urine. *Journal of the Science of Food and Agriculture*, *94*(12), 2541–2546. https://doi.org/10.1002/jsfa.6593

Obernberger, I., Brunner, T., & Bärnthaler, G. (2006). Chemical properties of solid biofuels-significance and impact. *Biomass and Bioenergy*, *30*(11), 973–982. https://doi.org/10.1016/j.biombioe.2006.06.011

Onabanjo, T., Patchigolla, K., Wagland, S. T., Fidalgo, B., Kolios, A., McAdam, E., Parker, A., Williams, L., Tyrrel, S., & Cartmell, E. (2016). Energy recovery from human faeces via gasification: A thermodynamic equilibrium modelling approach. *Energy Conversion and Management*, *118*, 364–376. https://doi.org/10.1016/j.enconman.2016.04.005

Osei, J., Gawu, S. K., Schäfer, A. I., Atipoka, F. A., & Momade, F. W. (2016). Impact of laterite characteristics on fluoride removal from water. *Journal of Chemical Technology and Biotechnology*, *91*(4), 911–920. https://doi.org/10.1002/jctb.4656

OSHA. (2010). Carbon Dioxide Health Hazard Information Sheet. *The FSIS Environmental Safety and Health Group (ESHG)*, 2–4. https://www.osha.gov/dts/chemicalsampling/data/CH_225400.html

Otieno, A. O., Home, P. G., Raude, J. M., Murunga, S. I., Ngumba, E., Ojwang, D. O., & Tuhkanen, T. (2021). Pineapple peel biochar and lateritic soil as adsorbents for recovery of ammonium nitrogen from human urine. *Journal of Environmental Management*, *293*(May), 112794. https://doi.org/10.1016/j.jenvman.2021.112794

Özacar, M. (2003). Equilibrium and kinetic modelling of adsorption of phosphorus on calcined alunite. *Adsorption*, *9*(2), 125–132. https://doi.org/10.1023/A:1024289209583

Ozawa, T. (1965). A New Method of Analyzing Thermogravimetric Data. *Bulletin of the Chemical Society of Japan*, *38*(11), 1881–1886. https://doi.org/10.1246/bcsj.38.1881

Öztürk, N., & Bektaş, T. E. (2004). Nitrate removal from aqueous solution by adsorption onto various materials. *Journal of Hazardous Materials*, *112*(1–2), 155–162. https://doi.org/10.1016/j.jhazmat.2004.05.001

Palmonari, A., Cavallini, D., Sniffen, C. J., Fernandes, L., Holder, P., Fagioli, L., Fusaro, I., Biagi, G., Formigoni, A., & Mammi, L. (2020). Short communication: Characterization of molasses chemical composition. *Journal of Dairy Science*, *103*(7), 6244–6249. https://doi.org/10.3168/jds.2019-17644

Parikh, J., Channiwala, S. A., & Ghosal, G. K. (2007). A correlation for calculating elemental composition from proximate analysis of biomass materials. *Fuel*, *86*(12–

13), 1710–1719. https://doi.org/10.1016/j.fuel.2006.12.029

Patel, S. U., Jeevan Kumar, B., Badhe, Y. P., Sharma, B. K., Saha, S., Biswas, S., Chaudhury, A., Tambe, S. S., & Kulkarni, B. D. (2007). Estimation of gross calorific value of coals using artificial neural networks. *Fuel*, *86*(3), 334–344. https://doi.org/10.1016/j.fuel.2006.07.036

Perera, M. K., & Englehardt, J. D. (2020). Simultaneous nitrogen and phosphorus recovery from municipal wastewater by electrochemical pH modulation. *Separation and Purification Technology*, *250*, 117166. https://doi.org/10.1016/j.seppur.2020.117166

Pillai, M. G., Simha, P., & Gugalia, A. (2014). Recovering urea from human urine by bio-sorption onto Microwave Activated Carbonized Coconut Shells: Equilibrium, kinetics, optimization and field studies. *Journal of Environmental Chemical Engineering*. https://doi.org/10.1016/j.jece.2013.11.027

Pilusa, T. J., Huberts, R., & Muzenda, E. (2013). Emissions analysis from combustion of eco-fuel briquettes for domestic applications. *Journal of Energy in Southern Africa*, *24*(4), 30–36. https://doi.org/10.17159/2413-3051/2013/v24i4a3143

Pitawala, H. M. T. G. A., Karunaratne, D. G. G. P., & Silva, N. (2013). Removal of aqueous phosphate and phenol by adsorption on clayey peat, laterite and red earth. *Journal of Geological Society of Sri Lanka*, *15*, 57–67.

Pradhan, S. K., Mikola, A., Heinonen-Tanski, H., & Vahala, R. (2019). Recovery of nitrogen and phosphorus from human urine using membrane and precipitation process. *Journal of Environmental Management*, *247*, 596–602. https://doi.org/10.1016/j.jenvman.2019.06.046

Putnam, D. (1971). Composition and concentrative properties of human urine. *NASA Contractor Reports*, *July*.

Qin, Y., Zhu, X., Su, Q., Anumah, A., Gao, B., Lyu, W., Zhou, X., Xing, Y., & Wang, B. (2019). Enhanced removal of ammonium from water by ball-milled biochar. *Environmental Geochemistry and Health*, *5*. https://doi.org/10.1007/s10653-019-00474-5

Ragheb, S. M. (2013). Phosphate removal from aqueous solution using slag and fly ash. *HBRC Journal*, *9*(3), 270–275. https://doi.org/10.1016/j.hbrcj.2013.08.005

Ramakrishnaiah, V. (2012). Removal of Phosphate From Wastewater Using Low-Cost Adsorbents. *Internatentionional Journal of Engineering Inv*, *1*(7), 44–50.

Randall, D. G., Krähenbühl, M., Köpping, I., Larsen, T. A., & Udert, K. M. (2016a). A novel approach for stabilizing fresh urine by calcium hydroxide addition. *Water Research*, *95*, 361–369. https://doi.org/10.1016/j.watres.2016.03.007

Randall, D. G., Krähenbühl, M., Köpping, I., Larsen, T. A., & Udert, K. M. (2016b). A novel approach for stabilizing fresh urine by calcium hydroxide addition. *Water Research*, *95*, 361–369. https://doi.org/10.1016/j.watres.2016.03.007

Raveendran, K., Ganesh, A., & Khilar, K. C. (1996). Pyrolysis characteristics of biomass and biomass components. *Fuel*, *75*(8), 987–998. https://doi.org/10.1016/0016-2361(96)00030-0

Reid, W. V., Ali, M. K., & Field, C. B. (2020). The future of bioenergy. *Global Change Biology*, *26*(1), 274–286. https://doi.org/10.1111/gcb.14883

Ren, L. F., Deng, J., Li, Q. W., Ma, L., Zou, L., Laiwang, B., & Shu, C. M. (2019). Low-temperature exothermic oxidation characteristics and spontaneous combustion risk of pulverised coal. *Fuel*, *252*(March), 238–245. https://doi.org/10.1016/j.fuel.2019.04.108

Rocha, J., & Klinowski, J. (1990). 29Si and 27Al magic-angle-spinning NMR studies of the thermal transformation of kaolinite. *Physics and Chemistry of Minerals*, *17*(2), 179–186. https://doi.org/10.1007/BF00199671

Rose, C., Parker, A., Jefferson, B., & Cartmell, E. (2015). The characterization of feces and urine: A review of the literature to inform advanced treatment technology. *Critical Reviews in Environmental Science and Technology*, *45*(17), 1827–1879. https://doi.org/10.1080/10643389.2014.1000761

Ruiz-Aquino, F., Ruiz-Ángel, S., Santiago-García, W., Fuente-Carrasco, M. E., Sotomayor-Castellanos, J. R., & Carrillo-Parra, A. (2019). Energy characteristics of wood and charcoal of selected tree species in Mexico. *Wood Research*, *64*(1), 71–82.

Ryason, P. R., & Harkins, J. (1967). Studies on a new method of simultaneously removing sulfur dioxide and oxides of nitrogen from combustion gases. *Journal of the Air Pollution Control Association*, *17*(12), 796–799. https://doi.org/10.1080/00022470.1967.10469072

Saastamoinen, H., & Leino, T. (2019). Fuel Staging and Air Staging to Reduce Nitrogen Emission in the CFB Combustion of Bark and Coal. *Energy and Fuels*, *33*(6), 5732–5739. https://doi.org/10.1021/acs.energyfuels.9b00850

Saeed, A. A. H., Harun, N. Y., Bilad, M. R., Afzal, M. T., Parvez, A. M., Roslan, F. A. S., Rahim, S. A., Vinayagam, V. D., & Afolabi, H. K. (2021). Moisture content impact on properties of briquette produced from rice husk waste. *Sustainability (Switzerland)*, *13*(6). https://doi.org/10.3390/su13063069

Sait, H. H., Hussain, A., Salema, A. A., & Ani, F. N. (2012). Pyrolysis and combustion kinetics of date palm biomass using thermogravimetric analysis. *Bioresource Technology*, *118*, 382–389. https://doi.org/10.1016/j.biortech.2012.04.081

Salar-García, M. J., Ortiz-Martínez, V. M., Gajda, I., Greenman, J., Hernández-Fernández, F. J., & Ieropoulos, I. A. (2017). Electricity production from human urine in ceramic microbial fuel cells with alternative non-fluorinated polymer binders for cathode construction. *Separation and Purification Technology*, *187*, 436–442. https://doi.org/10.1016/j.seppur.2017.06.025

Saleem, J., Shahid, U. Bin, Hijab, M., Mackey, H., & McKay, G. (2019). Production and applications of activated carbons as adsorbents from olive stones. *Biomass Conversion and Biorefinery*, *9*(4), 775–802. https://doi.org/10.1007/s13399-019-00473-7

Sanchez, M. E., Otero, M., Gómez, X., & Morán, A. (2009). Thermogravimetric kinetic analysis of the combustion of biowastes. *Renewable Energy*, *34*(6), 1622–1627. https://doi.org/10.1016/j.renene.2008.11.011

Sarkar, M., Banerjee, A., Pramanick, P. P., & Sarkar, A. R. (2006). Use of laterite for the removal of fluoride from contaminated drinking water. *Journal of Colloid and Interface Science*, *302*(2), 432–441. https://doi.org/10.1016/j.jcis.2006.07.001

Sarkhot, D. V., Ghezzehei, T. A., & Berhe, A. A. (2013a). Effectiveness of biochar for sorption of ammonium and phosphate from dairy effluent. *Journal of Environmental Quality*, *42*(5), 1545–1554. https://doi.org/10.2134/jeq2012.0482

Sarkhot, D. V., Ghezzehei, T. A., & Berhe, A. A. (2013b). Effectiveness of Biochar for Sorption of Ammonium and Phosphate from Dairy Effluent. *Journal of Environmental Quality*, *42*(5), 1545–1554. https://doi.org/10.2134/jeq2012.0482

Schieb, T. (1976). Criteria for a recommended standard: occupational exposure to oxides of nitrogen (nitrogen dioxide and nitric oxide). *US Department of Health, Education, and Welfare, Public Health Service, Center for Disease Control, National Institute for Occupational Safety and Health.*

Sha, D., Li, Y., Zhou, X., Zhang, J., Zhang, H., & Yu, J. (2021). Influence of Volatile Content on the Explosion Characteristics of Coal Dust. *ACS Omega*, *6*(41), 27150–27157. https://doi.org/10.1021/acsomega.1c03803

Shaaban, A., Se, S. M., Mitan, N. M. M., & Dimin, M. F. (2013). Characterization of biochar derived from rubber wood sawdust through slow pyrolysis on surface porosities and functional groups. *Procedia Engineering*, *68*, 365–371. https://doi.org/10.1016/j.proeng.2013.12.193

Shakya, A., & Agarwal, T. (2019). Removal of Cr(VI) from water using pineapple peel derived biochars: Adsorption potential and re-usability assessment. *Journal of Molecular Liquids*, *293*, 111497. https://doi.org/10.1016/j.molliq.2019.111497

Shen, J., & Duvnjak, Z. (2005). Adsorption kinetics of cupric and cadmium ions on corncob particles. *Process Biochemistry*, *40*(11), 3446–3454. https://doi.org/10.1016/j.procbio.2005.02.016

Shirai, H., Ikeda, M., & Aramaki, H. (2013). Characteristics of hydrogen sulfide formation in pulverized coal combustion. *Fuel*, *114*, 114–119. https://doi.org/10.1016/j.fuel.2012.03.028

Sial, T. A., Khan, M. N., Lan, Z., Kumbhar, F., Ying, Z., Zhang, J., Sun, D., & Li, X. (2019). Contrasting effects of banana peels waste and its biochar on greenhouse gas emissions and soil biochemical properties. *Process Safety and Environmental Protection*, *122*, 366–377. https://doi.org/10.1016/j.psep.2018.10.030

Sica, M., Duta, A., Teodosiu, C., & Draghici, C. (2014). Thermodynamic and kinetic study on ammonium removal from a synthetic water solution using ion exchange resin. *Clean Technologies and Environmental Policy*, *16*(2), 351–359. https://doi.org/10.1007/s10098-013-0625-3

Simha, P., Lalander, C., Vinnerås, B., & Ganesapillai, M. (2017). Farmer attitudes and perceptions to the re–use of fertiliser products from resource–oriented sanitation systems – The case of Vellore, South India. *Science of the Total Environment*, *581–582*, 885–896. https://doi.org/10.1016/j.scitotenv.2017.01.044

Sittisun, P., Tippayawong, N., & Wattanasiriwech, D. (2015). Thermal degradation characteristics and kinetics of oxy combustion of corn residues. *Advances in Materials Science and Engineering*, *2015*. https://doi.org/10.1155/2015/304395

Somorin, T., Parker, A., McAdam, E., Williams, L., Tyrrel, S., Kolios, A., & Jiang, Y. (2020). Pyrolysis characteristics and kinetics of human faeces, simulant faeces and wood biomass by thermogravimetry–gas chromatography–mass spectrometry methods. *Energy Reports*, *6*, 3230–3239. https://doi.org/10.1016/j.egyr.2020.11.164

State, E., Polytechnic, T. F., Ekiti, A., & State, E. (2018). *2018 Volume 7 , Issue 1 : 10-18 Physico-Chemical Properties of Lateritic Soils in Ado-Ekiti , South Western Nigeria Abstract : Universal Journal of Environmental Research and Technology*. *7*(1), 10–18.

Stoops, G., & Marcelino, V. (2018). Lateritic and Bauxitic Materials. In *Interpretation of Micromorphological Features of Soils and Regoliths* (pp. 691–720). Elsevier. https://doi.org/10.1016/b978-0-444-63522-8.00024-3

Strande, L., Mariska, R., & Brdjanovic, D. (2014). Enduse of Treatment Products. In *Faecal Sludge Management: Systems Approach for Implementation and Operation*. http://www.eawag.ch/forschung/sandec/publikationen/ewm/dl/fsm_book.pdf

Sulaymon, A. H., Mohammed, A. A., & Al-Musawi, T. J. (2013). Competitive biosorption of lead, cadmium, copper, and arsenic ions using algae. *Environmental Science and Pollution Research*, *20*(5), 3011–3023. https://doi.org/10.1007/s11356-012-1208-2

Sumaraj, & Padhye, L. P. (2017). Influence of surface chemistry of carbon materials on their interactions with inorganic nitrogen contaminants in soil and water. *Chemosphere*, *184*, 532–547. https://doi.org/10.1016/j.chemosphere.2017.06.021

Supatata, N., Buates, J., & Hariyanont, P. (2013). Characterization of Fuel Briquettes Made from Sewage Sludge Mixed with Water Hyacinth and Sewage Sludge Mixed with Sedge. *International Journal of Environmental Science and Development*, *4*(2), 179–181. https://doi.org/10.7763/ijesd.2013.v4.330

Tanui, J. K., Kioni, P. N., Kariuki, P. N., & Ngugi, J. M. (2018). Influence of processing conditions on the quality of briquettes produced by recycling charcoal dust. *International Journal of Energy and Environmental Engineering*, *9*(3), 341–350. https://doi.org/10.1007/s40095-018-0275-7

Tokan, A., Sambo, A. S., & Kyauta, J. S. (2014). Effects of Particle Size on the Thermal Properties of Sawdust, Corncobs and Prosopis Africana Charcoal Briquettes. *American Journal of Engineering Research (AJER)*, *03*(January), 369–374. www.ajer.org

Townsend, C. L., & Maynard, R. L. (2002). Effects on health of prolonged exposure to low concentrations of carbon monoxide. *Occupational and Environmental Medicine*, *59*(10), 708–711. https://doi.org/10.1136/oem.59.10.708

Trinh, T. K., & Kang, L. S. (2011). Response surface methodological approach to optimize the coagulation-flocculation process in drinking water treatment. *Chemical Engineering Research and Design*, *89*(7), 1126–1135. https://doi.org/10.1016/j.cherd.2010.12.004

Udert, K. M., Larsen, T. A., Biebow, M., & Gujer, W. (2003). Urea hydrolysis and precipitation dynamics in a urine-collecting system. *Water Research*, *37*(11), 2571–2582. https://doi.org/10.1016/S0043-1354(03)00065-4

Ugwu, K. (2013). Evaluation of Binders in the Production of Briquettes from Empty Fruit Bunches of Elais Guinensis. *International Journal of Renewable and Sustainable Energy*, *2*(4), 176. https://doi.org/10.11648/j.ijrse.20130204.17

UNICEF/WHO. (2021). Progress on Household Drinking Water, Sanitation and Hygiene (2000-2020). Who/Unicef Joint Monitoring Programme for Water Supply, Sanitation and Hygiene. *World Health Organization and the United Nations Children's Fund*, 1–4.

Urban, D. L., & Antal, M. J. (1982). Study of the kinetics of sewage sludge pyrolysis using DSC and TGA. *Fuel*, *61*(9), 799–806. https://doi.org/10.1016/0016-2361(82)90306-4

Usman, A. R. A., Abduljabbar, A., Vithanage, M., Ok, Y. S., Ahmad, M., Ahmad, M., Elfaki, J., Abdulazeem, S. S., & Al-Wabel, M. I. (2015). Biochar production from date palm waste: Charring temperature induced changes in composition and surface chemistry. *Journal of Analytical and Applied Pyrolysis*, *115*, 392–400. https://doi.org/10.1016/j.jaap.2015.08.016

Uzun, H., Yıldız, Z., Goldfarb, J. L., & Ceylan, S. (2017). Improved prediction of higher heating value of biomass using an artificial neural network model based on proximate analysis. *Bioresource Technology*, *234*, 122–130. https://doi.org/10.1016/j.biortech.2017.03.015

Vijayaraghavan, K., Padmesh, T. V. N., Palanivelu, K., & Velan, M. (2006). Biosorption of nickel(II) ions onto Sargassum wightii: Application of two-parameter and three-parameter isotherm models. *Journal of Hazardous Materials*, *133*(1–3), 304–308. https://doi.org/10.1016/j.jhazmat.2005.10.016

Vinnerås, Björn, Nordin, A., Niwagaba, C., & Nyberg, K. (2008). Inactivation of bacteria and viruses in human urine depending on temperature and dilution rate. *Water Research*, *42*(15), 4067–4074. https://doi.org/10.1016/j.watres.2008.06.014

Vinnerås, Bjorn, Palmquist, H., Balmér, P., & Jönsson, H. (2006). The characteristics of household wastewater and biodegradable solid waste - A proposal for new Swedish design values. *Urban Water Journal*, *3*(1), 3–11. https://doi.org/10.1080/15730620600578629

Viskari, E.-L., Grobler, G., Karimäki, K., Gorbatova, A., Vilpas, R., & Lehtoranta, S. (2018). Nitrogen Recovery With Source Separation of Human Urine—Preliminary Results of Its Fertiliser Potential and Use in Agriculture. *Frontiers in Sustainable Food Systems*, *2*. https://doi.org/10.3389/fsufs.2018.00032

Vyazovkin, S., Burnham, A. K., Criado, J. M., Pérez-Maqueda, L. A., Popescu, C., & Sbirrazzuoli, N. (2011). ICTAC Kinetics Committee recommendations for performing kinetic computations on thermal analysis data. *Thermochimica Acta*, *520*(1–2), 1–19. https://doi.org/10.1016/j.tca.2011.03.034

Vyazovkin, S., & Wight, C. A. (1998). Isothermal and non-isothermal kinetics of thermally stimulated reactions of solids. *International Reviews in Physical Chemistry*, *17*(3), 407–433. https://doi.org/10.1080/014423598230108

W.A.Ufot, E. M. I. E. A. (2013). Determination of Combustion Characteristics of Compressed Pulverized Coal-Rice Husk Briquettes. *International Journal of Applied Science and Technology*, *3*(2), 61–64.

Wang, B., Lehmann, J., Hanley, K., Hestrin, R., & Enders, A. (2015). Adsorption and desorption of ammonium by maple wood biochar as a function of oxidation and pH. *Chemosphere*. https://doi.org/10.1016/j.chemosphere.2015.05.062

Wang, C., Gu, L., Liu, X., Zhang, X., Cao, L., & Hu, X. (2016). Sorption behavior of Cr(VI) on pineapple-peel-derived biochar and the influence of coexisting pyrene. *International Biodeterioration and Biodegradation*, *111*, 78–84. https://doi.org/10.1016/j.ibiod.2016.04.029

Wang, J., Ye, X., Zhang, Z., Ye, Z. L., & Chen, S. (2018). Selection of cost-effective magnesium sources for fluidized struvite crystallization. *Journal of Environmental Sciences (China)*, *70*, 144–153. https://doi.org/10.1016/j.jes.2017.11.029

Ward, B. J., Yacob, T. W., & Montoya, L. D. (2014). Evaluation of solid fuel char briquettes from human waste. *Environmental Science and Technology*, *48*(16), 9852–9858. https://doi.org/10.1021/es500197h

Wei, X., Viadero, R. C., & Bhojappa, S. (2008). Phosphorus removal by acid mine drainage sludge from secondary effluents of municipal wastewater treatment plants. *Water Research*, *42*(13), 3275–3284. https://doi.org/10.1016/j.watres.2008.04.005

WHO. (1981). Environmental Health Criteria 19: Hydrogen Sulfide. *Environmental Health Criteria*. https://doi.org/10.1016/0278-6915(83)90075-3

WHO. (2006). *WHO Guidelines for the Safe Use of Wasterwater Excreta and Greywater - World Health Organization - Google Books*. https://books.google.fi/books?hl=en&lr=&id=uJJ3UIPGtFIC&oi=fnd&pg=PR9&dq=who+2006+reuse+of+huma+excreta+standards+and+guidelines&ots=wQboTWmibd&sig=25U5IInpqPdLtZEVDyt_kDteVYk&redir_esc=y#v=onepage&q=who 2006 reuse of huma excreta standards and guidelines

Winker, M., Vinnerås, B., Muskolus, A., Arnold, U., & Clemens, J. (2009). Fertiliser products from new sanitation systems: Their potential values and risks. *Bioresource Technology*, *100*(18), 4090–4096. https://doi.org/10.1016/j.biortech.2009.03.024

World Health Organization, & UNICEF. (2017). Progress on DrinkingWater, Sanitation and Hygiene 2017 Update and SDG Baselines. In *Who* (Issue February). http://apps.who.int/iris/bitstream/handle/10665/258617/9789241512893-eng.pdf?sequence=1

Wu, D., Zhang, B., Li, C., Zhang, Z., & Kong, H. (2006). Simultaneous removal of

ammonium and phosphate by zeolite synthesized from fly ash as influenced by salt treatment. *Journal of Colloid and Interface Science*, *304*(2), 300–306. https://doi.org/10.1016/j.jcis.2006.09.011

Wunderlich, S. (2015). *Nutrient Recovery from Wastewater Using Biochar and Zeolite*. 2013–2015.

Xiong, J., Qin, Y., Islam, E., Yue, M., & Wang, W. (2011). Phosphate removal from solution using powdered freshwater mussel shells. *Desalination*, *276*(1–3), 317–321. https://doi.org/10.1016/j.desal.2011.03.066

Xu, K., Zhang, C., Dou, X., Ma, W., & Wang, C. (2019). Optimizing the modification of wood waste biochar via metal oxides to remove and recover phosphate from human urine. *Environmental Geochemistry and Health*, *41*(4), 1767–1776. https://doi.org/10.1007/s10653-017-9986-6

Xu, L., & Yuan, J. (2015). Online identification of the lower heating value of the coal entering the furnace based on the boiler-side whole process models. *Fuel*, *161*(August), 68–77. https://doi.org/10.1016/j.fuel.2015.08.009

Yabe, J., Nakayama, S. M. M., Ikenaka, Y., Yohannes, Y. B., Bortey-Sam, N., Kabalo, A. N., Ntapisha, J., Mizukawa, H., Umemura, T., & Ishizuka, M. (2018). Lead and cadmium excretion in feces and urine of children from polluted townships near a lead-zinc mine in Kabwe, Zambia. *Chemosphere*, *202*, 48–55. https://doi.org/10.1016/j.chemosphere.2018.03.079

Yacob, T. W., (Chip) Fisher, R., Linden, K. G., & Weimer, A. W. (2018). Pyrolysis of human feces: Gas yield analysis and kinetic modeling. *Waste Management*, *79*, 214–222. https://doi.org/10.1016/j.wasman.2018.07.020

Yahav Spitzer, R., Mau, V., & Gross, A. (2018). Using hydrothermal carbonization for sustainable treatment and reuse of human excreta. *Journal of Cleaner Production*,

205, 955–963. https://doi.org/10.1016/j.jclepro.2018.09.126

Yank, A., Ngadi, M., & Kok, R. (2016). Physical properties of rice husk and bran briquettes under low pressure densification for rural applications. *Biomass and Bioenergy*, *84*, 22–30. https://doi.org/10.1016/j.biombioe.2015.09.015

Yao, Y., Gao, B., Chen, J., & Yang, L. (2013). Engineered biochar reclaiming phosphate from aqueous solutions: Mechanisms and potential application as a slow-release fertilizer. *Environmental Science and Technology*, *47*(15), 8700–8708. https://doi.org/10.1021/es4012977

Yao, Y., Gao, B., Chen, J., Zhang, M., Inyang, M., Li, Y., & Alva, A. (2013). Bioresource Technology Engineered carbon (biochar) prepared by direct pyrolysis of Mg-accumulated tomato tissues : Characterization and phosphate removal potential. *Bioresource Technology*, *138*, 8–13. https://doi.org/10.1016/j.biortech.2013.03.057

Yao, Y., Gao, B., Zhang, M., Inyang, M., & Zimmerman, A. R. (2012). Effect of biochar amendment on sorption and leaching of nitrate, ammonium, and phosphate in a sandy soil. *Chemosphere*, *89*(11), 1467–1471. https://doi.org/10.1016/j.chemosphere.2012.06.002

Zahoor, M. (2011). Effect of agitation speed on adsorption of imidacloprid on activated carbon. *Journal of Chemical Society of Pakistan*, *33*(3), 305. https://www.researchgate.net/publication/265865554

Zevenhoven, R., & Kilpinen, P. (2001). *Control of pollutants in flue gases and fuel gases*.

Zhai, Y., Wang, T., Zhu, Y., Peng, C., Wang, B., Li, X., Li, C., & Zeng, G. (2018). Production of fuel pellets via hydrothermal carbonization of food waste using molasses as a binder. *Waste Management*, *77*, 185–194.

https://doi.org/10.1016/j.wasman.2018.05.022

Zhang, Gaosheng, Liu, H., Liu, R., & Qu, J. (2009). Removal of phosphate from water by a Fe-Mn binary oxide adsorbent. *Journal of Colloid and Interface Science*, *335*(2), 168–174. https://doi.org/10.1016/j.jcis.2009.03.019

Zhang, Guojie, Sun, Y., & Xu, Y. (2018). Review of briquette binders and briquetting mechanism. *Renewable and Sustainable Energy Reviews*, *82*(January 2017), 477–487. https://doi.org/10.1016/j.rser.2017.09.072

Zhang, J., Liu, J., Evrendilek, F., Xie, W., Kuo, J., Zhang, X., & Buyukada, M. (2019). Kinetics, thermodynamics, gas evolution and empirical optimization of cattle manure combustion in air and oxy-fuel atmospheres. *Applied Thermal Engineering*, *149*, 119–131. https://doi.org/10.1016/j.applthermaleng.2018.12.010

Zhang, Liang, Hong, S., He, J., Gan, F., & Ho, Y. S. (2011). Adsorption characteristic studies of phosphorus onto laterite. *Desalination and Water Treatment*, *25*(1–3), 98–105. https://doi.org/10.5004/dwt.2011.1871

Zhang, Ling, Wu, W., Liu, J., Zhou, Q., Luo, J., Zhang, J., & Wang, X. (2014). Removal of phosphate from water using raw and activated laterite: Batch and column studies. *Desalination and Water Treatment*, *52*(4–6), 778–783. https://doi.org/10.1080/19443994.2013.826786

Zhang, Y., Li, Z., & Mahmood, I. B. (2014). Recovery of NH 4+ by corn cob produced biochars and its potential application as soil conditioner. *Frontiers of Environmental Science and Engineering*, *8*(6), 825–834. https://doi.org/10.1007/s11783-014-0682-9

Zhang, Z., & Baixiaofeng. (2009). Comparison about the three central composite designs with simulation. *Proceedings - International Conference on Advanced Computer Control, ICACC 2009*, *3*, 163–167.

https://doi.org/10.1109/ICACC.2009.48

Zhou, Y., Zhang, L., & Cheng, Z. (2015). Removal of organic pollutants from aqueous solution using agricultural wastes: A review. *Journal of Molecular Liquids*, *212*, 739–762. https://doi.org/10.1016/j.molliq.2015.10.023

Zhu, K., Fu, H., Zhang, J., Lv, X., Tang, J., & Xu, X. (2012). Studies on removal of NH4+-N from aqueous solution by using the activated carbons derived from rice husk. *Biomass and Bioenergy*, *43*, 18–25. https://doi.org/10.1016/j.biombioe.2012.04.005

Zhu, R., Zhu, L., Zhu, J., Ge, F., & Wang, T. (2009). Sorption of naphthalene and phosphate to the CTMAB-Al13 intercalated bentonites. *Journal of Hazardous Materials*, *168*(2–3), 1590–1594. https://doi.org/10.1016/j.jhazmat.2009.03.057

APPENDICES

Appendix I: Composition and Structures of Lateritic Soil (LS) and Pineapple Peel Biochar (PPB)

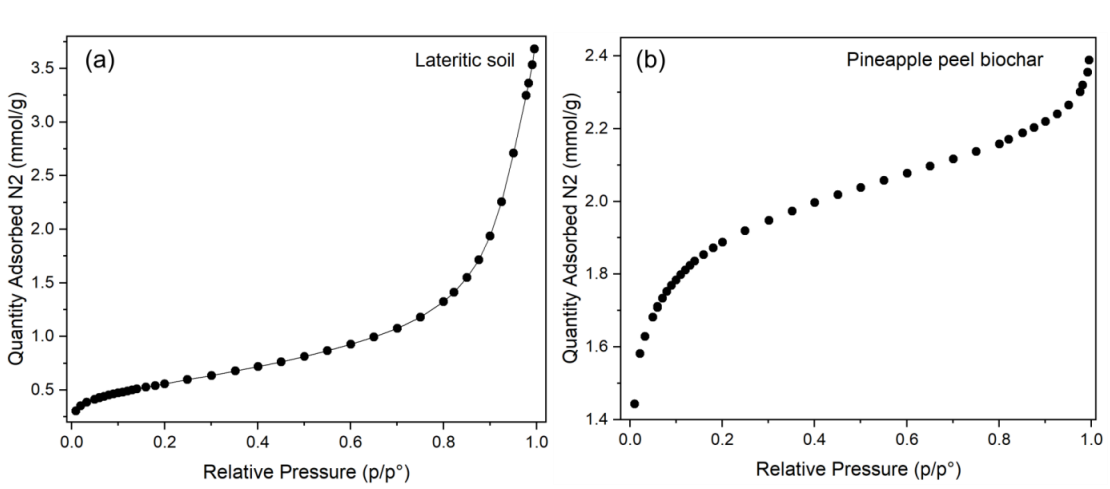

Figure A1: Nitrogen Adsorption Isotherm at 77 K of (a) Lateritic Soil, and (b) Pineapple Peel Biochar

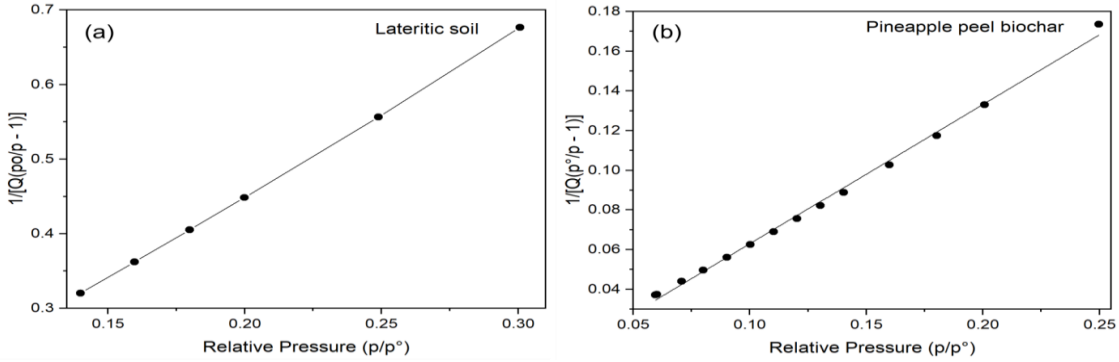

Figure A2: BET Plots of (a) Lateritic Soil, and (b) Pineapple Peel Biochar Determined using a Linear Section of Fig. A1 above at Relative Pressures (p/p^o) Over the Range of 0.05 – 0.3

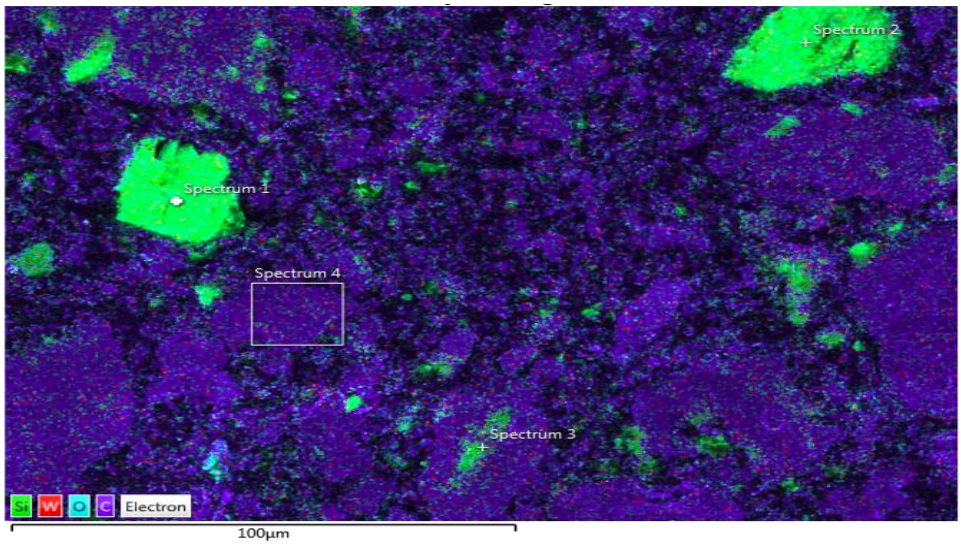

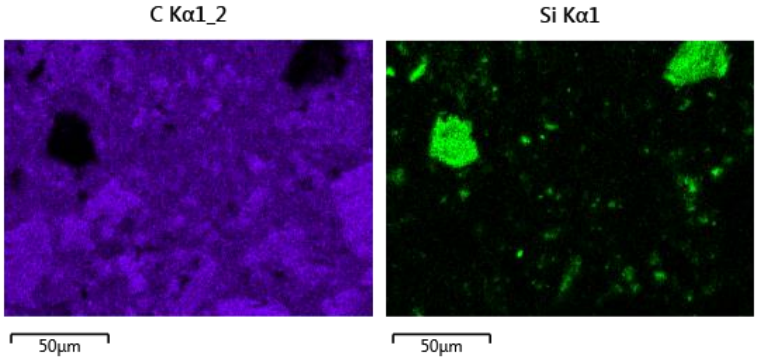

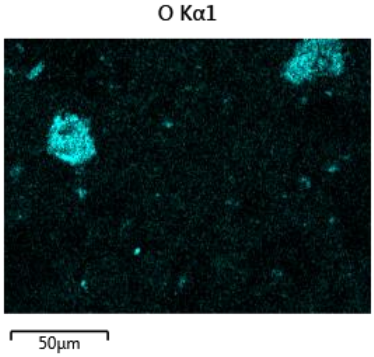

Figure A3: EDS Mapping of Lateritic Soil

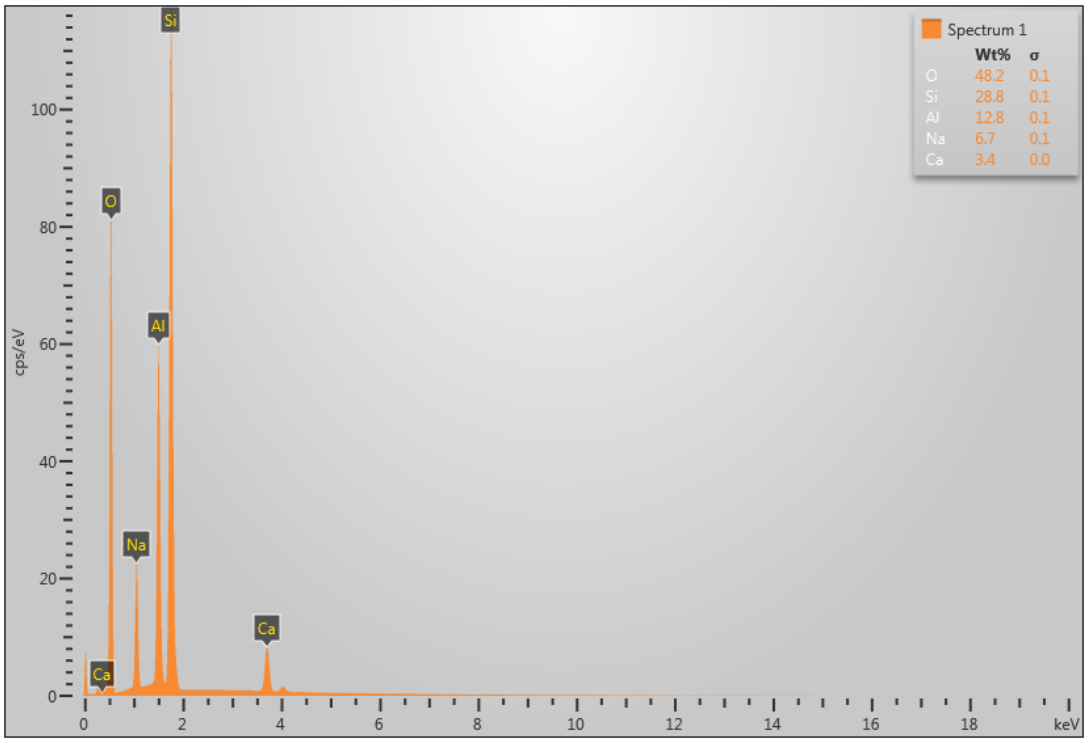

Figure A4 (a): EDS Graph of Lateritic Soil at Spectrum 1

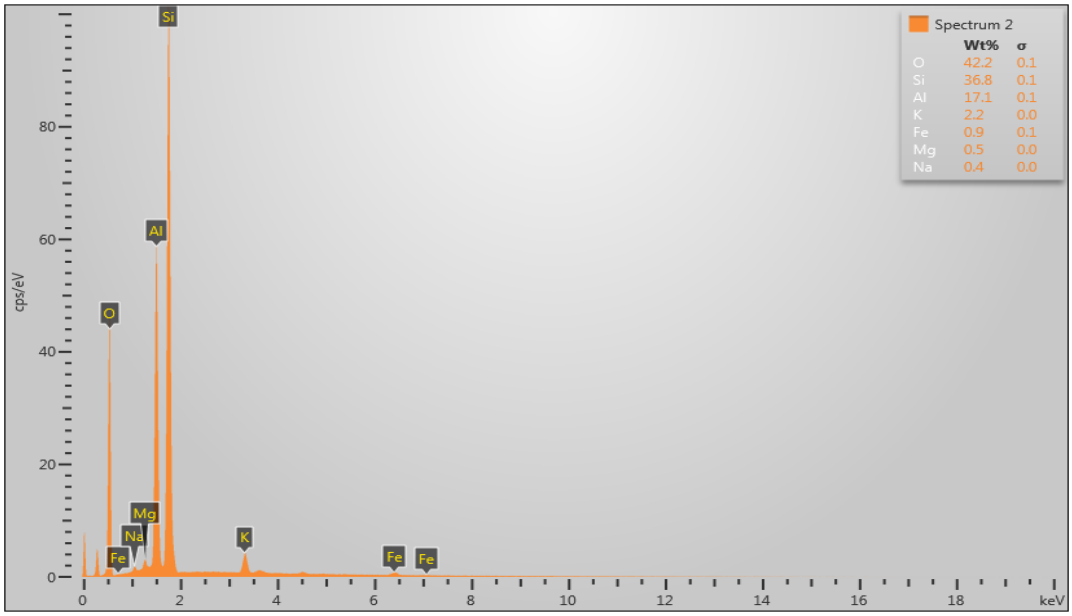

Figure A4 (b): EDS Graph of Lateritic Soil at Spectrum 2

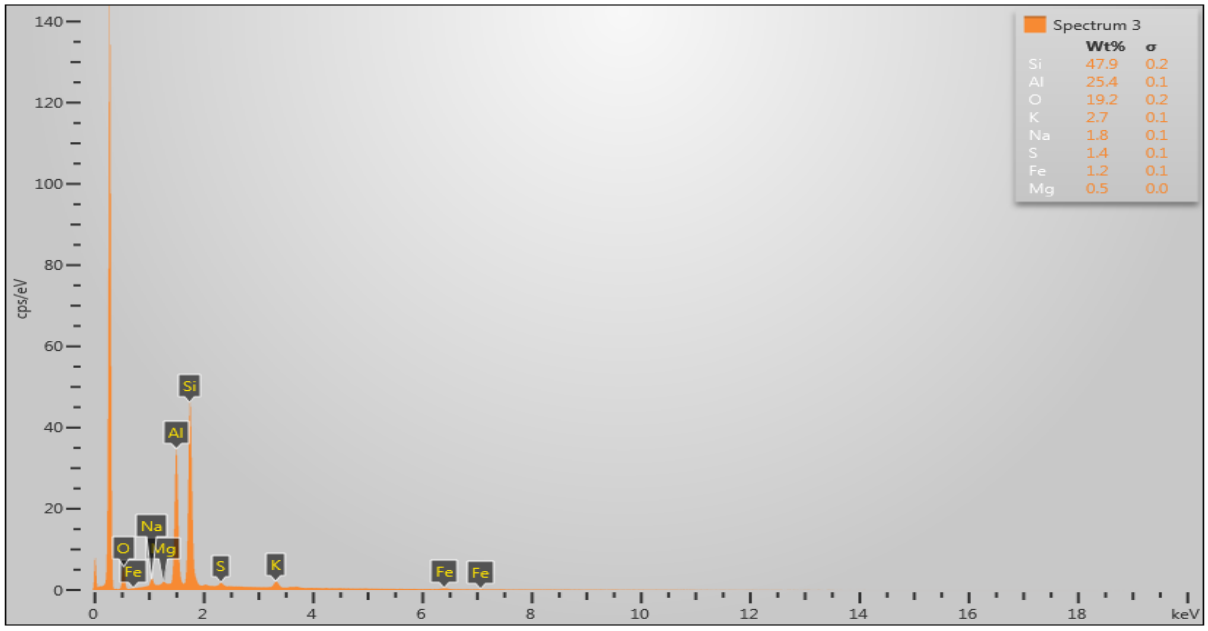

Figure A4 (c): EDS Graph of Lateritic Soil at Spectrum 3

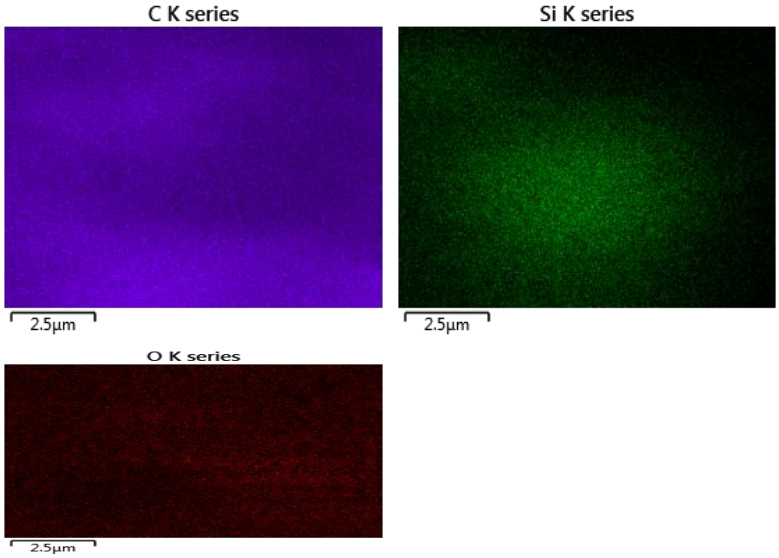

Figure A5: EDS Mapping of Pineapple Peel Biochar

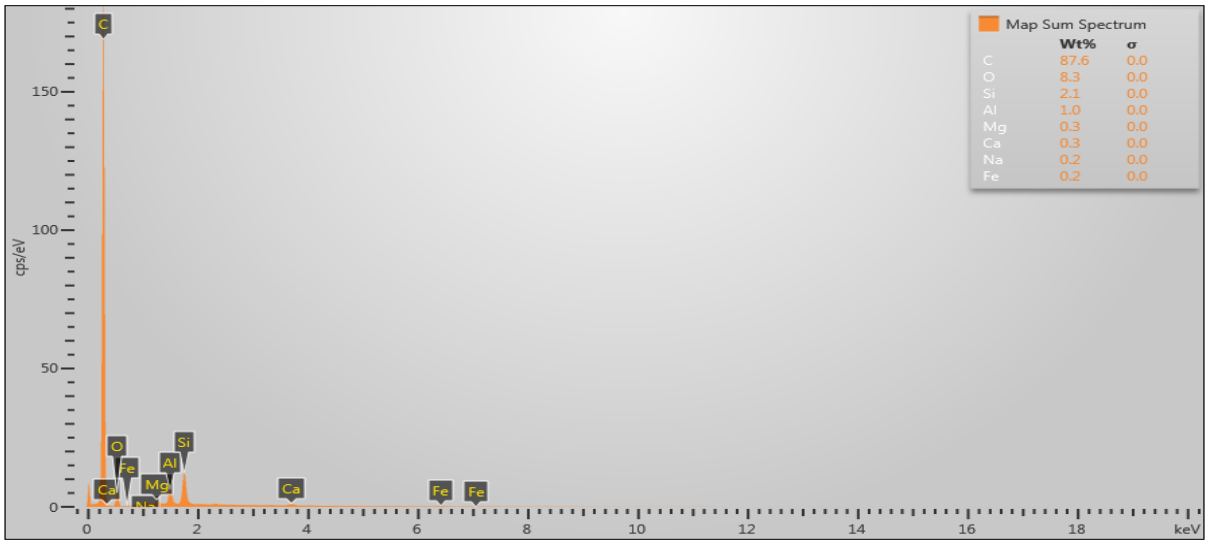

Figure A6: EDS Graph of Pineapple Peel Biochar

Appendix II: Langmuir, Freundlich, and Dubinin-Radushkevich Isotherm and Equilibrium Data for NH_4^+-N Adsorption on Lateritic Soils and Pineapple Peel Biochar

Table B1: Langmuir Isotherm Data of Lateritic Soil

Sample	Initial Conc. (mg/L)	$1/C_e$	$1/q_e$	Equation	R^2
Lateritic soil	569.24	0.002	0.095	y=17.914x+0.0518	0.983
	451.59	0.003	0.103		
	398.92	0.003	0.107		
	341.77	0.004	0.106		
	161.36	0.008	0.202		
	156.88	0.009	0.204		

Table B2: Langmuir Isotherm Data of Pineapple Peel Biochar

Sample	Initial Conc. (mg/L)	$1/C_e$	$1/q_e$	Equation	R^2
Pineapple peel biochar	569.24	0.002	0.078	y=12.273x+0.0444	0.979
	451.59	0.003	0.080		
	398.92	0.003	0.083		
	341.77	0.004	0.085		
	161.36	0.009	0.155		
	156.88	0.009	0.162		

Table B3: Freundlich Isotherm Data of Lateritic Soil

Sample	Initial Conc. (mg/L)	log C_e	log q_e	Equation	R^2
Lateritic soil	569.24	2.686	1.021	y= 0.5814x - 0.5009	0.946
	451.59	2.573	0.985		
	398.92	2.510	0.975		
	341.77	2.425	0.972		
	161.36	2.086	0.695		
	156.88	2.071	0.690		

Table B4: Freundlich Isotherm Data of Pineapple Peel Biochar

Sample	Initial Conc. (mg/L)	log C_e	log q_e	Equation	R^2
Pineapple peel biochar	569.24	2.669	1.105	y= 0.5405x - 0.2836	0.928
	451.59	2.546	1.096		
	398.92	2.484	1.082		
	341.77	2.389	1.071		
	161.36	2.041	0.809		
	156.88	2.032	0.789		

Table B5: Dubinin-Radushkevich Isotherm Data of Lateritic Soil

Sample	Initial Conc. (mg/L)	$[RT\ln(1+1/Ce)]^2$	lnqe	Equation	R^2
Lateritic soil	569.24	25.35	2.352	y=-0.0019x+2.3734	0.995
	451.59	42.58	2.268		
	398.92	56.85	2.244		
	341.77	84.00	2.239		
	161.36	400.07	1.599		
	156.88	428.24	1.589		

Table B6: Dubinin-Radushkevich Isotherm Data of Pineapple Peel Biochar

Sample	Initial Conc. (mg/L)	$[RTln(1+1/Ce)]^2$	lnqe	Equation	R^2
Pineapple peel biochar	569.24	27.33	2.545	y=-0.0015x+2.5957	0.999
	451.59	48.17	2.523		
	398.92	64.17	2.492		
	341.77	99.19	2.465		
	161.36	491.47	1.863		
	156.88	512.07	1.818		

Table B7: Ammonium Nitrogen (NH4+-N) Adsorbed (mg/g) at Initial Concentration of 569.24 mg/Ls

Initial Conc.	Contact time(min)	NH_4^+-N adsorbed by lateritic soil	NH_4^+-N adsorbed by pineapple peel biochar
569.24	30	6.45±0.11	9.71±0.08
	60	9.76±0.06	12.68±0.04
	90	10.51±0.04	12.75±0.09
	120	10.51±0.06	12.74±0.04

Table B8: Ammonium Nitrogen (NH_4^+-N) Adsorbed (mg/g) at Initial Concentration of 451.59 mg/L

Initial Conc.	Contact time (min)	NH_4^+-N adsorbed by lateritic soil	NH_4^+-N adsorbed by pineapple peel biochar
451.59	30	6.25±0.02	9.10±0.02
	60	9.29±0.01	12.46±0.01
	90	9.66±0.07	12.47±0.06
	120	9.66±0.02	12.47±0.04

Table B9: Ammonium Nitrogen (NH_4^+-N) Adsorbed (mg/g) at Initial Concentration of 398.92 mg/L

Initial Conc.	Contact time (min)	NH_4^+-N adsorbed by lateritic soil	NH_4^+-N adsorbed by pineapple peel biochar
398.92	30	5.65±0.02	9.34±0.06
	60	8.96±0.02	11.95±0.16
	90	9.43±0.03	12.09±0.02
	120	9.43±0.02	12.09±0.04

Table B10: Ammonium Nitrogen (NH_4^+-N) Adsorbed (mg/g) at Initial Concentration of 341.77 mg/L

Initial Conc.	Contact time (min)	NH_4^+-N adsorbed by lateritic soil	NH_4^+-N adsorbed by pineapple peel biochar
341.77	30	4.16±0.10	8.31±0.07
	60	7.56±0.03	11.76±0.02
	90	9.38±0.02	11.77±0.02
	120	9.38±0.02	11.77±0.01

Table B11: Ammonium Nitrogen (NH_4^+-N) Adsorbed (mg/g) at Initial Concentration of 161.36 mg/L

Initial Conc.	Contact time (min)	NH_4^+-N adsorbed by lateritic soil	NH_4^+-N adsorbed by pineapple peel biochar
161.36	30	3.96±0.05	5.79±0.03
	60	4.75±0.03	6.39±0.04
	90	4.95±0.04	6.44±0.02
	120	4.95±0.08	6.44±0.03

Table B12: Ammonium Nitrogen (NH_4^+-N) Adsorbed (mg/g) at Initial Concentration of 156.88 mg/L

Initial Conc.	Contact time (min)	NH_4^+-N adsorbed by lateritic soil	NH_4^+-N adsorbed by pineapple peel biochar
156.88	30	3.36±0.05	5.09±0.02

	60	4.48±0.08	6.15±0.06
	90	4.90±0.03	6.16±0.05
	120	4.91±0.03	6.16±0.02

Appendix III: Calibration Curves, Equilibrium, and Langmuir, Freundlich, and Dubinin-Radushkevich Isotherm Data for P Adsorption on Lateritic Soils and Pineapple Peel Biochar

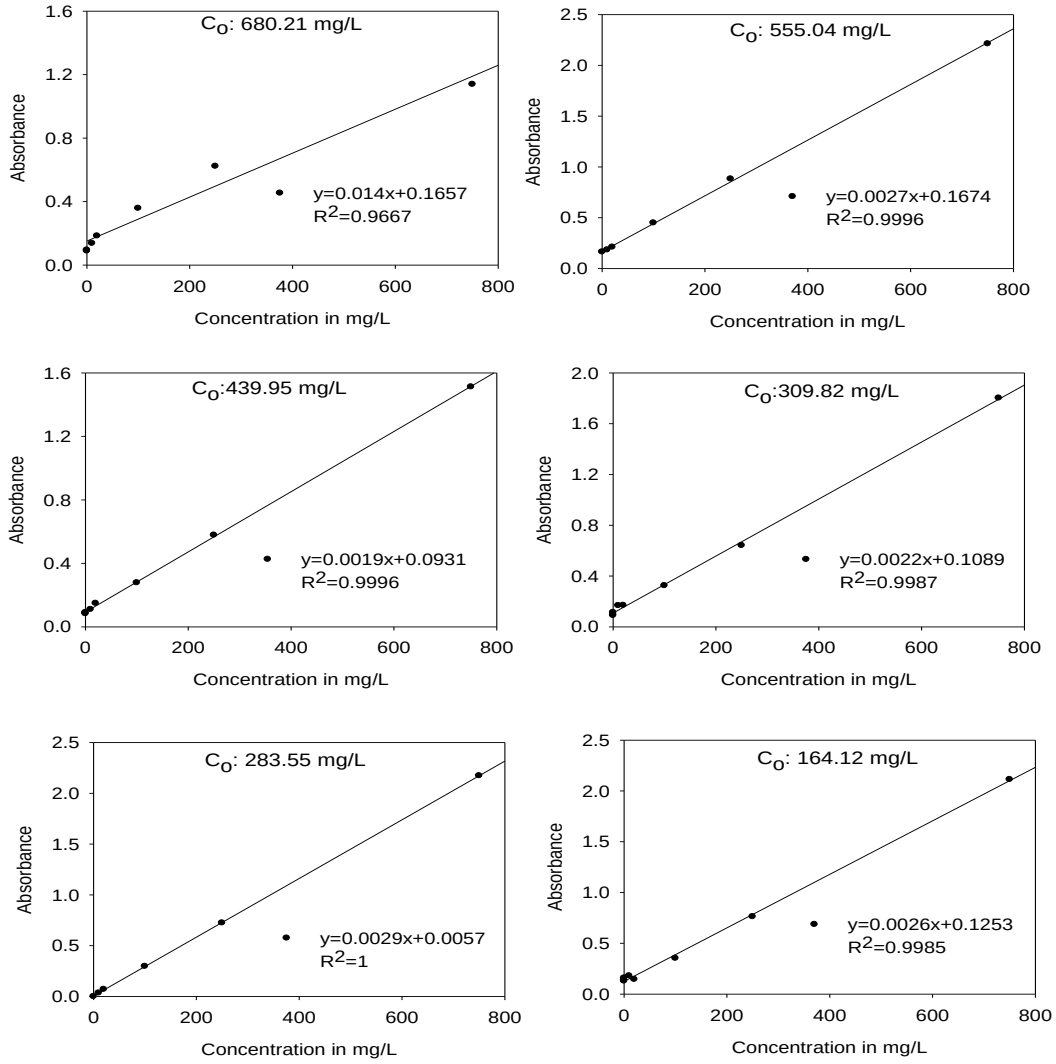

Figure C1: Calibration Curves for P Adsorption at Different Initial Concentrations (C_o)

Table C1: Phosphorous (P) Adsorbed (mg/g) at Initial Concentration of 680.21 mg/L

Initial Conc.	Contact time(min)	P adsorbed by lateritic soil	P adsorbed by pineapple peel biochar
680.21	30	14.38±0.05	56.74±0.08
	60	15.27±0.06	41.88±0.05
	90	15.36±0.03	39.87±0.05
	120	15.36±0.09	38.88±0.04

Table C2: Phosphorous (P) Adsorbed (mg/g) at Initial Concentration of 555.04 mg/L

Initial Conc.	Contact time (min)	P adsorbed by lateritic soil	P adsorbed by pineapple peel biochar
555.04	30	9.45±0.03	27.48±0.02
	60	12.35±0.01	24.51±0.08
	90	13.34±0.09	25.12±0.06
	120	13.34±0.07	23.38±0.09

Table C3: Phosphorous (P) Adsorbed (mg/g) at Initial Concentration of 439.95 mg/L

Initial Conc.	Contact time (min)	P adsorbed by lateritic soil	P adsorbed by pineapple peel biochar
439.95	30	8.75±0.05	15.56±0.07
	60	11.94±0.10	14.67±0.06
	90	12.80±0.03	14.67±0.02
	120	12.80±0.06	14.15±0.03

Table C4: Phosphorous (P) Adsorbed (mg/g) at Initial Concentration of 309.82 mg/L

Initial Conc.	Contact time (min)	P adsorbed by lateritic soil	P adsorbed by pineapple peel biochar
309.82	30	4.96±0.11	13.01±0.08
	60	7.60±0.09	12.36±0.02
	90	8.75±0.02	14.38±0.04
	120	8.75±0.03	12.78±0.03

Table C5: Phosphorous (P) Adsorbed (mg/g) at Initial Concentration of 283.55 mg/L

Initial Conc.	Contact time (min)	P adsorbed by lateritic soil	P adsorbed by pineapple peel biochar
283.55	30	4.78±0.05	7.54±0.03
	60	5.68±0.03	10.06±0.02
	90	7.58±0.06	9.46±0.03
	120	7.58±0.02	9.61±0.03

Table C6: Phosphorous (P) Adsorbed (mg/g) at Initial Concentration of 164.12 mg/L

Initial Conc.	Contact time (min)	P adsorbed by lateritic soil	P adsorbed by pineapple peel biochar
164.12	30	1.79±0.05	-1.23±0.02
	60	2.64±0.08	0.80±0.06
	90	4.95±0.03	1.57±0.08
	120	4.95±0.02	0.71±0.04

Table C7: Langmuir Isotherm Data of Lateritic Soil

Sample	Initial Conc. (mg/L)	$1/C_e$	$1/q_e$	Equation	R^2
lateritic soil	680.21	0.001	0.065	y=22.553x+0.0221	0.984
	555.04	0.002	0.075		
	439.95	0.003	0.078		
	309.82	0.004	0.114		
	283.55	0.005	0.132		
	164.12	0.008	0.202		

Table C8: Freundlich Isotherm Data of Lateritic Soil

Sample	Initial Conc. (mg/L)	Log C_e	Log q_e	Equation	R^2
lateritic soil	680.21	2.746	1.186	y= 0.7776x - 0.9223	0.966
	555.04	2.652	1.125		
	439.95	2.528	1.107		
	309.82	2.379	0.942		
	283.55	2.348	0.879		
	164.12	2.095	0.695		

Table C9: Dubinin-Radushkevich Isotherm Data of Lateritic Soil

Sample	**Initial Conc. (mg/L)**	**{RTln(1+1/Ce)}^{2}**	**Lnqe**	**Equation**	**R^2**
lateritic soil	680.21	19.218	2.732	y=-0.0029x+2.6215	0.858
	555.04	29.690	2.591		
	439.95	52.336	2.549		
	309.82	103.557	2.169		
	283.55	119.827	2.026		
	164.12	382.774	1.599		

Appendix IV: Graphical Presentation of the Interaction of Contact Time, Adsorbent Loading and Agitation Speed on Ammonium Nitrogen (NH_4^+-N) Adsorption on Pineapple Peel Biochar (PPB)

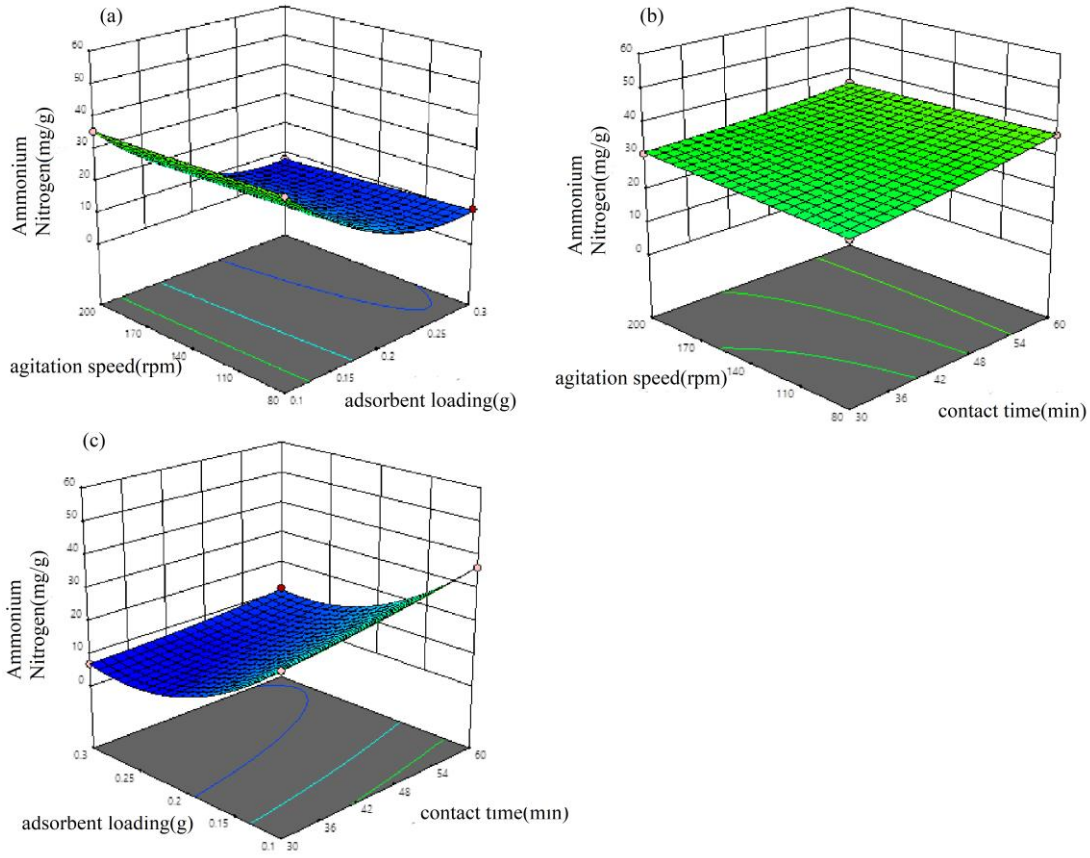

Figure D1:(a)Interactive Effect of Agitation Speed and Adsorbent Loading at Constant Time of 60 min;(b)Interactive Effect of Agitation Speed and Contact Time at Constant Loading of 0.1g;(c)Interactive Effect of Adsorbent Loading and Contact Time at Constant Speed of 80rpm

Appendix V: Graphical Presentation of the Interaction of Contact Time, Adsorbent Loading and Agitation Speed on Phosphorous (P) Adsorption on Lateritic Soil

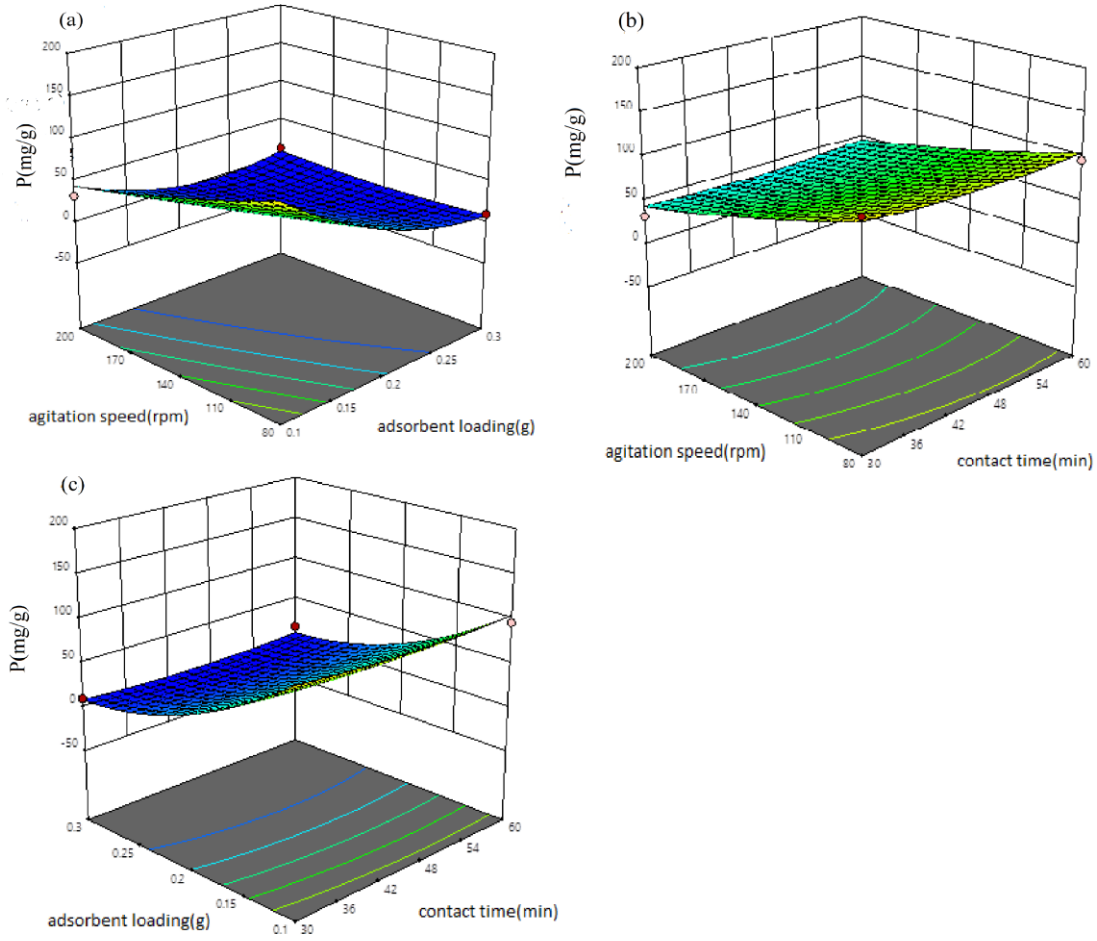

Figure E1:(a)Interactive Effect of Agitation Speed and Adsorbent Loading at Constant Time of 30 min;(b)Interactive Effect of Agitation Speed and Contact Time at Constant Loading of 0.1g;(c)Interactive Effect of Adsorbent Loading and Contact Time at Constant Speed of 80rpm

Appendix VI: Emissions Monitored During Combustion of Charcoal and Co-combustion of Charcoal with Briquettes

Table F1: Emission from Charcoal Combustion

Time(min)	Temp(°C) of Stack	CO (ppm)	CO_2 (ppm)	SO_2	H_2S (ppm)	NO	NO_2	O %
0	24	0	0	0	0	0	0	20.9
2	222	90	3000	0	0	0	0	20.6
8	209	1359	5000	0	2	0	0	20.3
16	180	1169	4000	0	2	0	0	20.3
25	160	856	3000	0	0	0	0	20.5
29	202	1539	7000	0	2	0	0	20.1
35	197	1065	5000	0	0	0	0	20.4
37	174	747	4000	0	0	0	0	20.5

Table F2: Emission from Co-combustion of Charcoal with Briquettes

Time(min)	Temp(°C) of Stack	CO (ppm)	CO_2 (ppm)	SO_2	H_2S (ppm)	NO	NO_2	O %
0	33	0	0	0	0	0	0	20.9
2	450	2	14000	0	0	0	0	20.5
5	475	554	22000	0	2	0	0	18.4
8	435	1859	15000	0	3	24	0	19.3
12	352	3845	12000	0	6	30	0	19.4
17	295	2881	8000	0	6	18	0	19.9
21	237	316	2000	0	0	0	0	20.8
25	252	3105	7000	0	6	17	0	19.9

Appendix VII: Pictures of Equipment Used in the Study

Plate G1: Equipment Used in Nh4+-N and P Determination

Plate G2: Combustion and Emission Monitoring using E8500P Industrial Integrated Emissions System Combustion Gas Analyser

Plate G3: Image of Ignited Charcoal and Briquettes in the Cook Stove